AD NUMBER
ADB265760
NEW LIMITATION CHANGE

TO
Approved for public release, distribution unlimited

FROM
Distribution authorized to U.S. Gov't. agencies only; Proprietary Info.; Oct 2000. Other requests shall be referred to US Army Medical Research and Materiel Comd., 504 Scott St., Fort Detrick, MD 21702-5012.

AUTHORITY

USAMRMC ltr, DTD 01 Jul 2003

AD_____

Award Number: DAMD17-97-1-7030

TITLE: Magnetic Resonance Arterial Spin Tagging for Non-Invasive
Pharmacokinetic Analysis of Breast Cancer

PRINCIPAL INVESTIGATOR: Michael H. Buonocore, M.D.

CONTRACTING ORGANIZATION: University of California
Davis, California   95616-8671

REPORT DATE: October 2000

TYPE OF REPORT: Annual

PREPARED FOR: U.S. Army Medical Research and Materiel Command
Fort Detrick, Maryland   21702-5012

DISTRIBUTION STATEMENT: Distribution authorized to U.S.
Government agencies only (proprietary information, Oct 00).
Other requests for this document shall be referred to U.S.
Army Medical Research and Materiel Command, 504 Scott Street,
Fort Detrick, Maryland   21702-5012.

20010502 187

NOTICE

USING GOVERNMENT DRAWINGS, SPECIFICATIONS, OR OTHER DATA INCLUDED IN THIS DOCUMENT FOR ANY PURPOSE OTHER THAN GOVERNMENT PROCUREMENT DOES NOT IN ANY WAY OBLIGATE THE U.S. GOVERNMENT. THE FACT THAT THE GOVERNMENT FORMULATED OR SUPPLIED THE DRAWINGS, SPECIFICATIONS, OR OTHER DATA DOES NOT LICENSE THE HOLDER OR ANY OTHER PERSON OR CORPORATION; OR CONVEY ANY RIGHTS OR PERMISSION TO MANUFACTURE, USE, OR SELL ANY PATENTED INVENTION THAT MAY RELATE TO THEM.

LIMITED RIGHTS LEGEND

Award Number: DAMD17-97-1-7030
Organization: University of California
Location of Limited Rights Data (Pages):

Those portions of the technical data contained in this report marked as limited rights data shall not, without the written permission of the above contractor, be (a) released or disclosed outside the government, (b) used by the Government for manufacture or, in the case of computer software documentation, for preparing the same or similar computer software, or (c) used by a party other than the Government, except that the Government may release or disclose technical data to persons outside the Government, or permit the use of technical data by such persons, if (i) such release, disclosure, or use is necessary for emergency repair or overhaul or (ii) is a release or disclosure of technical data (other than detailed manufacturing or process data) to, or use of such data by, a foreign government that is in the interest of the Government and is required for evaluational or informational purposes, provided in either case that such release, disclosure or use is made subject to a prohibition that the person to whom the data is released or disclosed may not further use, release or disclose such data, and the contractor or subcontractor or subcontractor asserting the restriction is notified of such release, disclosure or use. This legend, together with the indications of the portions of this data which are subject to such limitations, shall be included on any reproduction hereof which includes any part of the portions subject to such limitations.

THIS TECHNICAL REPORT HAS BEEN REVIEWED AND IS APPROVED FOR PUBLICATION.

Earl Grout Jr.

21 Feb. 2001

REPORT DOCUMENTATION PAGE		*Form Approved* *OMB No. 074-0188*

Public reporting burden for this collection of information is estimated to average 1 hour per response, including the time for reviewing instructions, searching existing data sources, gathering and maintaining the data needed, and completing and reviewing this collection of information. Send comments regarding this burden estimate or any other aspect of this collection of information, including suggestions for reducing this burden to Washington Headquarters Services, Directorate for Information Operations and Reports, 1215 Jefferson Davis Highway, Suite 1204, Arlington, VA 22202-4302, and to the Office of Management and Budget, Paperwork Reduction Project (0704-0188), Washington, DC 20503

1. AGENCY USE ONLY (Leave blank)	2. REPORT DATE October 2000	3. REPORT TYPE AND DATES COVERED Annual (30 Sep 99 – 29 Sep 00)	
4. TITLE AND SUBTITLE Magnetic Resonance Arterial Spin Tagging for Non-Invasive Pharmacokinetic Analysis of Breast Cancer		**5. FUNDING NUMBERS** DAMD17-97-1-7030	
6. AUTHOR(S) Michael H. Buonocore, M.D.-Ph.D.			
7. PERFORMING ORGANIZATION NAME(S) AND ADDRESS(ES) University of California Davis, California 95616-8671 E-MAIL: mhbuonocore@ucdavis.edu		**8. PERFORMING ORGANIZATION REPORT NUMBER**	
9. SPONSORING / MONITORING AGENCY NAME(S) AND ADDRESS(ES) U.S. Army Medical Research and Materiel Command Fort Detrick, Maryland 21702-5012		**10. SPONSORING / MONITORING AGENCY REPORT NUMBER**	

11. SUPPLEMENTARY NOTES

This report contains colored photos

12a. DISTRIBUTION / AVAILABILITY STATEMENT DISTRIBUTION STATEMENT: Distribution authorized to U.S. Government agencies only (proprietary information, Oct 00). Other requests for this document shall be referred to U.S. Army Medical Research and Materiel Command, 504 Scott Street, Fort Detrick, Maryland 21702-5012.	12b. DISTRIBUTION CODE

13. ABSTRACT (Maximum 200 Words)

This research project concerns the development of MRI arterial spin tagging to non-invasively measure breast tissue perfusion. The specific aims are to (1) refine arterial spin tagging pulse sequences, (2) develop automated data analysis software, and (3) compare the technique to first-pass contrast-enhanced MRI and biopsy. The scope of effort has been mainly limited to technical developments. During the first two years, the spin-tagging pulse sequences were developed for the GE 1.5T Horizon LX CV/I MRI system at UC Davis. New image processing software, and software for statistical analysis of spin tagging and contrast enhanced dynamic scans, were written for use in the clinical setting. Year three the project included a clinical comparison with first-pass, contrast-enhanced MRI in 60 patients with unbiopsied breast masses, for aim (3). However, these studies were not done, due to the inability to recruit patients. The grant funds were not spent. Official approval has been granted for a one-year no-cost extension. A new co-investigator and patient referral pattern should improve patient recruitment in this upcoming fourth year of the project.

14. SUBJECT TERMS Breast Cancer			15. NUMBER OF PAGES 180
			16. PRICE CODE
17. SECURITY CLASSIFICATION OF REPORT Unclassified	18. SECURITY CLASSIFICATION OF THIS PAGE Unclassified	19. SECURITY CLASSIFICATION OF ABSTRACT Unclassified	20. LIMITATION OF ABSTRACT Unlimited

NSN 7540-01-280-5500

Standard Form 298 (Rev. 2-89)
Prescribed by ANSI Std. Z39-18
298-102

Table of Contents

Introduction

This research project concerns the development of MRI arterial spin tagging to non-invasively measure breast tissue perfusion. MR dynamic first-pass contrast-enhanced imaging has shown that malignant and benign breast lesions can be distinguished. However, it may have limited importance in clinical breast diagnosis due to significant false-negatives and false-positives. The arterial spin tagging technique was developed to measure tissue perfusion parameters without intravenous contrast, and has been successfully demonstrated in brain and kidney. The specific aims are to (1) refine arterial spin tagging pulse sequences and imaging protocols, (2) develop automated data analysis software for measurement of breast tissue parameters, and (3) compare the technique to first-pass contrast-enhanced MRI and biopsy. We will test the hypothesis that arterial spin tagging provides accurate and precise discrimination between normal tissue, benign and malignant lesions, when differences in perfusion and T_1 exist. Lesions will have been previously detected by clinically accepted diagnostic imaging procedures, and by biopsy. Statistical analysis will be performed to access the correspondence between arterial spin tagging and biopsy, and to establish the relative value of spin tagging compared to first-pass contrast-enhanced MRI. We hope to establish that, relative to using first-pass contrast-enhanced imaging, false positives and negatives are reduced using arterial spin tagging by virtue of increased image signal-to-noise ratio (SNR), higher spatial resolution, and the unique ability to obtain estimates of macromolecular bound fluid fractions. The scope of effort on the project is mainly limited to the technical aspects of development of a new methodology. However, the project also includes a rigorous performance comparison with the current gold-standard methodology. The technique will be evaluated in sixty patients, with roughly equal numbers of benign and malignant lesions.

Body

Summary of Project Accomplishments

Report for 2000

David Zhu completed his dissertation (attached as Appendix) and compiled the software on CD-ROM (enclosed), a poster was presented at the BCRP meeting in Atlanta (attached as Appendix), and a publication is currently being written. Comparison of the arterial spin tagging sequence with the dynamic contrast enhanced first pass study, intended for year 3, has not yet been achieved. Sixty patients should have been studied at this point in the project, but only two have been studied. It was not possible to find a replacement physician for the original co-Investigator on the project, Rebecca Zulim, who left UCDMC November 1, 1998. I submitted a revised project schedule and budget in May 1999 based upon having Dr. Philip Schneider as a collaborator, and these were approved, but they were not implemented due to the lack of patient recruitment into the study. Although Dr. Schneider agreed to serve as a collaborator for this period, patient recruitment was ineffective. Over the past year, exactly $12,971 was spent from grant funds, for support of Dr. Zhu during the last three months (Oct 1999 – Dec 1999) of his employment at UC Davis, and 3% PI salary support. No salary support was provided to the co-I. As of Sept 2000, $71,408 (27.2% of total award) remain unexpended.

From the 1999 Annual Report ...

UCD Medical Center Radiology Department upgraded all their MRI systems from Signa Genesis 5.x to Signa LX 8.2.5, resulting in several months during which our pulse sequences were not compatible with any of the MRI systems to which we had access. Substantial time was needed to convert the pulse sequences to the LX 8.2.5 platform from the Genesis 5.x platform. This time period for upgrading the UCD Med Center MRI systems was not planned in advance, and the time to convert our research software was not written into the approved Work Statement. The graduate student on this project, David Zhu, and I succeeded in converting the arterial spin tagging pulse sequences, and on further developing new arterial spin tagging sequences based on our "odd-hybrid" EPI technique [Buonocore MH, Zhu DC. High spatial resolution EPI using an odd number of interleaves. Magnetic Resonance in Medicine 41 (6): 1199-1205 (1999)]. Also, advances have been made in our image processing software for the project. The major deficiency in our progress is with the third technical objective. Comparison of the arterial spin tagging sequence with the dynamic contrast enhanced first pass study has not yet been achieved. Rebecca Zulim, the co-I on the project, left UCDMC November 1, 1998, and a replacement was not immediately found. The budget and schedule was officially pushed back 6 months, into the 3rd year which had a light work schedule in the original proposal. The project now continues into the 3rd year, as dictated by approved revised schedule and budget. Dr. PD Schneider of the UC Davis Cancer Center is the co-investigator on the project.

From the 1998 Annual Report ...

There are two substantial contributions of the work. The first is the development of robust pulse sequences and analysis methods to derive accurate T1 estimates with inherently noisy and confounded signal data. The second is the development of the software program (BrView), to allow rapid review, quantitative analysis, and assessment of the multitude of different breast images and timeseries data that is obtained in each patient study.

Accomplishments relating to Approved Statement of Work

Technical objective 1

Task 1: *Months 1-6: Implementation and testing of magnetization transfer pulses for both arterial tagging and first-pass contrast enhanced sequences.*

Report for 2000

Magnetization transfer (MT) was fully tested with the EPI-based spin tagging sequence.

From 1999 Annual Report ...

Magnetization transfer (MT) has been implemented with the EPI-based spin tagging sequence (see Figure 1). The MT radiofrequency (RF) pulse selectively excites the protons of the macromolecules and its hydration layer by a 900 flip angle. Two gradient spoiling pulses (in the x- and y- directions) are applied immediately after the RF pulse to spoil the transverse magnetization. The usual RF excitation pulse for data acquisition is applied immediately after these spoiling pulses. Due to hardware and or compiler problems that are currently being investigated by GE, this pulse sequence has been implemented only on pulse sequence simulation software (EPIC), not yet on the MRI system. The hardware problems are somehow preventing this sequence from running successfully on the MRI system. Testing of MT using the fast SPGR-based sequence revealed that it would not be effective. Because the magnetization transfer RF pulse is long duration (16 ms), the "small TR" (optr) period of the fast SPGR sequence was effectively doubled in length, thus sacrificing short scan time and distorting the signal upon which the perfusion measurement is based.

From 1998 Annual Report ...

Magnetization transfer pulses have not been implemented yet. Mainly, this delay was due to the fact that the MRI system at UC Davis Medical Center is scheduled to be upgraded to the new Horizon LX system soon, and we opted to defer this pulse sequence development until we were using this new LX software platform. There have been multiple delays, but this upgrade is scheduled to occur by January 1999. The existing pulse sequence will be converted from the 5.4 OS platform to the LX2 platform (a substantial change), and the magnetization transfer pulses will be implemented.

Because of concerns regarding the ultimate utility of the magnetization transfer technique, we have decided that implementation and testing of arterial spin-tagging sequence based on echo planar imaging (EPI) data acquisition is a higher priority. EPI based spin-tagging technique can theoretically improve the accuracy of the T_1 estimation, which we have studied and worked with extensively (see below). The major problem with magnetization transfer is that it represents a perturbation on an already small signal. Therefore, whether we will observe a magnetization transfer effect is questionable. Nevertheless, it will be implemented as part of the project.

Task 2: *Months 1-9: Implementation and testing of interleaved high-resolution imaging technique, for both arterial tagging and first-pass contrast enhanced sequences.*

Report for 2000

Conversion of the Fast SPGR Based Arterial Spin Tagging Sequence

The authors completed the conversion and testing of the fast SPGR-based arterial spin tagging pulse sequence, from the Genesis 5.4 platform to the LX 8.2.5 platform.

Development of an EPI-Based Arterial Spin Tagging Sequence

In October 1999, the authors formulated an alternative approach to eliminate the requirement of polarity alternation, which was successfully implemented. The following steps are performed at each interleaf: (1) non-selective RF inversion pulse, (2) 20 EPI acquisitions, each of which is preceded by a 10^0 RF pulse (Figure 2). These 20 acquisitions are played out with a repetition time (*optr* in Figure 2) of 100 ms. Each acquisition defines one point on a T_1 recovery curve. The total time for each interleaf (*TR* in Figure 5.10) is 2 seconds. Data for the other interleaves is collected in the same fashion in subsequent TR intervals (see Dissertation). The completed set of images, showing T1 recovery of the magnetization, is acquired in two seconds times the number of interleaves.

From 1999 Annual Report ...

Summary

Since the completion of the upgrade of the UC Davis Imaging Center MRI system, and since it's designation as the Research MRI system for UC Davis, we have thoroughly studied the EPIC LX 8.2.5 programming language for pulse sequence development, and the operation of this new MRI system. The transition to the new research MRI required a complete rewrite of all pulse sequence software that we had developed for this project. In addition, we revised the pulse sequences to utilize the high performance gradients (40 mT/m peak, 150 mT/m/ms rise) of the system. We believe these revised sequences will provide better arterial spin tagged data for perfusion measurement. All of the other sequences in our breast imaging protocol were set up for the new LX 8.2.5 platform as well.

Conversion of the Fast SPGR Based Arterial Spin Tagging Sequence

The authors converted the fast SPGR-based arterial spin tagging pulse sequence from the Genesis 5.4 platform to the LX 8.2.5 platform. The converted sequence was also improved to achieve higher resolution with a shorter overall scan time. The new MR system has higher peak gradient amplitude and slew rate. Fast data acquisition, which requires the higher read-out gradient amplitude (4.0 g/cm) could be specified, and consequently the data acquisition period (optr) was shorten from 16.62 ms to 12.5 ms. Since optr was shortened, a larger matrix in the phase encode direction could be specified. The resolution is now 256 × 256 matrix using a one-half phase field of view acquisition. Previously we used a 256 × 240 matrix with one-half phase field of view acquisition. The total time for the image acquisition (the TR period), including the global inversion RF pulse, has been decreased from 2.7 seconds to 2.22 seconds. The performance of this new sequence has been confirmed using phantoms and one test subject.

Development of an EPI-Based Arterial Spin Tagging Sequence

The EPI-based arterial spin tagging sequence was rewritten and verified on the research MRI system. The data acquisition scheme is based on our recently published high-resolution odd-number interleaf EPI sequence [Buonocore MH, Zhu DC. High spatial resolution EPI using an odd number of interleaves. Magnetic Resonance in Medicine 41 (6): 1199-1205 (1999)]. This sequence was first developed and verified on the Signa Advantage 1.5 T GE MR system. Unfortunately, under the new LX system, the polarity alternation scheme for each successive interleaf we had implemented caused the system to hang, and substantial time was expended understanding the problem.

From 1998 Annual Report ...

An interleaved arterial spin-tagging technique, that allows high resolution (e.g. 256 × 256 or more) has been implemented and tested. We also implemented a rectangular data acquisition technique, which acquires data sets that have different numbers of points along the frequency and phase encode direction. The 256 × 240 interleaved acquisition provides the best spatial versus temporal resolution tradeoff, and has been used for all of our recent studies.

7

Task 3: *Months 1-9: Analysis of spin tagging sequence to understand causes of existing baseline offsets, effects of inversion slice transition profiles, and effects of RF flip angle profile on the measurements, with implementation and testing pulse sequence modifications to minimize these imperfections.*

Report for 2000

The EPI arterial spin tagging sequence was not formally evaluated.

From 1999 Annual Report ...

Regarding the spin tagging sequence utilizing fast SPGR, these issues were treated in the 1998 report. The EPI arterial spin tagging sequence has not been evaluated, but the same solutions for the inversion slice transition profiles, and effects of RF flip angle profile, will apply.

From 1998 Annual Report ...

Matching of inversion and excitation slice profiles was greatly improved by using customized RF pulses designed with the Shinnar-Le Roux (SLR) algorithm. The new data processing technique (based on a semi-log linear regression of inversion time (TI) dependent signal) significantly reduced the previously reported problem in measuring the longitudinal relaxation time (T1) caused by baseline offsets, and by the uncertainty in the effective inversion time. The optimal RF flip angle for spin excitation during spatial encoding was found to be 10 degrees, based on experiments over a range of flip angles.

Technical objective 2

Task 4: *Months 3-15: Software for automatic estimation and error analysis of perfusion, tissue water longitudinal relaxation time, and extracellular fluid volume fraction from mathematical models and user-defined ROIs from spin tagging timeseries. Implementation of pharmacokinetic model calculations and error analysis for first-pass contrast enhanced imaging.*

Report for 2000

No new software was developed.

From 1999 Annual Report ...

From October 1998 through April 1999 (during which time there was no MRI system for us to develop on, or do patient studies), image processing software development continued. Improvements in the BreastView program, development of "dispAlls" program for analysis of general MRI images, and implementation of statistical analysis of breast lesions based on Bayesian approach, was completed. Statistical analysis of available breast lesion data continued (See below). The most important new function of BreastView is that for analysis of the first-pass contrast enhanced images. The program creates an image based upon the time derivative of the rate of rise of the signal, so that the contrast enhancement effect can be better visualized (See Figures 4 and 5).

From 1998 Annual Report ...

A software program (BrView) has been written in C, X Window System, and Motif, and implemented on an SGI O2 computer (paid for by grant funds) for analyzing and visualizing the MR images and timeseries. Much effort has been expended on developing the capability to easily review all of the images taken in each study, and cross-reference pixel locations. Much more effort than anticipated was required for development of a robust technique for identifying so-called "suspicious regions"

based on the T1 and perfusion measurements. The measurement of T1, upon which the perfusion measurement entirely depends, is based on a semi-log linear regression technique developed by the investigators. The T1, perfusion (f/λ) and standard errors of these quantities are estimated automatically using this robust technique. The so-called feature images display these quantities in color and grayscale. These quantities are used to calculate a "suspicion index" for each pixel, and thereby identify regions of breast tissue suspicious for malignancy.

The implementation of the pharmacokinetic model calculations and error analysis for first-pass contrast enhanced imaging has not been completed. Thus far, the software allows the user to click on the reference image of the dynamic study, to display the time profile of the signal at that pixel. The implementation of the pharmacokinetic model is currently a major focus of the current effort.

> Task 5: *Months 3-15: Software for registration (including implementation and testing of motion correction and physiological noise reduction algorithms) and overlay of images from high resolution* T*₁ weighted, spin tagging, and contrast enhanced studies.*

Report for 2000

BreastView

BreastView now performs a simple analysis of first-pass contrast enhanced images. The program creates a contrast enhancement-weighted image based upon the maximum time derivative of the rate of rise of the signal, so that the contrast effect can be better visualized.

The dispAlls program

There were no further enhancements of this program.

From the 1999 Annual Report ...

First described in the 1998 Annual Report, the BreastView program has been continually upgraded and enhanced with the latest algorithms for processing and analysis of breast imaging studies, including those for spin-tagged and dynamic contrast enhanced images. The specific developments this year of BreastView, and of another program, dispAlls, are described.

BreastView

Between October 1998 and April 1999, the BreastView program was made "clinician-friendly". The graphical user interface now guides the user through the entire visualization and analysis process for a breast imaging study. A "Help" button, linked to extensive set of manual pages, now appears on the first page of the interface. Clicking the Help button brings up an html file with necessary operating instructions. The help files were written for clinicians. The clinician can now begin using the program without first studying the written instructions. If an inappropriate option is selected, the program now provides help to the user to select a more appropriate option or operation. Several new features and functions have been implemented. The most important new function of BreastView is the analysis of the first-pass contrast enhanced images. The program creates a contrast enhancement-weighted image based upon the time derivative of the rate of rise of the signal, so that the contrast effect can be better visualized.

The dispAlls program

This program has been written for quickly viewing and performing ROI analysis on one or a series of images. The program is particularly useful for quickly reviewing the timeseries of signal changes in an ROI from the dynamic contrast enhanced studies. The program displays one image, or a sequence of images, with or without an image header. It performs ROI analysis and plots the calculated values.

Using the BrView software program, image pixels containing high values of perfusion (f/λ), and moderate to high values of T_1, and low standard errors, are identified as suspicious, and assigned a "suspicion index" based on finding similar abnormal values at spatially adjacent pixels. Suspicious pixels can be overlaid on the high-resolution T_1 and T_2 clinical images by color mapping, and simultaneously presented with the first-pass contrast enhanced timeseries at these pixels. This provides the user with a comprehensive anatomical and functional view of the suspicious regions, and facilitates making a decision regarding the malignant nature of the lesion. Finally, a motion artifact estimation and correction algorithm has been developed and implemented in a separate software program.

Technical objective 3

Task 6: *Months 9-24: 60 patients with malignant and benign breast lesions will be imaged using T₁ weighted, first-pass contrast enhanced, and arterial spin tagging MRI pulse sequences.*

Report for 2000

No additional subjects have been done.

From the 1999 Annual Report ...

Unfortunately, no additional subjects have been done. This is due to the loss of Rebecca Zulim, MD, as the co-investigator, and the transition to a dedicated research MRI system that operated at LX 8.2.5, as described above. Through Sept 1998, eighteen subjects, including 11 patients referred by their physicians and seven self-referred volunteers, had participated in the breast studies. Three patients and two volunteers were eliminated from the analysis because the studies were not done according to protocol, due to excess motion, or the abnormal mass being too close to the chest wall to be measured reliably, or no patient biopsy to confirm the MR study result. There are total of 13 useful cases left for analysis. For all these cases, the suspicious pixels were identified based on the following criteria: T1n: > 0.5 sec f/□□.> 0.1 sec-1, STD of f/□: < 0.1 sec-1, and the suspicion level threshold was set at 20.2%. Analysis has been done using the program BreastView. Table 8.5 shows the result of these 13 cases.

From 1998 Annual Report ...

We have thus far recruited two subject studies for both first-pass contrast enhanced and arterial spin tagging MRI pulse sequences. Now that the software development is substantially completed, we are trying to improve the rate at which patients are recruited into the study. It is likely that the patient studies will extend into the third year of the proposal. We are currently discussing with physicians at a local Kaiser Hospital for recruitment of additional patients. Appropriate documentation will be submitted for approvals upon reaching a firm agreement.

Task 7 (listed as Task 6 in the original grant application): Months 12-36: Automated pharmacokinetic analysis, blinded image reading, and statistical comparison of arterial spin tagging, contrast enhanced MRI, and biopsy results.

Report for 2000

No new software was developed.

We developed an analysis program for the detection of the features of the dynamic contrast enhanced study, and have developed a statistical approach to the determination of the malignant status of the lesion.

Bayesian Statistical Analysis

The identification of a suspicious pixel based upon the index threshold, that was developed last year, is a simple approach to cancer detection. When a large number of studies become available, a Bayesian decision technique [53] will be applied. This technique will be used to provide ROC (receiver operating characteristic) curves that are commonly used for evaluation of diagnostic algorithms. To summarize the Bayesian technique, let vector space x = (T1, f/λ, STD of f/λ, etc.) for a ROI (region of interest) in a breast.

Automated pharmacokinetic analysis, blinded image reading, and statistical comparisons, have not been started.

Key Research Accomplishments

Report for 2000

A. EPI-based arterial spin tagging sequence, with MT pulse option, for Signa Horizon LX CV/i system.

From the 1999 Annual Report ...

A. Pulse sequences that are compatible with a Signa Horizon LX EchoSpeed CV/i system, running LX 8.2.5 system software:

    1. Fast SPGR-based arterial spin tagging sequence

    2. Odd-number interleaved EPI sequence

    3. Interleaved EPI-based arterial spin tagging sequence

B. Imaging processing software

    1. BreastView

    2. DispAlls

    3. Bayesian analysis of arterial spin tagged image data

From the 1998 Annual Report ...

A. Fast SPGR-based arterial spin tagging sequence for Signa Advantage MRI system, running 5.7 system software:

B. Imaging processing software (BrView)

Reportable Outcomes

Report for 2000

A. Buonocore MH, Zhu DC. Magnetic resonance arterial spin tagging for non-invasive pharmacokinetic analysis of breast cancer. Poster Presentation and Abstract. Proceedings of the Era of Hope, Dept. of Defense Breast Cancer Research Program Meeting, June 8-11, 2000, Hilton Atlanta and Towers, Atlanta, GA, Vol. 1, page 177.

B. Buonocore MH, Zhu DC, Zulim RA. Magnetic resonance arterial spin tagging for non-invasive pharmacokinetic analysis of breast cancer. Poster Presentation and Abstract. Proceedings of the UC Davis Cancer Center Symposium, Oct 6-7, 2000. UC Davis Cancer Center, Sacramento, CA.

C. David Zhu. PhD Dissertation. Magnetic resonance pulse sequences and analytical techniques for breast cancer detection and cardiovascular flow. UC Davis, Biomedical Engineering. Dec 1999.

D. David Zhu. PhD in Biomedical Engineering, Dec 1999.

E. David Zhu, PhD. Employment as GE Applications Engineer, beginning Jan 2000.

From the 1999 Annual Report ...

A. Buonocore MH, Zhu DC. High spatial resolution EPI using an odd number of interleaves. Magnetic Resonance in Medicine 41 (6): 1199-1205 (1999).

B. Buonocore MH, Zhu DC, Zulim RA. Analysis software for breast imaging studies. Proceedings of the International Society for Magnetic Resonance in Medicine, 7th Annual Meeting and Exhibition, 3: 2172 (1999).

C. Pulse sequences for Version 8.2.5 (MH Buonocore and D Zhu):

Arterial spin tagging sequence with Fast SPGR Acquisition

Odd-number interleaf EPI

Arterial spin tagging sequence with Odd-number interleaf EPI acquisition

Arterial Spin Tagging sequence with Even-number hybrid EPI acquisition

D. Breast Imaging Protocols (MH Buonocore and D Zhu)

Anatomical, spin tagged, and dynamic c-e breast imaging protocol

E. SGI Graphics Software for Breast image analysis (MH Buonocore and D Zhu):

BreastView (display program for breast imaging protocol)

DispAll (display program for general MRI images)

From the 1998 Annual Report ...

A. Buonocore MH, Zhu DC. Odd-number hybrid EPI. Proceeding of the International Society for Magnetic Resonance in Medicine, 6th Annual Meeting and Exhibition, on CD-ROM, p. 1967 (1998).

B. Buonocore MH, Zhu D, Pellot-Barakat C. Measurement of breast tissue perfusion using arterial spin tagging, Proceedings of the International Society for Magnetic Resonance in Medicine 5th Annual Meeting and Exhibition, 1: 311 (1997).

C. Buonocore MH, Zhu DC, Pellot-Barakat C, Zulim RA. Noninvasive measurement of blood flow through breast tumors. Book of Abstracts, California Breast Cancer Research Symposium. Sacramento Convention Center, Sacramento CA, Sept. 16, 1997.

D. Buonocore MH, Zhu DL, Pellot-Barakat C., Zulim RA. Non-invasive measurement of breast tissue perfusion using arterial spin tagging. Radiology, November 1997, 205 (P): 162.

E. Sequence and Protocols for arterial spin tagging for Version 5.7 Signa Advantage MRI

F. Software for display and analysis of breast images, written in C, X and Motif.

Conclusions

<u>Report for 2000</u>

Technical accomplishments over the past three years have been documented in a PhD Dissertation, a CD ROM of research software, and poster presentations. These will be used to accomplish the third Specific Aim of the project, to non-invasively measure perfusion parameters in breast masses prior to biopsy. These measurements may distinguish malignant from benign breast lesions.

<u>From the 1999 Annual Report ...</u>

We have successfully converted and enhanced the arterial spin tagging pulse sequences to work on a new research MRI system, and have made several enhancements. Understanding of the 8.2.5 pulse sequence language on the new system represents a major advance of the project. These pulse sequences will be used in all future work, and hopefully there will not be a substantial MRI system upgrade such as we experienced for a few years at least. Image display and statistical analysis software has been written for the spin tagging and contrast enhanced studies, and to allow analysis to be done by a busy clinician without computer expertise.

<u>From the 1998 Annual Report ...</u>

In this year of the project, we have developed the necessary pulse sequences for anatomical and functional imaging of breast tissue, and the necessary software for the analysis, display and interpretation of this data. These developments will allow us to evaluate complete breast imaging studies that are composed of anatomical scans, dynamic first pass contrast enhanced scans, and arterial spin tagging scans. The integrated nature of the software allows easy and consistent interpretation of both spatial dependencies as well as temporal dependencies of signal changes indicative of disease. The in-vitro and in-vivo studies done thus far indicate that first and foremost, arterial spin tagging is a sensitive and reliable method for measuring T1 and parameters related to tissue perfusion. Second, they indicate that arterial spin tagging is a viable alternative to dynamic first-pass contrast-enhanced imaging. The fact that arterial spin tagging can be easily added to any standard breast imaging protocol, without requiring special nursing or MR technologist expertise, means that it is especially attractive for routine clinical use. It could be used to supplement contrast-enhanced studies in the initial study of the patient, and used exclusively in follow-up studies. Since 10/1/98, six subjects have been studied without the dynamic first-pass contrast-enhanced scan, and two have been studied with this scan. Comparison of contrast-enhanced images versus arterial spin-tagged images has not yet been made. In particular, no statistical comparison of the dynamic study results (considered to be the gold standard for non-invasive assessment of malignant disease) with the arterial spin tagging results has been performed. However, there is considerable spatial overlap of suspicious regions obtained by these methods noted on visual inspection. Collecting data on human subjects, and statistical confirmation of this agreement, will be major focuses of next year's work.

References

<u>Report for 2000</u>

1. Buonocore MH, Zhu DC. Magnetic resonance arterial spin tagging for non-invasive pharmacokinetic analysis of breast cancer. Proceedings of the Era of Hope, Dept. of Defense Breast Cancer Research Program Meeting, Vol. 1, page 177 (2000).
2. Buonocore MH, Zhu DC, Zulim RA. Magnetic resonance arterial spin tagging for non-invasive pharmacokinetic analysis of breast cancer. Proceedings of the 6th Annual UC Davis Cancer Center Symposium, Oct 6-7, 2000.

From the 1999 Annual Report ...

3. Buonocore MH, Zhu DC. High spatial resolution EPI using an odd number of interleaves. Magnetic Resonance in Medicine 41 (6): 1199-1205 (1999).

4. Buonocore MH, Zhu DC, Zulim RA. Analysis software for breast imaging studies. Proceedings of the International Society for Magnetic Resonance in Medicine, 7th Annual Meeting and Exhibition, 3: 2172 (1999).

From the 1998 Annual Report ...

5. Buonocore MH, Zhu DC. Odd-number hybrid EPI. Proceeding of the International Society for Magnetic Resonance in Medicine, 6th Annual Meeting and Exhibition, on CD-ROM, p. 1967 (1998).

6. Buonocore MH, Zhu D, Pellot-Barakat C. Measurement of breast tissue perfusion using arterial spin tagging, Proceedings of the International Society for Magnetic Resonance in Medicine 5th Annual Meeting and Exhibition, 1: 311 (1997).

7. Buonocore MH, Zhu DL, Pellot-Barakat C., Zulim RA. Non-invasive measurement of breast tissue perfusion using arterial spin tagging. Radiology, November 1997, 205 (P): 162.

Appendices

Poster presentations (References 1. and 2. above, 11% of full size) (Pages 15-16, respectively)

PhD Dissertation (Title, Prefaces, Part I, Appendices A-D,F,G), David Zhu. (Pages 17-179)

E-3

MAGNETIC RESONANCE ARTERIAL SPIN TAGGING FOR NONINVASIVE PHARMACOKINETIC ANALYSIS OF BREAST CANCER

Michael H. Buonocore, David C. Zhu

University of California Davis Imaging Center, Sacramento, CA 95817

Abstract

This project is designed to develop and evaluate arterial spin tagging techniques for the noninvasive measurement of breast tissue perfusion. The long term goal is to show that arterial spin tagging can provide comparable tissue information to that obtained using dynamic first-pass contrast-enhanced imaging. Effort has focused on the pulse sequence, protocol and image processing software needed for analysis and visualization of the anatomic, functional, and dynamic breast images. Specific tasks and analyses of the sequence have been performed to understand and correct for driven equilibrium effects, and for inversion and excitation slice profile mismatch. Software development includes methods for estimating, at each point, the T1, the perfusion (as defined by f/λ and standard errors, and from these comprise a "suspicion index" that the tissue is abnormal. Algorithms for image registration and image display have been developed to allow direct comparison of high resolution T1, first spin echo T2 and proton density, perfusion, and contrast enhanced images. The research effort provides critical software for detailed and definitive review of the images, and automation for detailed and thorough statistical analysis of the very large data sets that are obtained.

Summary and poster guide

Tissue perfusion parameters are measured without the use of intravenous contrast, by measuring the change in MR signal which varies as a function of blood flow into the tissue (Fig. 1). The arterial spin tagging pulse sequences uses an inversion pulse and time delay to vary the amount of signal change due to flow (Fig. 2). Differences between normal tissue and abnormal tissue are significant (Table 1), as seen on plots of T1 and the apparent perfusion/f/λ (Fig. 3). Specialized software was written to allow rapid display, analysis and identification of breast regions that are suspicious for malignancy (Fig. 4a). Positive regions on contrast enhanced scans are also identified and compared with those obtained by spin tagging (Fig. 4b). So far, eleven patients and seven volunteers have participated. Three patient and two volunteer studies were eliminated due to technical factors. Thirteen cases were analyzed (Table 2).

Table 1: Selected cases using arterial spin tagging

Case 1: Palpable mass. Study date: Aug 6. Level of suspicion based on T_{1n} and perfusion: High. Clinical MR images: Negative (mass not clearly visualized, prior cyst visualized). Result based on spin tagging: Positive for malignancy. Biopsy: Positive for malignancy (spin tagging CONSISTENT with biopsy). Perfusion, T1 data shown in Fig. 3.

Case 2: Palpable mass. Study date: Aug 7. Level of suspicion based on T_{1n} and perfusion: High. Clinical MR images: Positive (lesion visualized). Assessment based on spin tagging: Positive for malignancy. Assessment based on dynamic contrast-enhanced study: Positive for malignancy. Biopsy: Negative for malignancy (spin tagging INCONSISTENT with biopsy). Images shown in Fig. 4.

Table 2: Summary of Breast Case Studies

Study	Palpable?	On MRI?	Suspicion	Assessment	Mass Type
05/03	No	Yes	Low	Negative	Benign
05/23	Yes	Indeter	Mod/High	Positive	Benign Fibroid
08/01	No	No	High	Positive	Malig. Ductal Ca
11/15	Yes	No	High	Positive	Malig. Ductal Ca
12/10	Yes	No	High	Benign	Benign
04/13	Yes	Indeter	Mod/High	Positive	Benign
07/27	Yes	No	Low	Positive	Benign
02/07	Yes	No	High	Negative	Benign
03/05	Yes	No	Low	Negative	Benign Fibroid
07/26	Yes	No	Low	Negative	Normal
11/16	Yes	No	Low	Negative	Benign Fibroid
12/14	No	No	Low	Negative	Normal

Suspicion level based on T_{1n} and /λ. Assessment based on level of suspicion. Mass type based on biopsy or reliable history. There are two one positive (TP), zero false negative (FN), three false positive (FP) and eight true negative (TN). Sensitivity is 100%, calculated as TP/ (TP+FN). Specificity is 72.7%, calculated as TN/ (FP+TN).

Figure 1. Spin tagging concept. MR signal from imaged slice is affected by the blood flow into the slice. When the non-selective inversion pulse is on, the blood flow does not change the total signal from the imaged slice. When the non-selective inversion pulse is off, the blood flow increases the total signal in the imaged slice. High flow in cancerous tissue show large change in signal when the non-selective pulse is turned on and off.
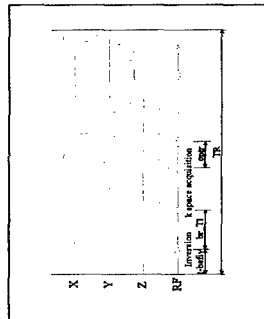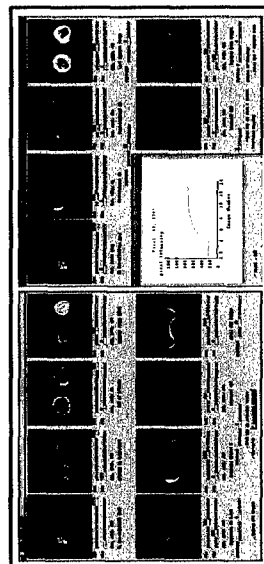

Figure 2. Spin-tagging pulse sequence. In each TR interval (2.7 s), an RF inversion pulse is applied first, followed by all phase encoding steps necessary to create one image. The inversion pulse inverts the magnetization in a non-selective or selective region. Ie, TI is the time interval that blood from outside the imaged slice flows into the imaged slice, thus affecting MR signal in proportion to the amount of flow. (see Fig. 1).
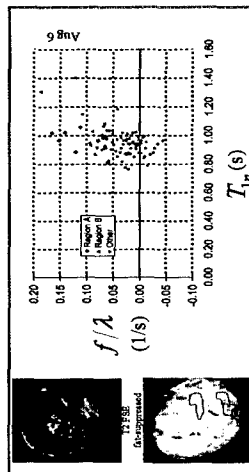

Figure 3. Graphical display of tissue parameters derived from arterial spin tagging. Aug 6 study (Case 1). Top Left: T2 fast spin echo (FSE) image done to show the palpable mass. Bottom left: "Spin tagging" image is a T1-weighted, and red pixels are those exceeding suspicion index threshold (likely to have high flow). A and B denote regions enclosed by the red lines. Right: Graph shows computed T1 and perfusion parameter /λ for tissues within regions A and B, and normal tissue outside of A and B. Note separation of pixels in Region A and B (A, B) from other pixels outside these regions, due to /λ.

Figure 4a: Display of diagnostic images. Aug 7 study (Case 2). Across, then down from top left: Computed T1 values, computed perfusion parameter, /λ, computed standard deviation of T1 values, pro-computed standard deviation of /λ. A accuracy). T1 weighted, suspicion index map, proton density with pixels exceeding high suspicion index threshold colored red. T1 weighted with near pixels colored red. T1 weighted axial. Suspicion index, and red pixels are derived from spin tagging sequence.

Figure 4b: Display of dynamic contrast-enhanced images. Aug 7 study (Case 2). Across, then down from top left: Computed T1 values, pre-contrast 3D T1 weighted, post-contrast 3D T1 weighted, last image of T1 weighted dynamic timeseries, plot of signal intensity versus time, showing increasing intensity in the suspicious region, computed dynamic rise image (max rate of change during contrast passage).

Conclusions

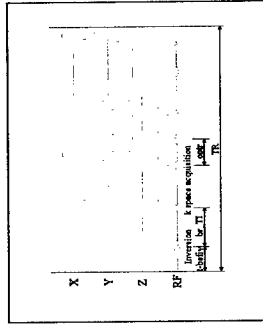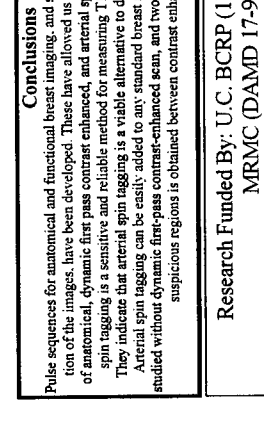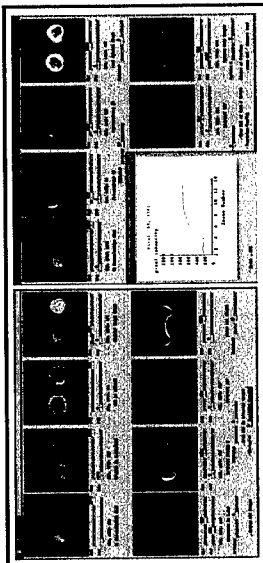Pulse sequences for anatomical and functional breast imaging, display and interpretation of the images, have been developed. These have allowed us to evaluate breast imaging studies composed of anatomical, dynamic first pass contrast enhanced, and arterial spin tagging scans. Studies indicate that arterial spin tagging is a sensitive and reliable method for measuring T1 and parameters related to tissue perfusion. They indicate that arterial spin tagging is a viable alternative to dynamic first-pass contrast-enhanced imaging. Arterial spin tagging can be easily added to any standard breast imaging protocol. Eleven subjects have been studied without dynamic first-pass contrast-enhanced scan, and two have been studied with this scan. Agreement of suspicious regions is obtained between contrast enhanced and spin tagging methods.

15

MAGNETIC RESONANCE ARTERIAL SPIN TAGGING FOR NONINVASIVE PHARMACOKINETIC ANALYSIS OF BREAST CANCER

[1]Michael H. Buonocore, [1]David C. Zhu, [2]Rebecca A. Zulim

University of California Davis Imaging Center[1] and Cancer Center[2], Sacramento, CA 95817

Abstract

This project is designed to develop and evaluate arterial spin tagging techniques for the noninvasive measurement of breast tissue perfusion. The long-term goal is to show that arterial spin tagging can provide comparable tissue information to that obtained using dynamic first-pass contrast-enhanced imaging. Effort has focused on the pulse sequence, protocol and image processing software needed for analysis and visualization of the anatomic, functional, and dynamic breast images. Specific tests and analyses of the sequence have been performed to understand and correct for driven equilibrium effects, and for structural and excitation slice profile statistical. Software development includes methods for estimating, at each pixel, the T1, the perfusion (as defined by f/λ, and standard errors, and from these compute a "suspicion index" that the tissue is abnormal. Algorithms for image registration and image display have been developed to allow direct comparison of high resolution T1, fast spin echo T2 and proton density, perfusion, and contrast enhanced images. The research effort provides crucial software for acquisition and definitive review of the images, and automation for detailed and thorough statistical analysis of the very large data sets that are obtained.

Summary and poster guide

Tissue perfusion parameters are measured without the use of intravenous contrast, by measuring the change in MR signal which varies as a function of blood flow into the tissue (Fig. 1). The arterial spin tagging pulse sequences uses an inversion pulse and time delay to vary the amount of signal change due to flow (Fig. 2). Differences between normal tissue and abnormal tissue are significant (Table 1), as seen on plots of T1 and the apparent perfusion f/λ (Fig. 3). Specialized software was written to allow rapid display, analysis and identification of breast regions that are suspicious for malignancy (Fig. 4a). Positive regions on contrast enhanced scans are also identified and compared with those obtained by spin tagging (Fig. 4b). So far, eleven patients and seven volunteers have participated. Three patient and two volunteer studies were eliminated for technical factors. Thirteen cases were analyzed (Table 2).

Table 1: Selected cases using arterial spin tagging

Case 1: Palpable mass. Study date: Aug 6. Level of suspicion based on T_{1n} and perfusion: High. Clinical MR images: Negative (mass not clearly visualized, prior cyst visualized). Result based on spin tagging: Positive for malignancy (spin tagging) CONSISTENT (with biopsy). Perfusion, T1 data shown in Fig. 3.

Case 2: Palpable mass. Study date: Aug 7. Level of suspicion based on T_{1n} and perfusion: High. Clinical MR images: Positive (lesion visualized). Assessment based on spin tagging: Positive for malignancy. Assessment based on dynamic contrast-enhanced study: Positive for malignancy. Biopsy: Negative for malignancy (spin tagging INCONSISTENT with biopsy). Images shown in Fig. 4.

Table 2: Summary of Breast Case Studies

Study	Palpable?	On MRI?	Suspicion	Assessment	Mass Type
05/05	No	Yes	Low	Negative	Benign Fibroid
05/23	Yes	Intermed.	Mod/High	Positive	Malig. Ductal Ca.
08/01	Yes	No	High	Positive	Malig. Ductal Ca.
11/15	Yes	No	Low	Negative	Benign
12/10	Yes	Intermed.	High	Positive	Benign
04/13	Yes	No	Low	Negative	Benign
07/27	No	No	Low	Negative	Benign
08/07	Yes	No	High	Positive	Benign
02/07	No	No	Low	Negative	Normal
05/05	No	No	Low	Negative	Benign Fibroid
07/28	Yes	No	Low	Negative	Normal
11/16	Yes	No	Low	Negative	Benign Fibroid
12/14	No	No	Low	Negative	Normal

Suspicion level based on T_{1n} and f/λ. Assessment based on level of suspicion. Mass type based on biopsy or reliable history. There are two true positives (TP), zero false negatives (FN), three false positives (FP) and eight true negatives (TN). Sensitivity is 100%, calculated by TP/(TP+FN). Specificity is 72.7%, calculated as 1-FP/(FP+TN).

Figure 1: Spin tagging concept. MR signal from imaged slice is affected by the blood flow into the slice. When the non-selective inversion pulse is on, the blood flow does not change the total signal from the imaged slice. When the non-selective inversion pulse is off, the blood flow increases the total signal in the imaged slice. High flow found is cancerous tissue show large changes in signal when the non-selective pulse is turned on and off.

Figure 2: Spin-tagging pulse sequence. In each TR interval (2.7 s), an RF inversion pulse is applied first, followed by all phase encoding steps necessary to create one image. The inversion pulse inverts the magnetization in a non-selective or selective region. b_r T1 is the time interval that blood from outside the imaged slice flows into the imaged slice, thus affecting MR signal in proportion to the amount of flow. (see Fig. 1).

Figure 3: Graphical display of tissue parameters derived from arterial spin tagging. Aug 6 study (Case 1). Top left: T2 fast spin echo (FSE) image does not show the palpable mass. Bottom left: "Spin tagging" image is a T1 weighted, and red pixels are those exceeding suspicion index threshold (likely to have high flow). A and B denote regions rendered by the red lines. Right: Graph shows computed T1 and perfusion parameter f/λ for tissue within regions A and B, and normal tissue outside of A and B. Note separation of pixels in Region A and B, from other pixels outside those regions, due to f/λ.

Figure 4a: Display of diagnostic images. Aug 7 study (Case 2). Across, then down from top left: Computed T1 value, computed perfusion parameter f/λ, computed standard deviation of f/λ (given f/λ accuracy), T1 weighted, suspicion index map, proton density with pixels exceeding high suspicion index threshold colored red, T2 weighted with same pixels colored red. T1 weighted scan. Suspicion index, and red pixels, are derived from spin tagging sequence.

Figure 4b: Display of dynamic contrast-enhanced images. Aug 7 study (Case 2). Across, then down from top left: Computed T1 value, precontrast 3D T1 weighted, post-contrast 3D T1 weighted, last image of T1 weighted dynamic timeseries, plot of signal intensity versus time, showing increasing intensity in the suspicious region, computed dynamic rise image (max rate of change during contrast passage).

Conclusions

Pulse sequences for anatomical and functional breast imaging, and software for the analysis, display and interpretation of the images, have been developed. These have allowed us to evaluate breast imaging studies composed of anatomical, dynamic first pass contrast enhanced, and arterial spin tagging scans. Studies indicate that arterial spin tagging is a sensitive and reliable method for measuring T1 and parameters related to tissue perfusion. They indicate that arterial spin tagging is a viable alternative to dynamic first-pass contrast-enhanced imaging.

Arterial spin tagging can be easily added to any standard breast imaging protocol. Eleven subjects have been studied without dynamic first-pass contrast-enhanced scan, and two have been studied with this scan. Agreement of suspicious regions is obtained between contrast enhanced and spin tagging methods.

Magnetic Resonance Pulse Sequences and Analytical Techniques for Breast Cancer Detection and Cardiovascular Flow

By

David Chao Dong Zhu

B.A. Molecular & Cell Biology, University of California, Berkeley, 1992
B.S. Electrical & Electronic Engineering, California State University, Sacramento, 1996
M.S. Biomedical Engineering, California State University, Sacramento, 1996

DISSERTATION

Submitted in partial satisfaction of the requirements for the degree of

DOCTOR OF PHILOSOPHY

in

Biomedical Engineering

in the
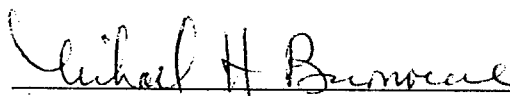
OFFICE OF GRADUATE STUDIES
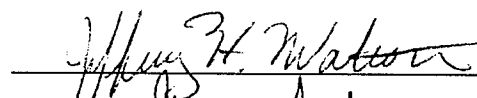
of the

UNIVERSITY OF CALIFORNIA

DAVIS

Approved:

Michael H Buonocore

Jeffrey H Walton

Gary S. Ford

Committee in Charge

1999

NoTE 03/31/01

This Appendix material includes only that part of the Dissertation which is relevant to the MRBCRP project.

Abstract

This dissertation involves the development of magnetic resonance pulse sequences and analytical techniques for two projects: breast cancer detection and cardiovascular flow study.

In the first project, arterial spin tagging techniques and analytical methods are developed and implemented to measure spin-lattice relaxation time T_1, relative blood perfusion, and magnetization transfer in breast tissue. Studies have shown that water content in malignant tumors is higher than in normal tissues. Studies have also shown that perfusion in malignant tumors is higher than in both normal tissues and benign lesions. Compared to the current widely used dynamic contrast enhancement techniques for breast cancer detection, the arterial spin tagging techniques may provide more sensitive and specific assessment of tissue parameters at higher spatial resolutions by virtue of their ability to improve signal to noise ratio (SNR) over reasonable scan times.

For the second project, a three-dimensional (3D) cine phase contrast pulse sequence (also called a 4D sequence in this dissertation) is developed and implemented. The sequence development is based on a two-dimensional (2D) cine phase contrast technique and a 3D non-cine phase contrast technique that have been developed and used in clinical studies. In the 2D technique, a sequence of images is acquired to capture the motion of blood flow throughout a cardiac cycle, but they are limited to one thin slice of the body. Images must be acquired at multiple slice

locations in order to show the volume change of flow patterns. The 3D technique

allows the acquisition of a slab of images, but does not provide the dynamic

information of cardiac flow. The 4D technique offers the convenience of volume

imaging of the 3D technique, and the dynamic cardiac flow information of the 2D

technique. The flow patterns based on the processed images can be used to assess the

cardiac condition of the subject.

Dedication

to

my father Mr. Guang Fu Zhu, whose early teaching and guiding have always inspired

me, and to my mother, my wife Leanna and my brothers.

Acknowledgments

First and foremost, I would like to thank my advisor Professor Michael Buonocore, who has worked closely with me during the development of this dissertation. His dedication to MR technology and his creativity have always inspired me. It is he who has guided me through the fascinating world of magnetic resonance imaging.

I want to thank Professor Gary Ford and Dr. Jeff Walton, who have provided helpful inputs to my dissertation. They have taken the time to serve on both my qualifying exam committee and dissertation committee. I also want to thank Dr. Claire Barakat, who worked with me on image processing techniques during the development of the breast cancer research project at its early stage.

The breast cancer research project in this dissertation has been supported by a grant from University of California Breast Cancer Research Program (Grant number: 1IB-0156), and a grant from US Army Breast Cancer Research Program (Grant numbers: BC961359 and DAMD17-97-1-7030).

It has been a great pleasure to study in the Biomedical Engineering Graduate Program at University of California Davis. I would like to thank the faculty in this program as well as in the Electrical and Computer Engineering Department and the Chemistry Department. I especially want to thank the faculty and staff in the

Department of Radiology. They have provided me with the necessary office space,

research support and a friendly working environment for my studies.

Table of Contents

Part I. Arterial Spin Tagging Techniques

for Breast Cancer Detection

Chapter

Pg. 25

List of Figures

List of Tables

Part I

Arterial Spin Tagging Techniques

for Breast Cancer Detection

Chapter 3

Introduction

Breast cancer is the leading cause of death from cancer among women in the western world. In the U.S., it accounts for approximately 26% of all cancer cases and 18% of all cancer deaths in women. Early detection and treatment have played important roles in improving the chance of survival in women with breast cancer [18,19,20]. However, early detection of cancer has not been easy, which is often misled by far more frequent incidences of benign disorders. The ratio of benign to malignant lesions is greater than 25:1 [18]. Few benign disorders are life-threatening. X-ray mammography is currently used as the primary screening tool for breast cancer. If suspicion regions were found with X-ray mammography, a patient would be sent to the pathology department for a biopsy, which serves as the final measurement of the malignancy of the suspicious regions. Although it is crucial to detect all the malignant cases, biopsies are expensive and invasive. It is economical and desirable to reduce the number of benign cases sent for biopsy. The sensitivity of X-ray mammography is greater than 90%. But the percentage of suspicious X-ray findings proven to be cancerous (the predictive value of X-ray) is only 10-54% [18]. Despite its low predictive value as well as the discomfort of breast compression and potential

radiation damage, X-ray mammography is convenient and economical. The cost of X-ray mammography is about $55 as compared to about $150 for breast ultrasound, $150 for fine-needle aspiration of palpable masses, and $850 for core biopsy of occult lesions [21]. Thus, X-ray mammography will continue to serve as an important role in breast screening.

Due to the drawbacks of X-ray mammography, researchers have studied other imaging modalities, such as ultrasonography, thermography, computed tomography (CT) and magnetic resonance imaging (MRI) [18, 22, 23]. Ultrasonography is an important complementary breast imaging tool, which can make the possible differentiation between cystic and solid masses [20]. But its ability in detecting tumors less than 1 cm and non-palpable malignancies is weak, with a detection accuracy of only about 30% and 8% respectively. In addition, the sensitivity is only about 64% [18]. Theromography is a modality based on the skin thermal image after the application of infra-red radiation. Although this method has been postulated as a risk indicator for subsequent development of breast cancer, it has not been proven to be useful for breast cancer detection [20]. CT has appeared to be more sensitive in detecting breast malignancies than X-ray mammography [18]. But CT of the breast requires intravenous injection of contrast media to achieve a good result. Besides this, the cost of contrast media, in addition to the small number of patients examined per hour and the potential radiation damage, have limited its application as a screening tool. It is used only occasionally as a diagnostic test [20]. MRI is new in breast

imaging. But its great sensitivity to soft tissue imaging and its non-invasiveness have provided a great potential for breast cancer detection.

In MRI, the most popular technique for breast cancer detection is MR dynamic first-pass contrast enhancement (commonly named Magnetic Resonance Mammography). MR dynamic first-pass contrast enhancement has shown its capability in distinguishing between malignant and benign breast lesions [18]. However, it may have limited importance in clinical breast diagnosis due to significant false-negatives and false-positives resulting from infectious lesions, proliferative dysplasia, myxoid fibroadenoma, and other benign breast lesions. Additionally, dynamic contrast enhancement cannot be used in screening, even within defined high-risk sub-populations (e.g. patients with dense breasts), due to the high cost of contrast material and its administration.

An arterial spin tagging technique [24] has been developed for measuring tissue parameters without the use of contrast materials, and has been previously demonstrated in brain and kidney. The spin tagging technique may provide more sensitive and specific assessment of tissue parameters, at higher spatial resolutions, by virtue of its ability to improve signal to noise ratio (SNR) over a reasonable scan time. This is another advantage over the dynamic contrast enhancement technique, which has a limited scan time and thus a limited resolution and SNR. A limited scan time is necessary to avoid the washout of contrast material.

Studies have shown that malignant tumors have higher water content than normal tissues and have higher perfusion than both normal tissues and benign lesions.

This is because malignant tumors induce high-level angiogenesis resulting in the increase of vascularity [25]. The rapid growth of malignant tumors suggests high metabolic rates at the tumors, which require an increased supply of nutrients and oxygen as well as the increased effort to remove the waste materials. Therefore, a higher blood perfusion and a higher blood volume at malignant tumors than normal tissue and benign lesions are expected [26, 27, 28]. High water content leads to a long MR spin-lattice relaxation time T_1. During the continuous research effort for this dissertation, the spin tagging technique that has been developed [29,30,31,32,33] measures T_1 and relative blood perfusion. These two parameters are used as the primary factors in determining the malignancy in the breast cancer detection technique developed. This technique is still in its exploration state, and improvement is still required.

Microcirculation in malignant tumors is complex. But macroscopically, tumor vasculature can be studied in terms of two idealized models: peripheral vascularization where vessels are localized primarily at the periphery, and central vascularization where vessels proliferate from the center like branches from a tree [28]. The spin tagging technique developed focused on investigating this macroscopic view of the tumor microcirculation, instead of the details of the microcirculation itself.

The rate of magnetization transfer between macromolecules and water has also been shown to be a valuable indicator of malignant disorder in the breast [34,35] and other parts of the body [36]. The level of magnetization transfer can be used to complement the application of T_1 and perfusion in malignancy detection.

Kallinowski's group found that perfusion has a wide range in malignant tumors [26]. Magnetization transfer might become more important if perfusion fails in tumor recognition.

Based on the above three parameters, and additional statistical factors, a simple malignancy decision technique based on thresholds and a more sophisticated decision technique based on Bayesian theory are developed. The former technique has been implemented in a visualization program (called BreastView) to aid researchers and clinicians in decision making. The ROC (receiver operating characteristic) curve based on the thresholds or the risk ratios used in Bayesian decision theory can be used to evaluate the technique presented.

The following six chapters (Chapters 4 to 9) will be dedicated to the discussion of the arterial spin tagging technique development and its application to breast cancer detection. Chapter 4 describes the concept of perfusion and the theory of the spin tagging technique. Chapter 5 discusses the arterial spin tagging pulse sequences developed. They include the fast SPGR (SPoiled Gradient Recalled) based and EPI (Echo Planer Imaging) based sequences. Magnetization transfer and its implementation are also discussed. In Chapter 6, the data processing techniques, including the semi-log linear regression technique and the minimum-mean-square-error technique, are discussed. Chapter 7 discusses the techniques of image processing. Chapter 8 contains the results and discussion. Chapter 9 summarizes this project, presents conclusions and suggests areas of further development.

Chapter 4

The Concept of Perfusion and the Theory of Spin Tagging

Before proceeding to the discussion of spin tagging, the concept of perfusion needs to be clarified. Buxton *et al* well defines the concept of perfusion appropriate for imaging in *Clinical Magnetic Resonance Imaging* edited by Edelman *et al* [37]. Considering a volume of tissue (V) supplied with arterial blood at a rate F (milliliters per minute) to the capillary beds within V, the perfusion (*f*) is then *f* = F/V (the milliliters of arterial blood delivered per minute per milliliter of tissue). With this definition of perfusion, *f* has dimensions of 1/minute and is thus a rate constant (Figure 4.1). This definition differs slightly from the standard definition of perfusion as milliliters of blood per minute per 100 g of tissue. The latter definition is more practical for experimental studies in which tissue samples are measured for concentrations of radioactive tracers, but the former definition is convenient for imaging studies where a known volume of tissue is imaged [37].

In our research protocol, approximately 10 slices within the breast, each with a thickness of 3 mm, are studied. Each slice is individually examined to investigate blood perfusion. The perfusion is measured at each voxel in these slices. In breast tissue, the blood vessels are composed of capillaries, connected by a few larger vessels (arterioles, metarteriles and venules). The diameters of capillary, arteriole, metarterile and venule are 5 to 10 μm, 5 to 100 μm, 10 to 20 μm and 5 to 100 μm respectively. Blood flows slowly from arteriole to metarterile to the capillary bed and then to the
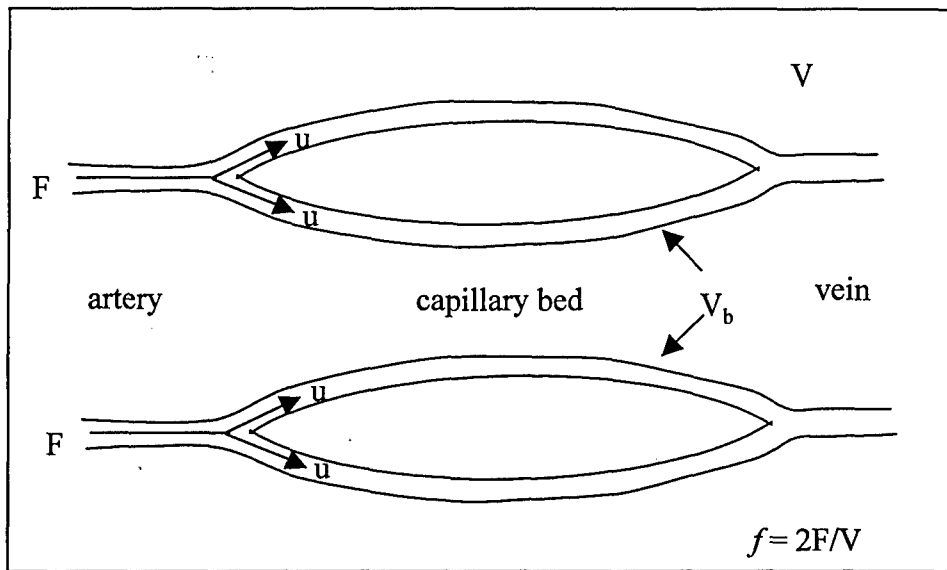
(a)
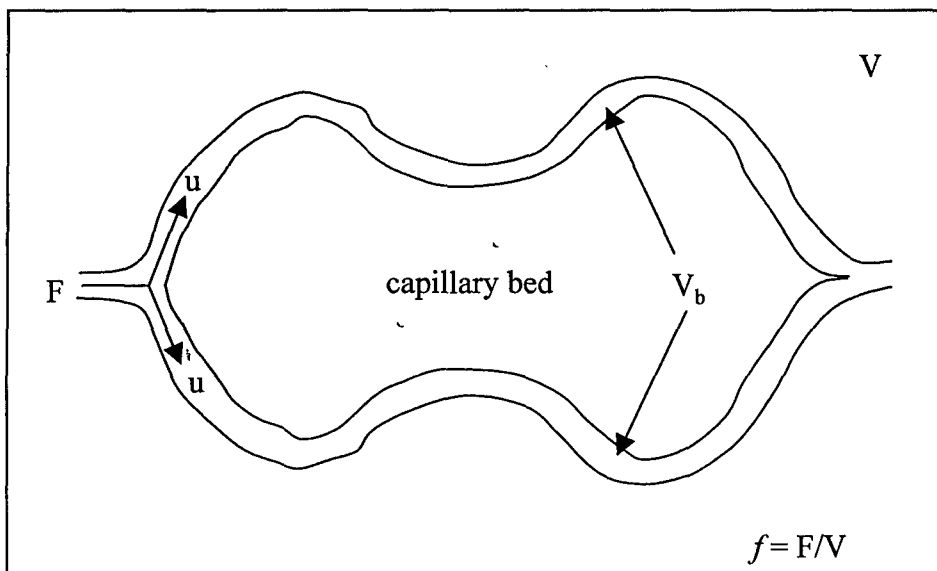
(b)

Figure 4.1. The meaning of perfusion. Two idealized capillary beds illustrate the distinction between blood volume (V_b), blood velocity (u) and perfusion (f). The V_b's as well as the u's are the same in Configurations (a) and (b), but f in Configuration (a) is twice as large as in Configuration (b). In Configuration (a), a tissue volume V is fed by two arteries each with flow F. In Configuration (b), the capillaries are twice as long so that the blood volume is the same, but fed by only one artery.

venules. Water molecules can move freely between the capillaries and their surroundings. The average velocity of blood flow in capillaries is 1 mm/sec [2]. The voxel resolution used in our research protocol is 1.33 mm × 1.33 mm × 3 mm, which is also the range used in typical clinical MR imaging. There are about 50 capillaries penetrating each voxel in various directions. Therefore, perfusion represents the combined activity of micro flows within a voxel (Figure 4.2). A two-component model is used to approximate the activity of the water molecules. In this model, water molecules in blood vessels entering a slice of breast tissue mix thoroughly with water molecules outside the vessels before they leave the slice. For this two-component model, the Bloch Equation for the breast tissue water magnetization at the slice of tissue investigated after any RF perturbation can be written as [24]

$$\frac{dM(t)}{dt} = \frac{M_0 - M(t)}{T_1} - k_{for} M(t) + k_{rev} M_m(t) + f M_a(t) - f\left(\frac{M(t)}{\lambda}\right) \quad (4.1)$$

where,

$M(t)$ = the longitudinal water magnetization of a voxel of breast tissue at time t,

M_0 = the value of $M(t)$ under fully relaxed conditions,

T_1 = the spin-lattice relaxation time constant of the breast tissue,

$M_m(t)$ = the longitudinal magnetization of macromolecules in a voxel of tissue,

k_{for}, k_{rev} = the magnetization transfer rate constants from water to macromolecules and vice versa,

The slice of tissue
to be investigated
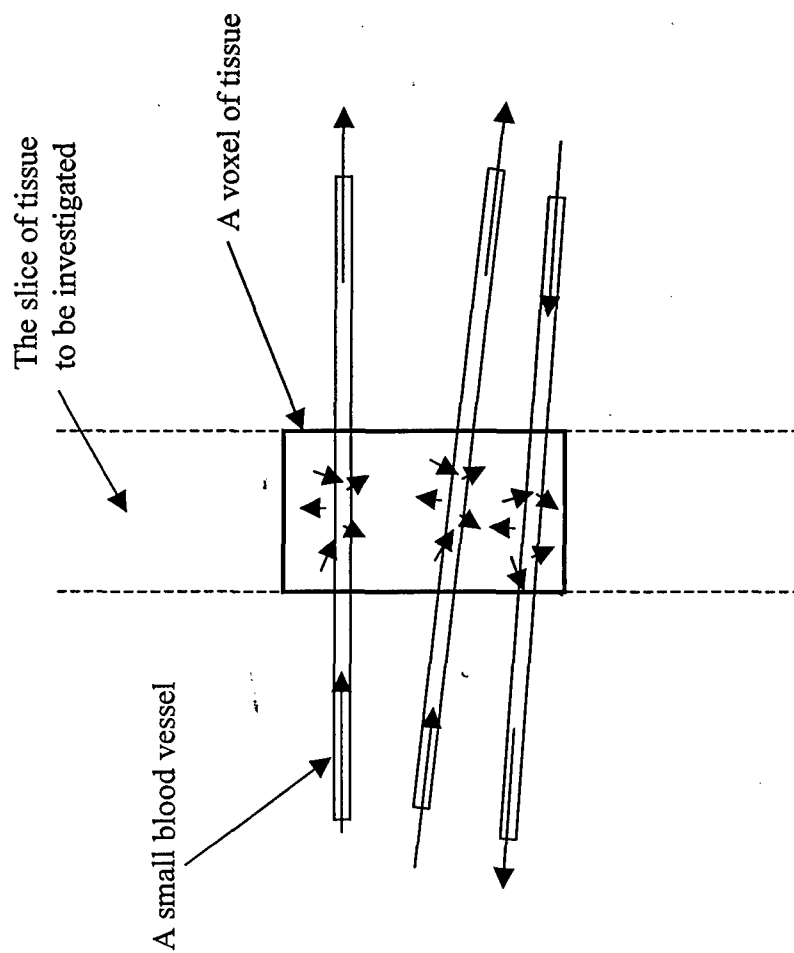
A voxel of tissue

A small blood vessel

Figure 4.2. Micro blood flow in breast tissue. The above drawing shows a slice of breast tissue to be investigated. A voxel within the slice is identified. As shown, small blood vessels randomly penetrate the voxel resulting in random directions of blood flow (indicated by long arrows). Water molecules (indicated by short arrows) move easily in and out of the blood vessels. The blood perfusion of the voxel represents the overall activity of the micro flows within it.

M_a = the longitudinal water magnetization per ml of arterial blood entering a

voxel from outside of the slice investigated,

f = perfusion in ml of arterial blood per second per voxel (with dimensions of

sec^{-1}),

λ = the ratio of water content between breast tissue overall and the arterial

blood within it.

To simplify Eq. (4.1), we need to make two assumptions. The first assumption

is that the effect of magnetization transfer is negligible, specifically,

$$\left| k_{rev}\, M_m(t) - k_{for}\, M(t) \right| \ll \left| \frac{M_0 - M(t)}{T_1} + f M_a(t) - f\left(\frac{M(t)}{\lambda}\right) \right|$$

Then Eq. (4.1) can be simplified to

$$\frac{dM(t)}{dt} = \frac{M_0 - M(t)}{T_1} + f M_a(t) - f\left(\frac{M(t)}{\lambda}\right) \qquad (4.2)$$

Eliminating the magnetization transfer terms can also be rationalized as being

included in T_1 relaxation. The effect of magnetization transfer has to be measured

using other means to improve the precision of Eq. (4.1), such as the use of binomial

pulses [38] or off-center RF irradiation [36,39].

Various spin tagging techniques have been used to estimate perfusion f (or

f/λ). Some are qualitative [40] and others are more quantitative [24,41,42]. The

various techniques are all based on three different spin states: equilibrium, saturation

and inversion.

The arterial spin tagging method presented in this dissertation is also based on two of these three states: the equilibrium and inversion states, which should give the maximum spin signal contrast. The measurement of both T_1 and f/λ are achieved. This general scheme of the pulse sequence is based on inversion recovery. Spins in a slab of breast tissue are inverted first using a RF pulse. The thickness of the slab can be controlled by the strength of the slab selective gradient (normally a Z gradient). Then the levels of recovery to equilibrium are measured at different times (Figure 4.3). The rate of recovery can be estimated from the recovery curve.

Parameters T_1 and f/λ in Eq. (4.2) can be estimated from two spin tagging conditions. Under Condition 1 (Selective tagging condition), spins in the slice of breast tissue to be investigated are inverted first, and then the signal corresponding to the overall spin magnetization from the same slice is acquired at a later time, which is varied to obtain a good spin recovery curve. Since the spins entering the slice of breast tissue are not perturbed, they are in equilibrium. Then,

$$M_a(t) = M_a^0$$

where,

M_a^0 = the value of $M_a(t)$ under the fully relaxed condition.

In the two-component model, we assume that the spins in arterial blood entering the slice can mix thoroughly with spins in the surrounding breast tissue before they leaving the slice. Thus in the equilibrium condition,
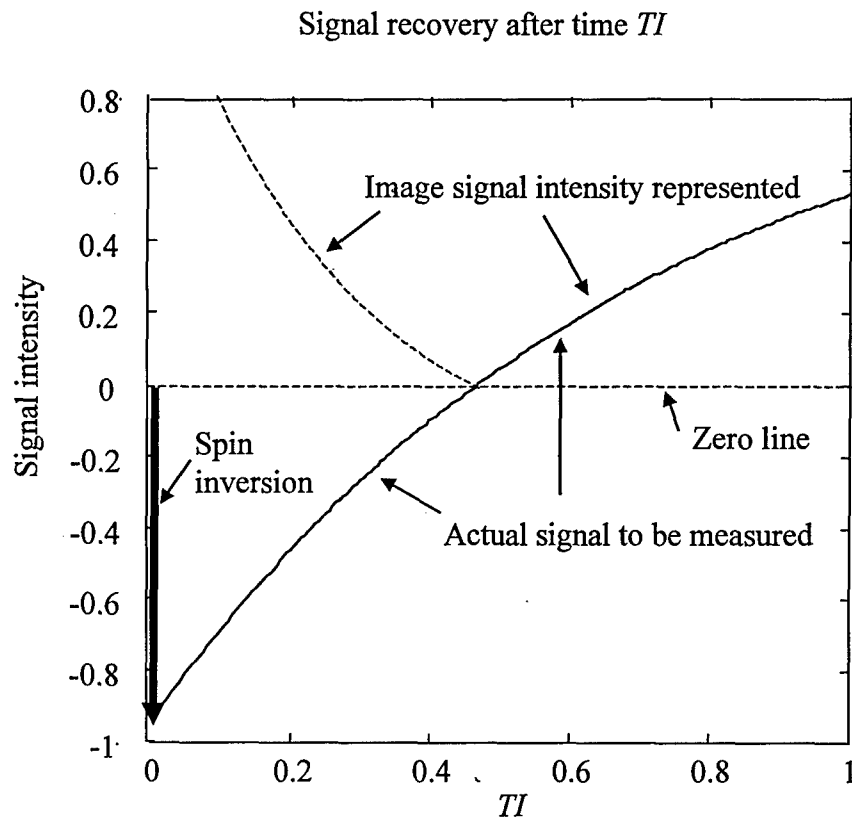
Signal recovery after time *TI*

Figure 4.3. Signal recovery after spin inversion. After the spin dipoles are inverted, they relax back to their equilibrium positions in an exponential fashion. Shown here is the signal acquired along a typical spin recovery curve. An image only shows the magnitude of the actual signal measured. The rate of recovery can be determined by the signal intensity in images acquired at different points of the recovery curve. *TI* is a point in time at which an image is acquired.

$$fM_a^0 = f\frac{M_0}{\lambda}$$

Eq. (4.2) then becomes

$$\frac{dM(t)}{dt} = M_0(\frac{1}{T_1} + \frac{f}{\lambda}) - M(t)(\frac{1}{T_1} + \frac{f}{\lambda}) \qquad (4.3)$$

Eq. (4.3) is the standard relaxation equation below

$$\frac{dM(t)}{dt} = \frac{M_0 - M(t)}{T_{1s}}$$

with

$$\frac{1}{T_{1s}} = b_s = \frac{1}{T_1} + \frac{f}{\lambda} \qquad (4.4)$$

where T_{1s} is the apparent spin-lattice relaxation time measured under the Selective condition. The subscript "s" means "under Selective condition".

Under Condition 2 (Non-selective tagging condition), spins are inverted everywhere, but signals are acquired only from the slice to be investigated. The spins inside and outside the slice of breast tissue are thus the same. Then

$$fM_a(t) = f\frac{M(t)}{\lambda}$$

and Eq. (4.2) becomes

$$\frac{dM(t)}{dt} = \frac{M_0 - M(t)}{T_1}$$

The T_1 measured in this case is the true T_1 without the influence of blood flow, which can be denoted as

$$T_{1n} = T_1 \tag{4.5}$$

and

$$b_n = \frac{1}{T_{1n}} \tag{4.6}$$

The subscript "n" denotes the T_1 and the b value measured under the Non-selective condition, distinguishing them from the Selective case.

Based on the b_s and b_n values obtained from the two tagging conditions, we can determine the perfusion parameter

$$\frac{f}{\lambda} = b_s - b_n \tag{4.7}$$

The term f/λ can be interpreted as the rate of spin replacement in a voxel in the direction perpendicular to the slice. Compared to normal breast tissue and benign lesions, we would expect a higher f/λ in malignant tumors.

In summary, this chapter has covered the concept of perfusion and its measurement in MRI. The theory of spin tagging has been thoroughly discussed, as well as how it is used to measure the perfusion parameter f/λ. The next chapter will cover the arterial spin tagging pulse sequences developed for the measurement of the T_1's under the Selective and Non-selective conditions, from which the perfusion

parameter f/λ can be calculated, and for the measurement of the level of

magnetization transfer between macromolecules and water.

Chapter 5

Arterial Spin Tagging Pulse Sequences

To capture the ideal spin recovery after the spin tagging inversion pulse, some design criteria need to be considered: (1) The slice profiles generated by the inversion RF pulse and the data acquisition RF pulse should match perfectly with each other during the Selective condition so that the inverted spins are the spins being measured. (2) The total time of whole-image data acquisition for each point of the recovery curve should be as short as possible to avoid the averaging effect. (3) The total scan time for the full breast examination should be reasonably short. (4) The data acquisition should not disturb the natural spin recovery after the inversion RF pulse excitation.

To satisfy Criterion 1, an optimized RF inversion pulse and an optimized RF acquisition pulse have been designed based on the Shinnar Le-Roux (SLR) algorithm [43,12,15]. These optimized RF pulses allow sharp rectangular slice profiles so that the spins being tagged are basically the spins being measured under the Selective condition (Figure 5.1). The section of inverted magnetization (slab) is created by applying the SLR inversion pulse in the presence of the slice selection gradient. The thickness of the inversion slab can be controlled by changing the gradient strength. By applying the SLR pulse without an associated slice selection gradient, a non-selective slab containing inverted spins in the entire sensitive volume of the transmit RF coil is created. To optimize the RF pulse profiles, tradeoffs have to be considered among the length, the amplitude and the bandwidth of the RF pulses. In general, a better slice
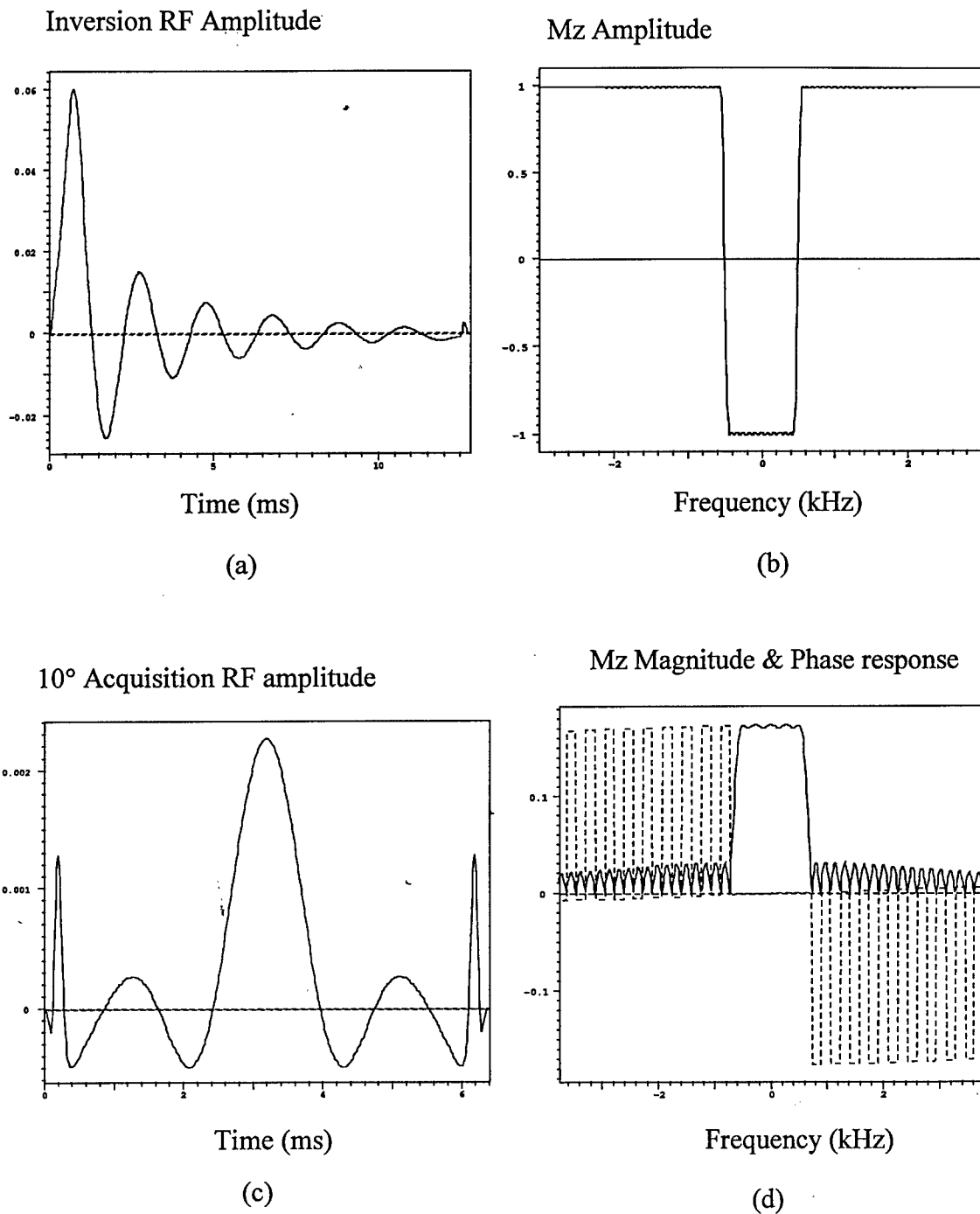
Figure 5.1. SLR inversion and data acquisition RF pulses. (a) and (b) show the
SLR inversion RF pulse and the near rectangular frequency response for the
longitudinal magnetization. (c) shows the 10° SLR data acquisition RF pulse.
(d) shows the magnitude of the frequency response of the longitudinal
magnetization and the associated phase.

profile is obtained by using a RF pulse with a longer pulse width, a higher amplitude and a larger bandwidth. However, a long data acquisition RF pulse can lead to a lengthening of the scan time because it is used many times for the completion of the data acquisition for the whole image. Its excitation effect on the moving spins due to perfusion might also change during a long RF excitation. The high amplitude of a RF pulse can go beyond the limitation of the hardware. For a fixed pulse length, a larger bandwidth can lead to a better slice profile, but it also induces a higher RF amplitude. There is a hardware limitation on the bandwidth itself, but it has not led to any problem for the RF pulse design in this dissertation. The final design of the RF pulses is shown on Table 5.1 below:

Table 5.1. The SLR RF Pulse Design Specifications

Parameters	Inversion Pulse	Data Acquisition Pulse
Pulse Type	Inversion	Spin echo
Phase Type	Maximum phase	Linear phase
Pulse duration (ms)	15.6	6.4
Pulse bandwidth (kHz)	0.95	1.25
Ripple in passband	1.50%	5%
Ripple in stopband	0.40%	5%
Resolution (# of points)	1560	640
Flip angle (degree)	180	10

The above design specifications were implemented using the RF design tool that comes with the EPIC software. The resulting attributes for the RF pulses are listed in Table 5.2 below:

Table 5.2. The RF Resulting Attributes Based on
the Design Specifications in Table 5.1

Parameters	Inversion Pulse	Data Acquisition Pulse
Actual Resolution (# of points)	1558	638
isoDelay (ms)	unknown	3.195
Pulse area (G ms)	0.0343	0.1216
Absolute width (ratio)	0.1091	0.2309
Effective width (ratio)	0.0445	0.1249
Duty cycle	13.22%	24.14%
Maximum pulse width	8.92%	24.14%
Maximum B1 (G)	0.219366	0.00838565
Maximum integral $B1^2$ (G^2)	0.0334052	5.62188×10^{-5}
Maximum RMS B1 (G)	0.0462748	0.00296381

IsoDelay: Time in μs from the zero phase reference of the pulse to the end of pulse.

Pulse area: The integrated area of the pulse.

Absolute width: The ratio of absolute pulse area, calculated by integrating the absolute value of pulse amplitude over time, to that of a hard pulse of unit amplitude and equal duration.

Hard pulse: A rectangular RF pulse, also called a standard RF pulse.

Effective width: Ratio of pulse energy to that of a hard pulse of unit amplitude and equal duration.

Duty cycle: Duty cycle of pulse defined by GE Medical Systems Inc.. It is the percentage of pulse duration in which amplitude exceeds 22.3% of maximum pulse amplitude.

Maximum pulse width: Percentage of pulse width that exceeds 22.4% of pulse's maximum amplitude that is found in the largest lobe of the pulse.

B1: The magnetic field of the RF pulse.

Maximum B1: Peak B1 field strength in Gauss.

Maximum integral $B1^2$: Peak integral of $B1^2$ in $Gauss^2$.

Maximum RMS B1: Peak RMS B1 in Gauss.

The above attributes are used to scale the amplitudes of the RF pulses against the actual amplitude of a 90° sinc RF pulse that causes a true 90° spin flip determined in a prescan. They are also used to calculate the heat absorption rate to the patient so that a maximum repetition rate of the RF pulse excitation can be set according to the safety guidelines that have been established by health agencies such as the FDA.

The RF pulses designed might not be optimized in terms of the flip angle and pulse width. They can be manipulated without changing the shape of the RF pulse or the slice profile. But the peak amplitude of the RF pulse is changed according to

$$B1_{peak} = B1_{peak}^{nominal} \frac{flip}{nom\_flip} \frac{nom\_pw}{pw} \qquad (5.1)$$

where,

flip = the flip angle of the RF pulse used,

pw = the pulse width of the RF pulse used,

nom_flip = the normal flip angle of the RF pulse designed,

nom_pw = the normal pulse width of the RF pulse designed,

$B1_{peak}$ = the peak amplitude of the RF pulse used,

$B1_{\text{peak}}^{\text{nominal}} = $ the peak amplitude of RF pulse at normal flip angle and pulse width.

Normally, only the flip angle is manipulated during scanning because the change of the pulse width leads to a change of the timing diagram. For the spin tagging sequence implemented here, the inversion pulse is fixed. The optimal flip angle for the data acquisition RF pulse has been determined by inspecting the resulting images at various flip angles.

To satisfy Criteria 2 and 3, fast data acquisition techniques should be used. These techniques can include fast SPGR (SPoiled Gradient Recalled), EPI (Echo Planar Image) and Spiral sequences. They all have their own technical advantages and disadvantages. The fast SPGR sequence has been tested repeatedly in both research and clinical environments. The image quality is good and the images contain few artifacts. It is much less demanding on the gradient amplitude and the receiver bandwidth than the other two sequences. However, it is much slower than the other two techniques and thus is more prone to motion artifacts. It also has more chance of disturbing the natural spin recovery due to the need of repeated application of the data acquisition RF pulse for the whole image. On the other hand, the EPI and Spiral sequences only require one application of the data acquisition RF pulse for the whole image or for many k_y lines in the case of interleaved data acquisition. They are more capable of preserving the natural spin recovery curve. They also reduce scan time and thus are less prone to motion artifacts. However, they demand a high amplitude and a fast slew rate that some MR systems cannot provide. Due to the use of fast alternating

gradient pulses, they also lead to serious artifacts and a lower image quality. EPI appears advantageous compared to Spiral imaging. An EPI sequence is easier to implement, allows for more control over the frequency and phase encoding directions, and is capable of asymmetric matrix data acquisition. The techniques for the EPI artifact removal and interleaved data acquisition have been fully developed. Although the Spiral sequence is more efficient in the use of the gradients, it is also more demanding on the gradients.

The Signa Advantage 1.5 T GE MR system (GE Medical Systems Inc., Milwaukee) has been the system available in the research site at University of California Davis Medical Center during the development of this project. This system could not support the EPI and spiral application for this project, so the arterial spin tagging sequence has been developed based on a fast SPGR data acquisition scheme. This spin tagging sequence has been fully tested on phantoms, normal subjects and patients, and has been proven to function as expected. The data used for analysis is mainly from the application of this sequence. In April 1999, the Signa Advantage system was upgraded to Signa Horizon LX 1.5 T GE MR system (GE Medical Systems Inc., Milwaukee). The spin tagging sequence based on the fast SPGR data acquisition scheme has been converted to run on this new system. But this new system still has problems supporting the polarity alternation of the EPI X gradient pulse train from one interleave to the next. Therefore, the EPI based arterial spin tagging pulse sequence has only been developed to run on computer simulation.

The 180° RF refocusing pulse has been eliminated from all of the three fast sequences to achieve fast data acquisition. Since each data acquisition period is very short, the transverse magnetization is not completely dephased. This problem is most severe for fast SPGR because its TR period is 15 ms as compared to about 100 ms for EPI or Spiral. To avoid the transverse magnetization being carried over to the next data acquisition periods, it needs to be dephased or randomized. This has been achieved by using a combination of gradient and RF spoiling [44]. The spoiling techniques will be investigated by looking into the fast SPGR pulse sequence following (Figure 5.2).

5.1. Arterial Spin Tagging Sequence Based on a Fast SPGR Data Acquisition Scheme

The fast SPGR sequence is a gradient recalled echo (GRE) based sequence, so it looks similar to the one discussed in Chapter 2 (Figure 2.6). The optional killer pulse in the X gradient has not been used. To achieve a short repetition period, a higher data acquisition frequency is normally used. This leads to a higher read-out gradient amplitude (the gxw pulse amplitude). Shorter pulse widths are also used in other gradients, except the slice-selection gradient that is determined by the slice thickness and the bandwidth of the RF pulse. The other method used to shorten the TR period is the concurrent application of the gradient pulses except during RF pulse excitation and data acquisition. This fast SPGR sequence has been implemented for clinical studies by GE Medical Systems Inc., and the image quality from this sequence has also been verified [44].
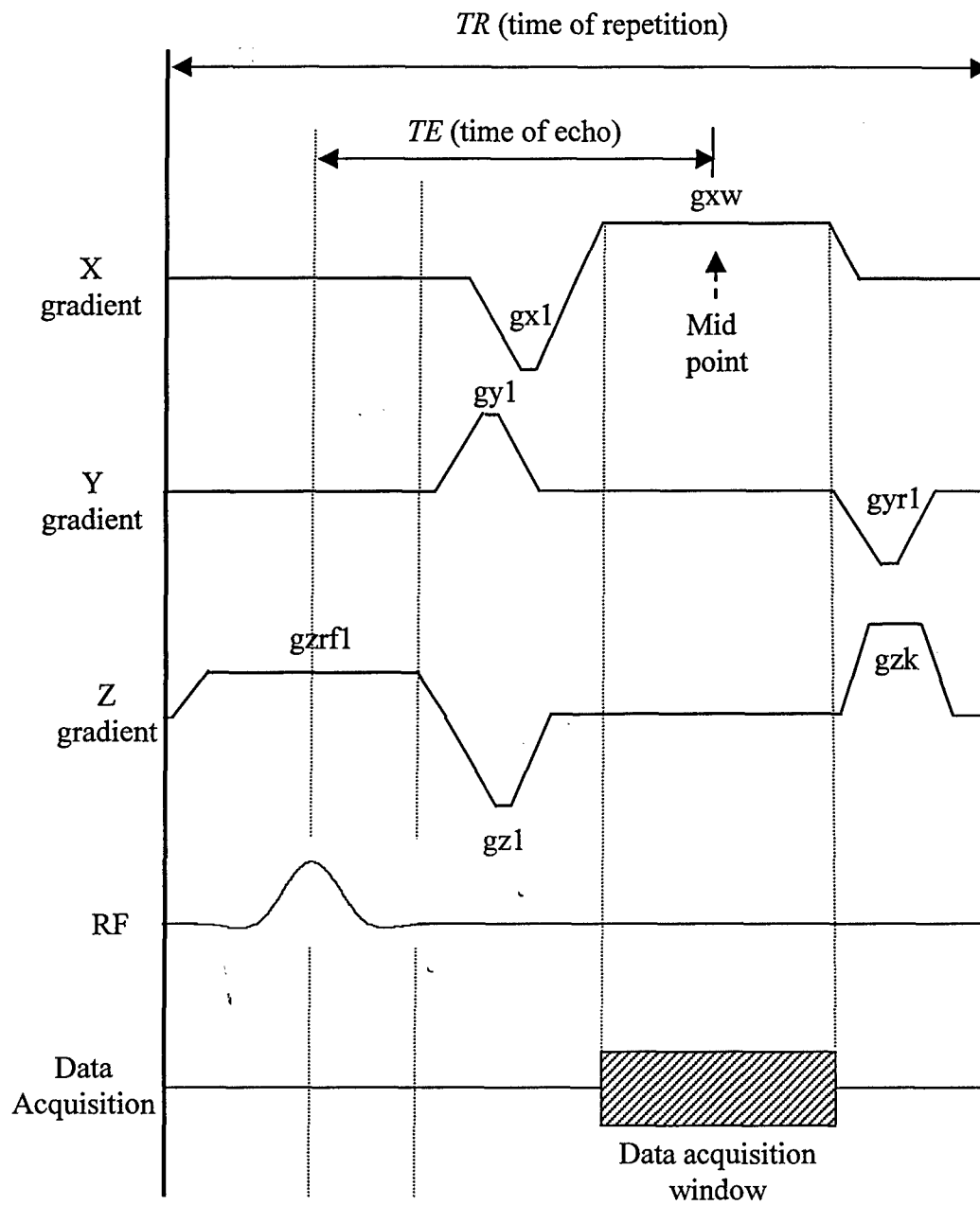
Figure 5.2. A fast SPGR sequence. The gradient and RF pulses played in
one repetition period of a fast SPoiled Gradient Recalled (SPGR) sequence.

The details for spoiling gradient pulse design are described by Zur and his colleagues. They suggested that a phase increment of 117° or 123° at each TR period would give adequate cancellation of transverse magnetization in clinical MRI [9]. In the SPGR sequence implemented by GE Medical Systems Inc., the pulse area of the spoiling gradient pulse has been designed to have at least 4π of phase dispersion across the slice at each TR period, combined with the net phase introduced in the slice-selection gradient pulse and its rewinding pulse. But the pulse area range is set between 100 ms•G/cm and 400 ms•G/cm. The pulse area calculation is given by the following equation:

$$area\_gzk = \frac{4}{\gamma \cdot \Delta z} - (t\_exa - \frac{pw\_gzrf1a}{2}) \cdot |a\_gzrf1| \qquad (5.2)$$

where,

area_gzk = the pulse area of the spoiling gradient pulse (sec · G/cm),

Δz = the slice thickness (cm),

γ = the gyromagnetic ratio for the proton = 4258 Hz/G,

a_gzrf1 = the amplitude of the gzrf1 pulse (G/cm),

pw_gzrf1a = the width of the ramp time of the gzrf1 trapezoid pulse (sec),

t_exa = the time from the start to the middle of RF pulse, including pw_gzrf1a (sec).

To achieve effective spoiling after just a few or no TR periods, RF spoiling is also implemented. For the SPGR sequence implemented by GE Medical Systems Inc., the RF spoiling use the following scheme:

(1) Initialization:

        fs_pi = phase board value for π radians = 32752,

        fs_2pi = phase board value for 2π radians = 65504,

        seq = the fast SPGR repetition number = 0,

        seed = 21001.

(2) Looping from one TR period to the next:

        phase = (phase + seq * seed + 3 * fs_pi) % fs_2pi – fs_pi;

        seq ++;

An application of an inversion RF pulse before the full data acquisition scheme is the basis of the arterial spin tagging sequence. An inversion RF pulse is applied first to tag the spins. Data is then acquired for the entire image using a fast SPGR data acquisition scheme. In the standard clinical sequence, data acquisition starts at one end of the k space and a significant amount of time elapses before $k_y = 0$ occurs. This time is too long to map out the T_1 recovery curve. The original clinical sequence must be modified to support a symmetric-k space data acquisition (Figure 5.3). Data acquisition starts at the $k_y = 0$ line of the k space, and then alternates below and above this k_y line until the lowest and highest k_y lines. This allows the signal of the reconstructed image to have the highest weighting on the data points at the beginning of the acquisition. Thus, the effective time of inversion, which is the time from spin inversion to the effective zero k space, can have a wide range and thus map the T_1 recovery curve. Since the RF phase is alternated in fast SPGR, the order of data acquisition has been constructed in a way such that this alternating RF phase pattern is retained in both the actual data acquisition as well as the whole data set. This allows for the correct image reconstruction using the algorithms installed in the MR system.
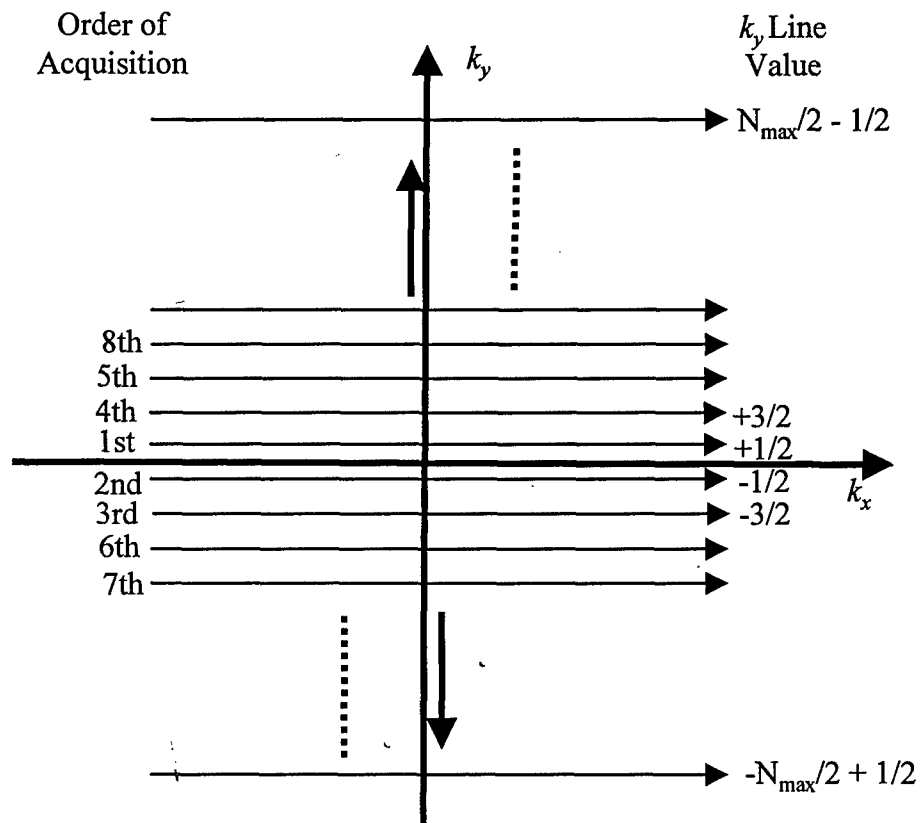
Figure 5.3. The k space for the fast SPGR symmetric data
acquisition. The total number of k_y lines is N_{max}.

The complete fast SPGR based arterial spin tagging pulse sequence is shown in Figure 5.4.

Odd-number interleaved k-space acquisition [45] has also been implemented to allow high spatial resolution in the phase-encoding direction. The k space is completed from different inversion periods (interleaves). By using an odd number of interleaves, the data combined would appear obtained from a single-shot acquisition. This would allow the simple image reconstruction as before. But the scan time would increase with the number of interleaves. Since then, a more effective technique to approach a sufficiently high resolution has been found by using the half phase field of view data acquisition. In this approach, the field of view (FOV) in the Y direction is only half of that in the X direction. This takes advantage of the fact that two breasts are scanned at a time. The long axis can be chosen as the frequency direction (X direction). The FOV required in the Y direction is obviously only half of that in the X direction. So only half of the phase-encoding steps are needed to achieve the same spatial resolution as before. This allows the doubling of the spatial resolution without any sacrifice of the scan time. Certainly, if the resolution is not sufficient after the application of this technique, the odd-number interleaved k-space acquisition can be added on to it. Or if the geometry of the object does not allow the half-phase FOV data acquisition technique, the odd-number interleaved k-space acquisition technique can be used.

For this fast SPGR spin tagging sequence operated in the Signa Advantage MR system, the following control variables have been used for all our studies:

$TE = 9.244$ ms (The minimum),
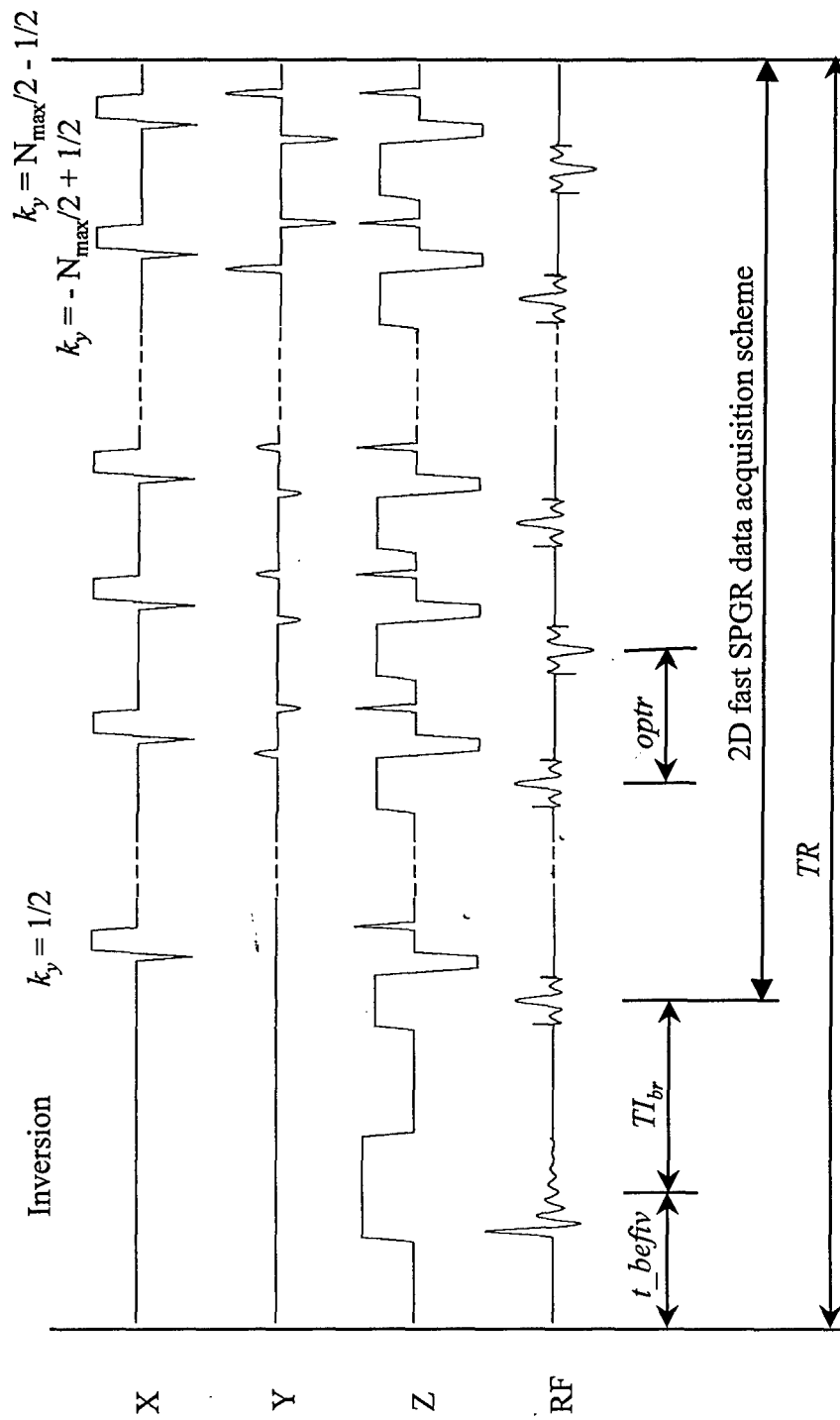
Figure 5.4. The fast SPGR based arterial spin tagging sequence. The parameter TR is fixed at 2.7 sec by default. An inversion tagging RF pulse is applied first, followed by phase encoding steps starting around zero k space. The time TI_{br} is changed by changing t_befiv. To show the details, the RF acquisition pulses are magnified, and t_befiv and TI_{br} are longer than they appear. N_{max} is the total number of k_y lines.

optr = the time of repetition for individual data acquisition frame = 16.62 ms

(The minimum),

Receiving bandwidth = 31.25 kHz,

Data acquisition flip angle = 10°,

Slice thickness = 3 mm,

Field of view (FOV) in X direction = 34 cm,

Field of view (FOV) in Y direction = 17 cm (by using half-phase FOV),

X matrix resolution = 256,

Y matrix resolution = 120,

Number of interleaves = 1 (single-shot),

Time of inversion = start with 615 ms, decrement to 15 ms with a step size of

100 ms.

The total scan time for the acquisition of data for the entire image (*TR* in

Figure 5.4) is 2.7 sec, including the inversion RF pulse. The data acquisition under the

Regular condition is designed simply by setting the amplitude of the inversion RF

pulse and the associated Z gradient pulse to zero, and thus keeping the same timing for

the gradient and RF pulses.

The Signa Horizon LX MR system has a higher gradient amplitude tolerance.

A fast data acquisition, which requires a higher read-out gradient amplitude, is used,

and thus the data acquisition period (*optr*) can be shortened to 12.5 ms. The *TE* now

becomes 5.2 ms. Since the *TR* is shortened, a higher Y matrix resolution can be used.

The default Y matrix resolution is set at 128. The total time for the whole image

acquisition, including the inversion RF pulse, is dropped down to 2.22 sec. This TR period should be designed within a reasonable range (2 sec to 3 sec for tissue) so that sufficient signal can be recovered to have a good SNR. The rest of the control variables remain the same.

For each breast study, approximately 10 equally spaced slices in the breasts are imaged with a total scan time of approximately 25 minutes. Two breasts are scanned simultaneously. At each slice location, 61 images are acquired in a continuous manner with a repetition time of 2.7 sec (or 2.22 sec in the LX system) based on the arterial spin tagging sequence (Figure 5.5). The image acquisition is based on the three conditions: Selective, Non-selective and Regular conditions. Under either the Selective or Non-selective condition, spins are inverted first and then data acquisition starts at a certain points (TI_{br}'s) of the recovery curve. For the Selective condition, only spins within the slice being measured are inverted. For the Non-selective condition, spins within the entire sensitive volume of the transmit RF coil are inverted. For either Selective or Non-selective condition, seven different time delays (or seven different TI_{br}'s) are used. Under each timing condition, four repeating images under the same constraints are acquired. The last three images of each timing condition are nearly at steady state and are extracted for analysis. Under the Regular condition, five repeated images are acquired under the same constraints. The last three images are nearly at steady state and their mean is used for analysis. Using the mean of three images instead of one helps to improve the signal-to-noise ratio (SNR). Through image comparison between the Regular condition and the Selective or Non-selective
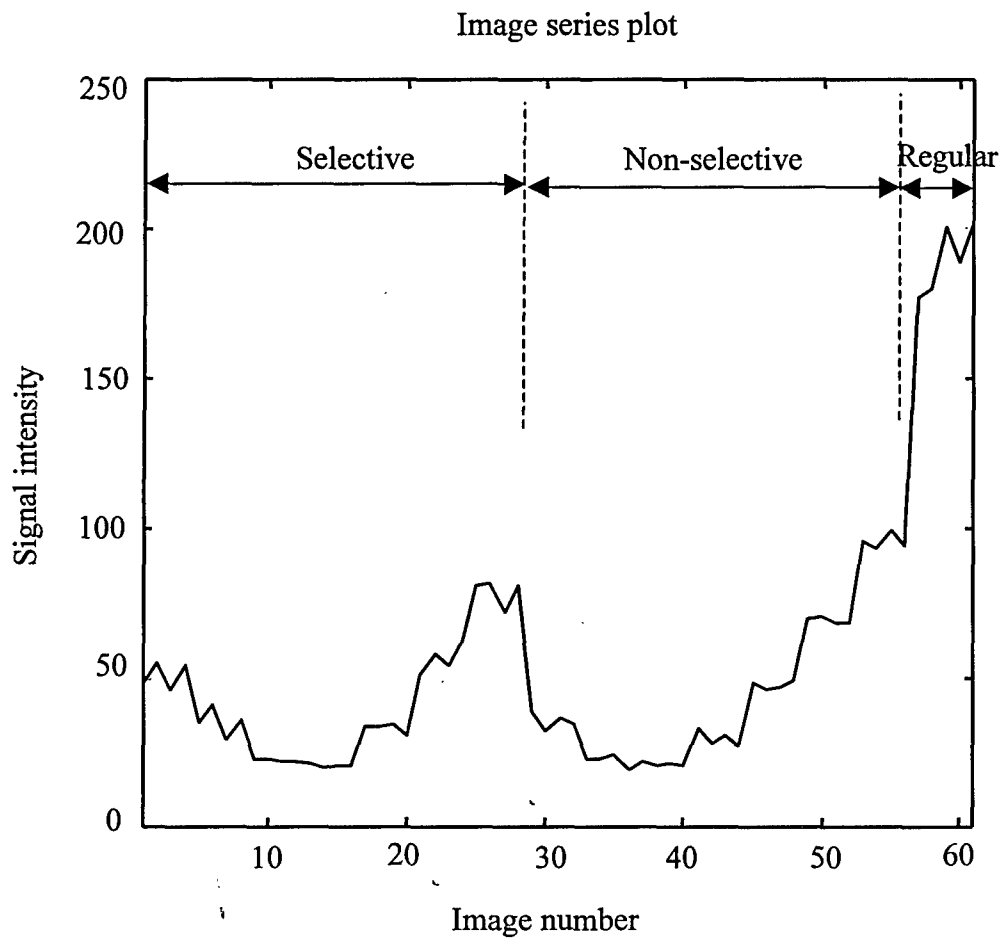
Figure 5.5. Image series plot using the fast SPGR based breast sequence. This plot shows the signal at the same pixel location across the 61 images acquired using this sequence. There are three imaging conditions: Selective, Non-selective and Regular conditions. For either Selective or Non-selective condition, seven *TI* timing conditions are used. Four repeated images are acquired at each *TI* timing condition. Images are acquired in a continuous manner with a repetition time of 2.7 seconds.

condition, T_{1s} or T_{1n} can be calculated respectively. The technique of calculation and derivation is discussed fully in Chapter 6.

Appendix A outlines the detail of the simulation and scanner operation for this SPGR based arterial spin tagging pulse sequence.

5.2. Arterial Spin Tagging Sequences Based on EPI Data Acquisition Scheme

In EPI, the full-image data acquisition can be completed after one RF excitation (Figure 5.6). EPI is still a derivative of a GRE sequence (Figure 2.6), although they appear quite different. A net zero phase accumulation in the X direction is still at the center of each X read-out pulse. A set-up pulse with an area equal to half of the read-out pulse is applied before the train of read-out pulses. A Y-gradient set-up pulse is applied before the train of X read-out pulses. This allows data acquisition to start at the top of the k_y line. Y-gradient blip pulses with an equal area are applied between the X read-out pulses. This allows the uniform decrementation of the k_y lines from the top of k space to the bottom of k space. The net zero phase accumulation in the Y direction occurs after half the data has been acquired. Thus, the net zero phase accumulation considering both the X and Y directions occurs at the center of the EPI train. Figure 5.7 shows the k space of an EPI sequence with a matrix resolution of 64 × 64.

However, there is a limitation on image matrix resolution using this one-shot technique because of the T_2 decay and the hardware limitations on the number of data points that can be acquired continuously. To achieve a good signal to noise ratio, all the data must be acquired before too much signal is lost due to T_2 decay (or T_2* decay
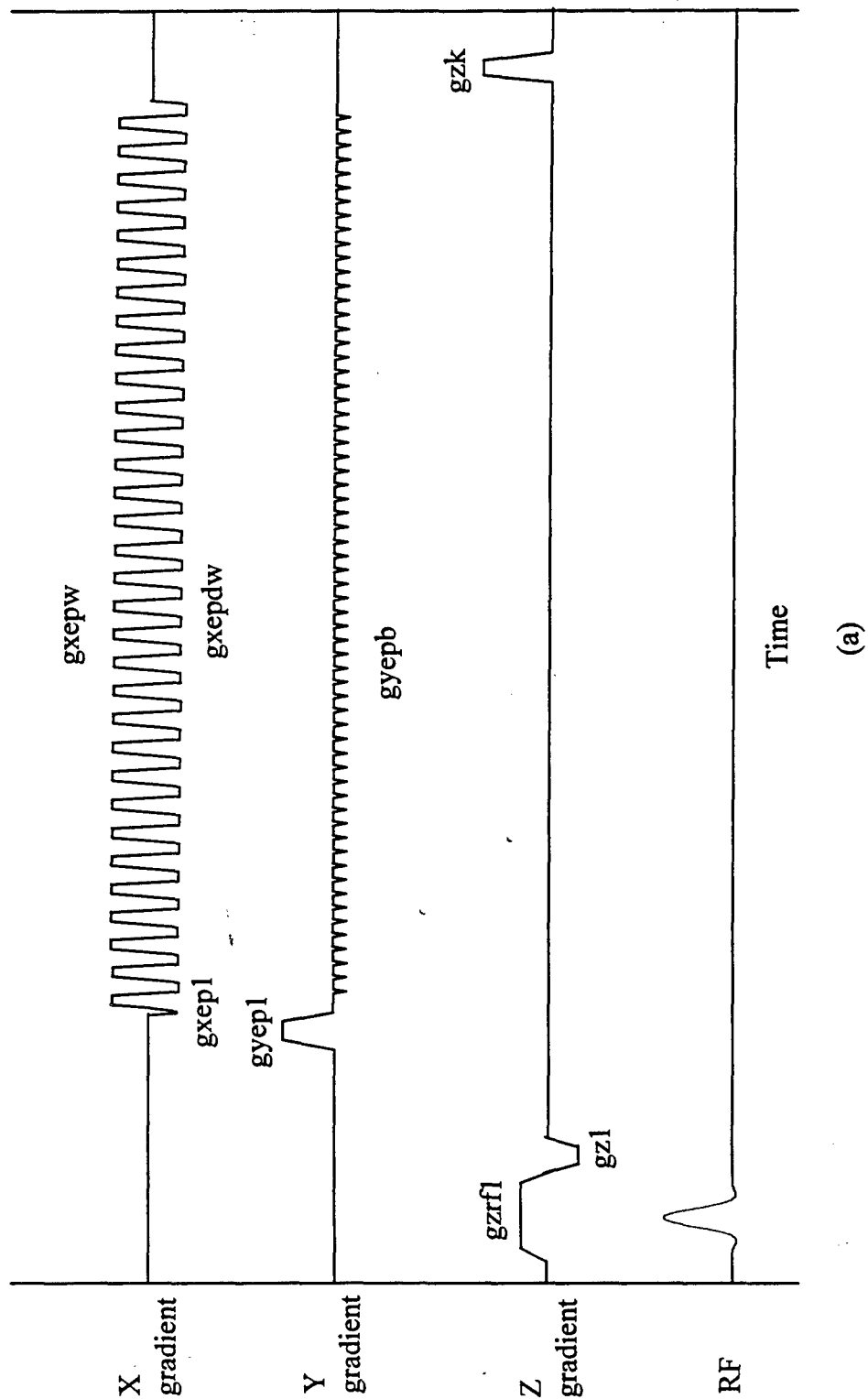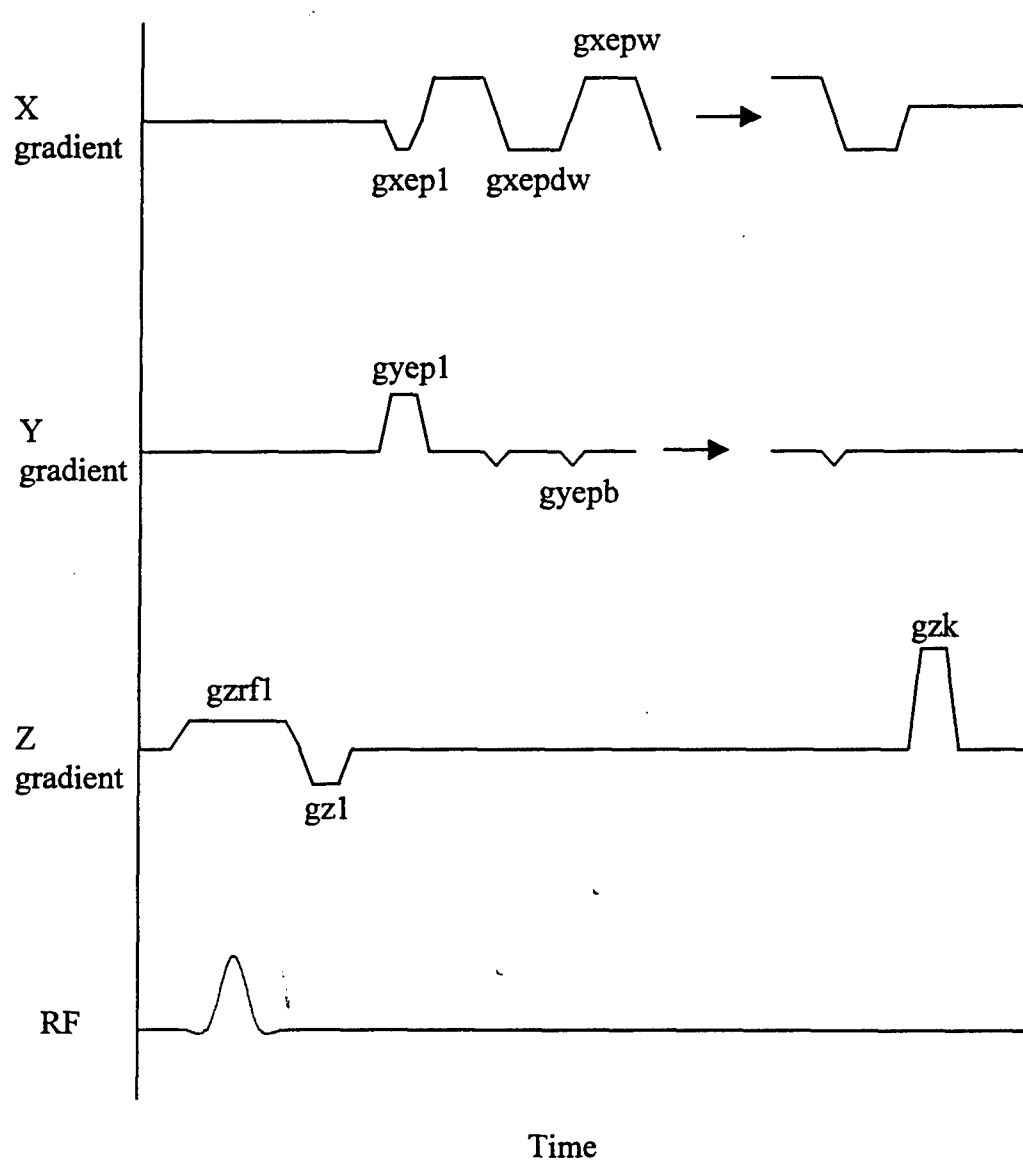
Figure 5.6. The pulse sequence for a regular 64 × 64 EPI. (a) This graph shows the simulation of the pulse sequence for the regular 64 × 64 EPI. (b) A magnification of part of the EPI train.

(a)

Time
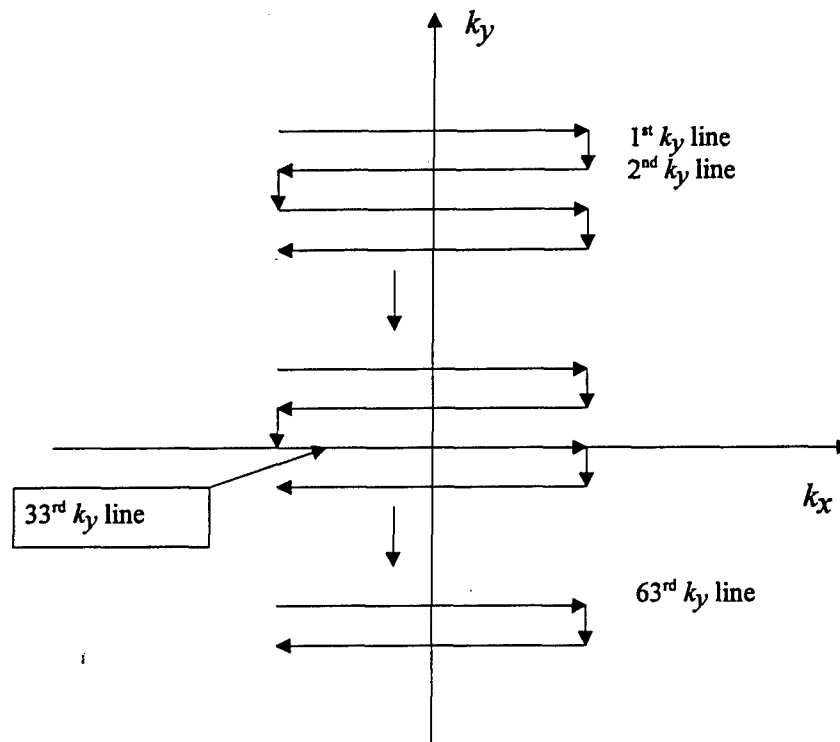
(b)

Figure 5.6. (continued)

Figure 5.7. The k space for a regular 64×64 EPI. This drawing shows the k space of the regular 64×64 EPI. The direction of data acquisition is from the top to the bottom, and from the left to the right and then from the right to the left and so on.

if field inhomogeneity exists). The number of data points that can be acquired continuously is limited by the receiver. The N/2 ghost also becomes more severe with the lengthening of the EPI gradient pulse train. In his master's thesis the author has developed an odd-number hybrid (or interleave) EPI technique for high-resolution imaging [45,46,47,48,49]. The data for a full k space is completed using an odd-number of interleaves (Figure 5.8). A time-shift is introduced incrementally to the interleaves (Figure 5.9). This interleave technique allows the combined data set to appear that it has been acquired in a one-shot EPI. The N/2 ghost appears the same as a one-shot EPI, and thus can be removed using the established N/2 ghost-removal algorithm [50].

To implement the spin tagging with interleaved EPI, the following steps are performed at each interleave: (1) inversion pulse and (2) 20 EPI acquisitions, each of which starts with a 10° RF pulse (Figure 5.10). Each of these 20 acquisitions, with a repetition time ($optr$ in Figure 5.10) of 100 ms, defines one point in the T_1 recovery curve. The total time for each interleave (TR in Figure 5.10) is 2 seconds. The data in the other interleaves is gathered in the same fashion. Since repeated RF pulses are applied to the same spins at the same slice location, transverse magnetization might not have completely dephased yet. RF spoiling should be added to the EPI sequence also. Figure 5.11 shows the looping technique used in the sequence.

5.3. The Implementation of Magnetization Transfer

Magnetization transfer (MT) is only implemented for the EPI based spin tagging sequence. It is not applicable to the fast SPGR based spin tagging sequence.
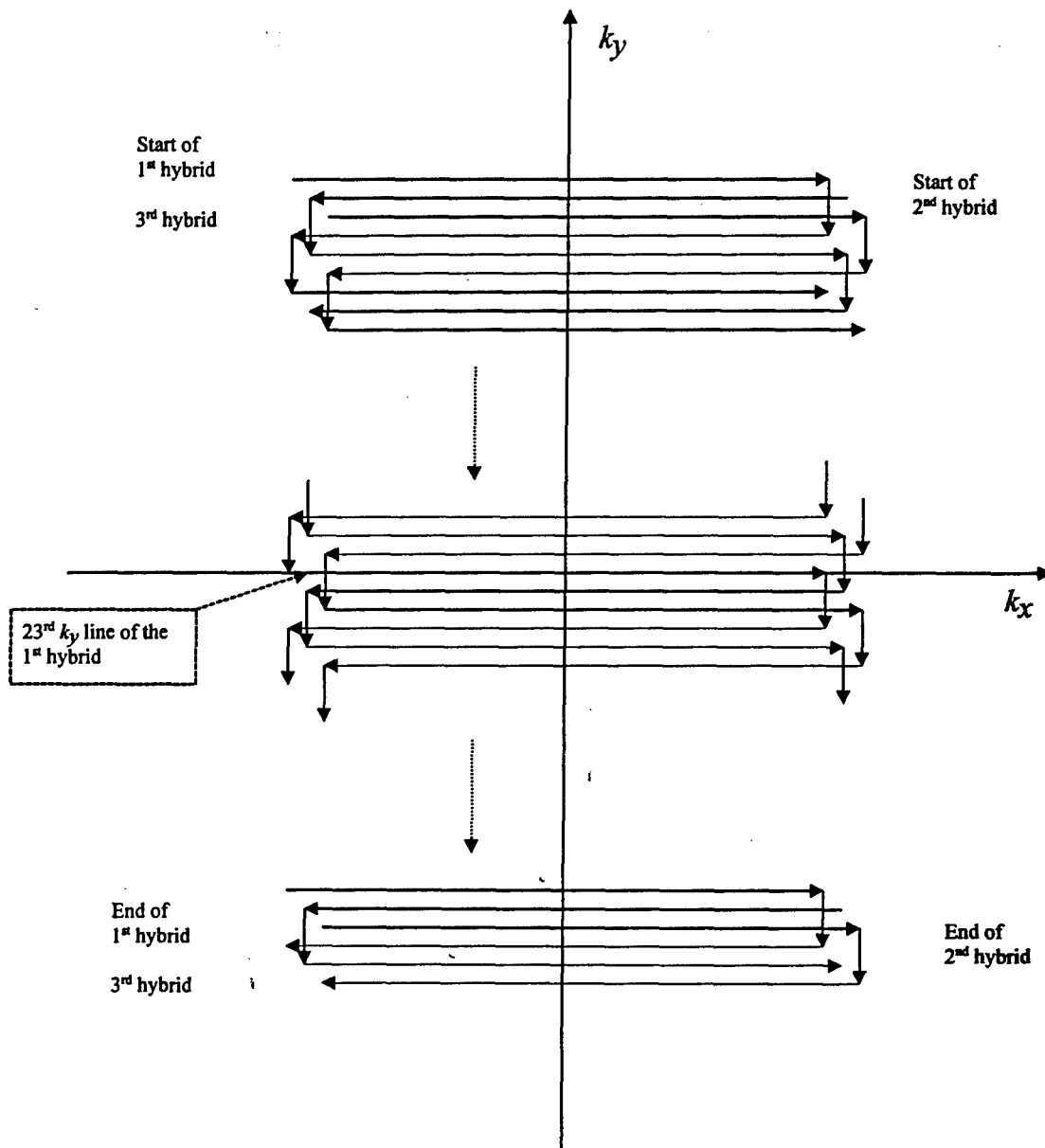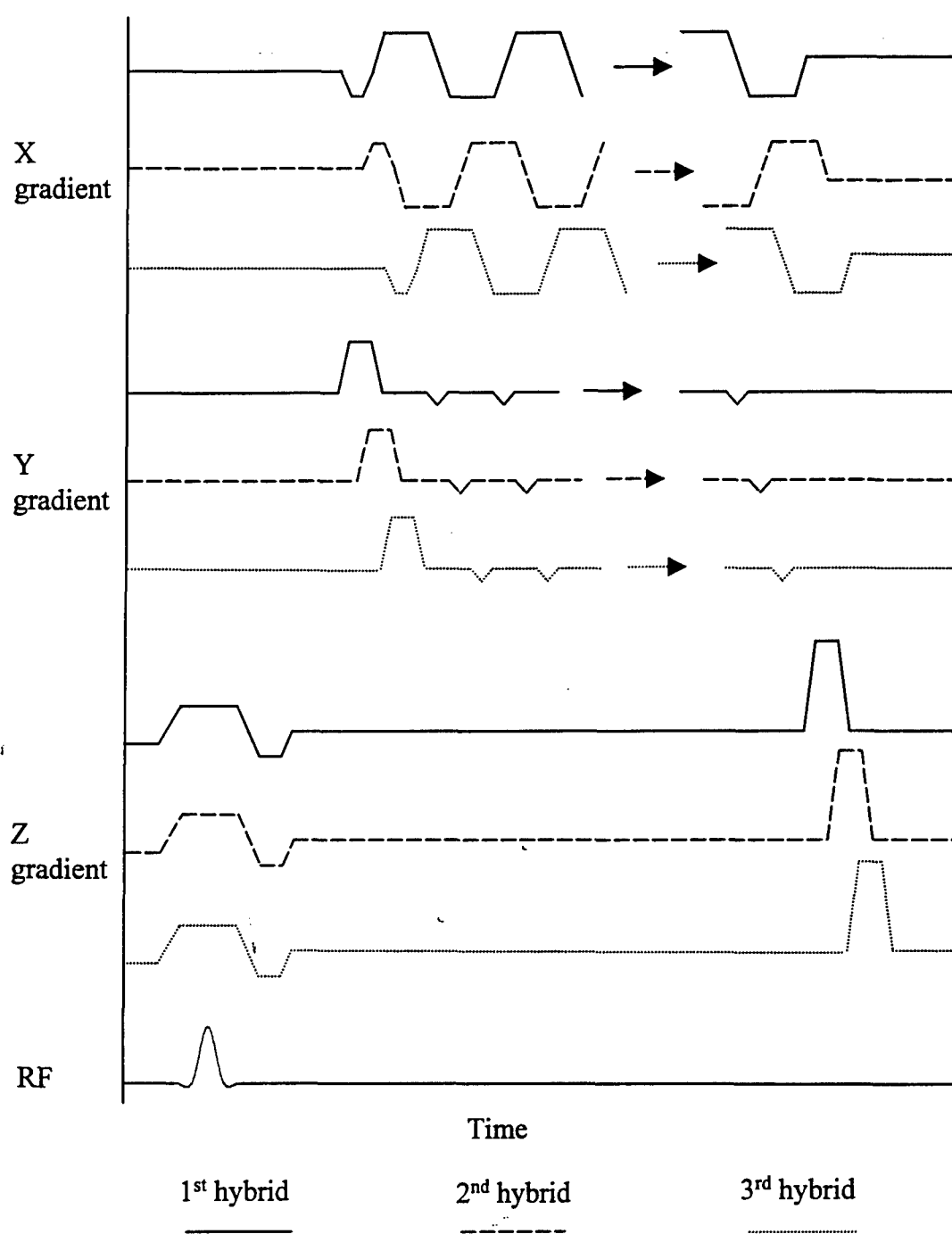
Figure 5.8. The *k* space for a 128 × 128 odd-number hybrid EPI. This drawing shows the *k* space of the 128 × 128 odd-number hybrid EPI that was developed. Three 128 × 44 hybrid scans are used. The starting direction of data acquisition for one hybrid scan is the opposite of the previous one. The data acquisition direction of odd-number hybrid scans is from the top to the bottom, and from the left to the right and then from the right to the left and so on. The data acquisition direction for even-number hybrid scans is just the reverse of that for odd-number hybrid scans.

RF is the same for all hybrid scans.

Figure 5.9. The pulse sequence for a 128 × 128 odd-number hybrid EPI. The drawing shows the sequence for the three hybrid scans used in the 128 × 128 odd-number hybrid EPI. The time delay and polarity change of the X gradient pulses are shown.
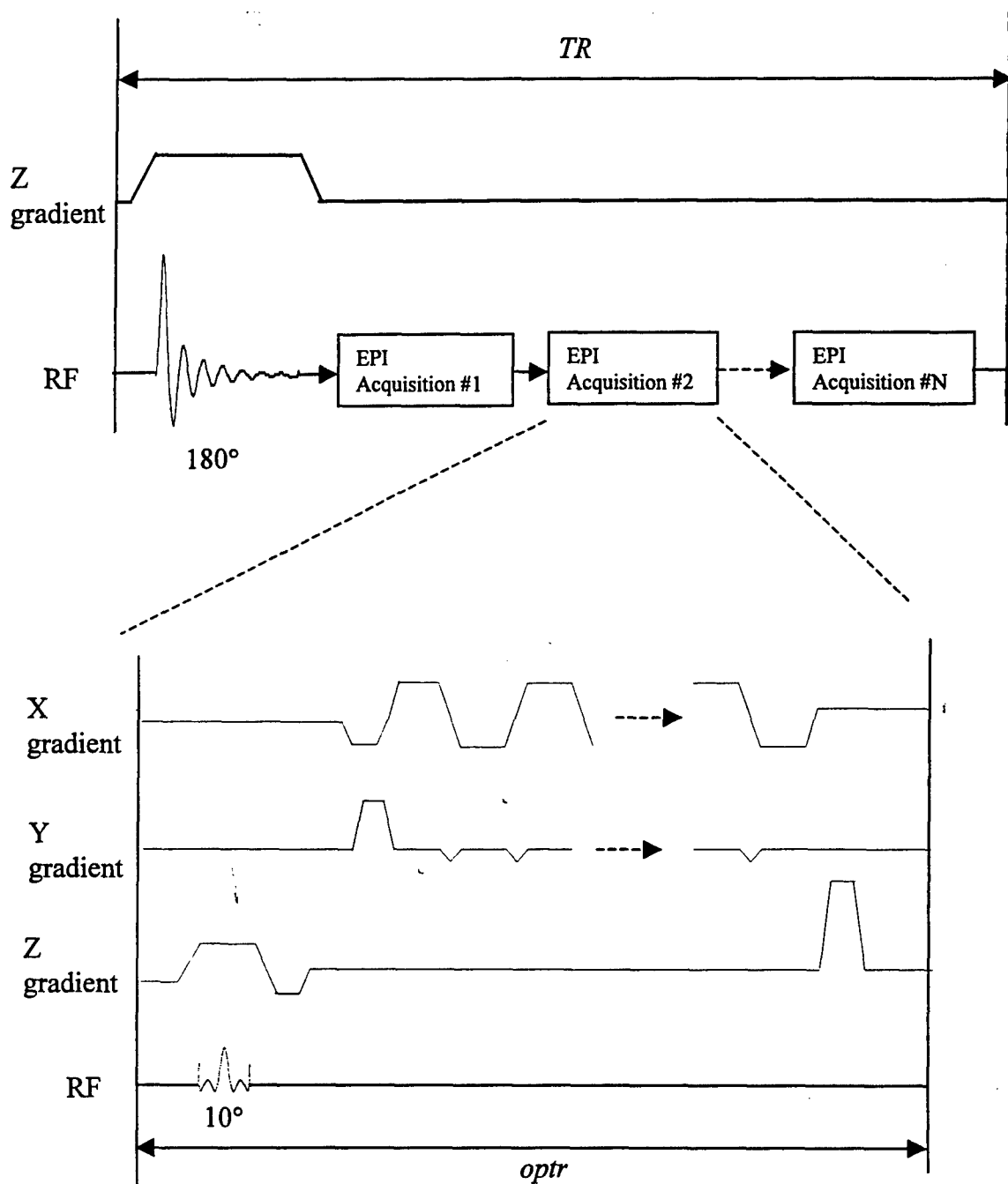
Figure 5.10. The EPI based spin tagging sequence. The odd-number interleave EPI
technique discussed is implemented in data acquisition. The upper figure shows
the timing diagram for each interleave acquisition. An 180° degree RF pulse is
followed by N repeated EPI data acquisitions (as shown in the lower figure).
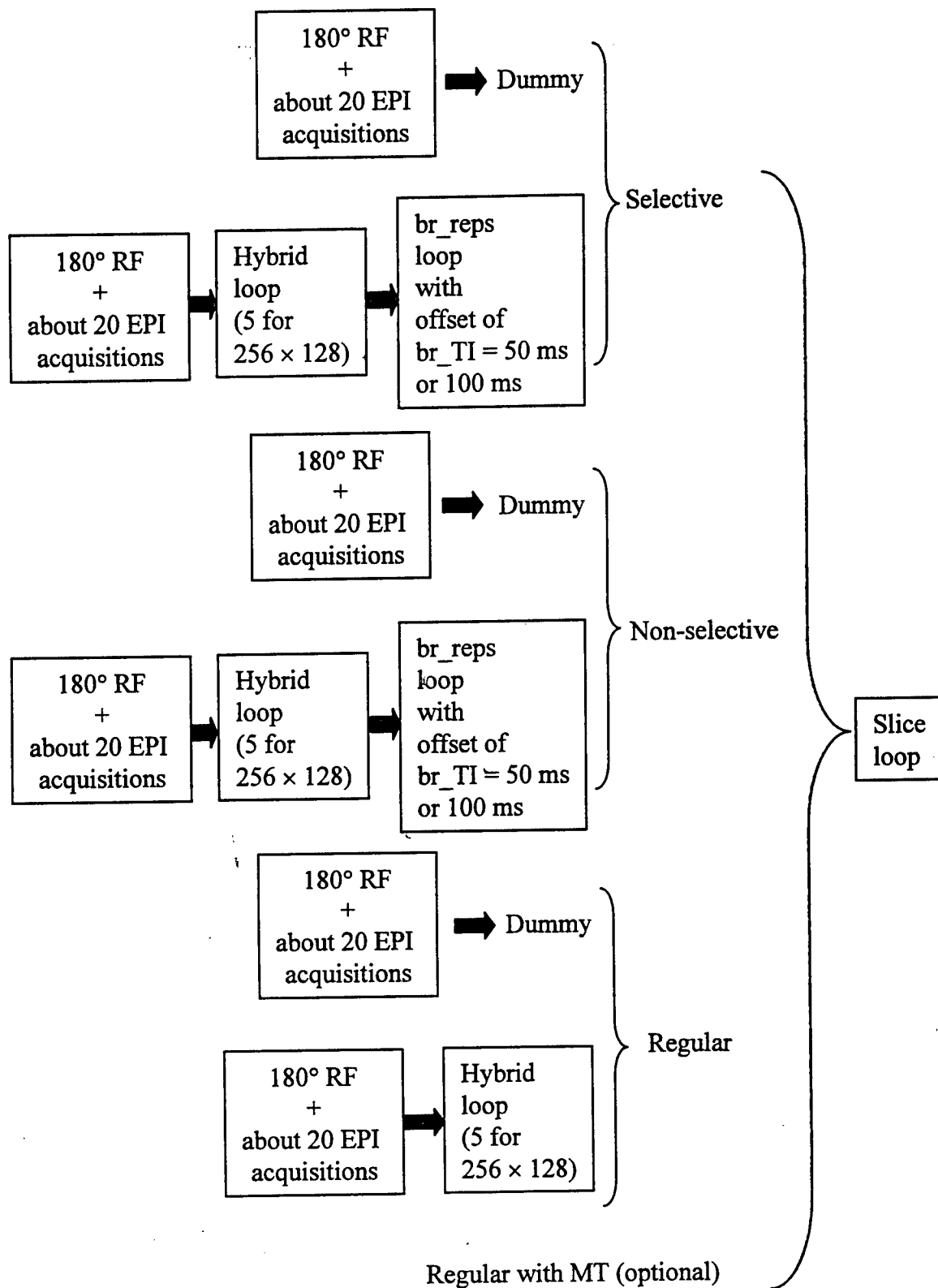
Figure 5.11. The looping technique for the EPI based spin tagging sequence.

The magnetization transfer pulse is a lengthy RF pulse, which could double the *optr* period of the fast SPGR sequence and thus destroy the time constraint of the spin tagging sequence. The magnetization transfer RF pulse selectively excites the spins of the macromolecules such as protein by a 90° flip angle. These spins have a Larmor frequency offset (either lower or higher) from that of spins in water due to the different micro-environments and thus can be selectively excited. Two gradient spoiling pulses in the X and Y directions follow this RF pulse to spoil the transverse magnetization of the spins. The data acquisition RF pulse is applied immediately after the spoiling pulses. Only the spins of water are left to be excited by this RF pulse because longitudinal magnetization of the spins from macromolecules has not yet recovered. The EPI train is followed as in a regular interleaved EPI sequence for data acquisition (Figure 5.12). The amount of magnetization transfer measured is still a relative figure rather than a quantitative one. The Larmor frequency of the spins of the macromolecules can be randomly distributed over a large range around the Larmor frequency of the spins in water. The ability of the magnetization transfer RF pulse and its associated spoiling gradient pulses are also limited in removing the effect of the magnetization transfer completely. Due to hardware problems, this pulse sequence has only been implemented using computer simulation.

This chapter has provided a detailed description on the fast SPGR based and the EPI based arterial spin tagging pulse sequences that were developed and implemented for this dissertation. The design of the optimized RF inversion and data acquisition pulses has also been discussed. The goal is to use these pulse sequences to
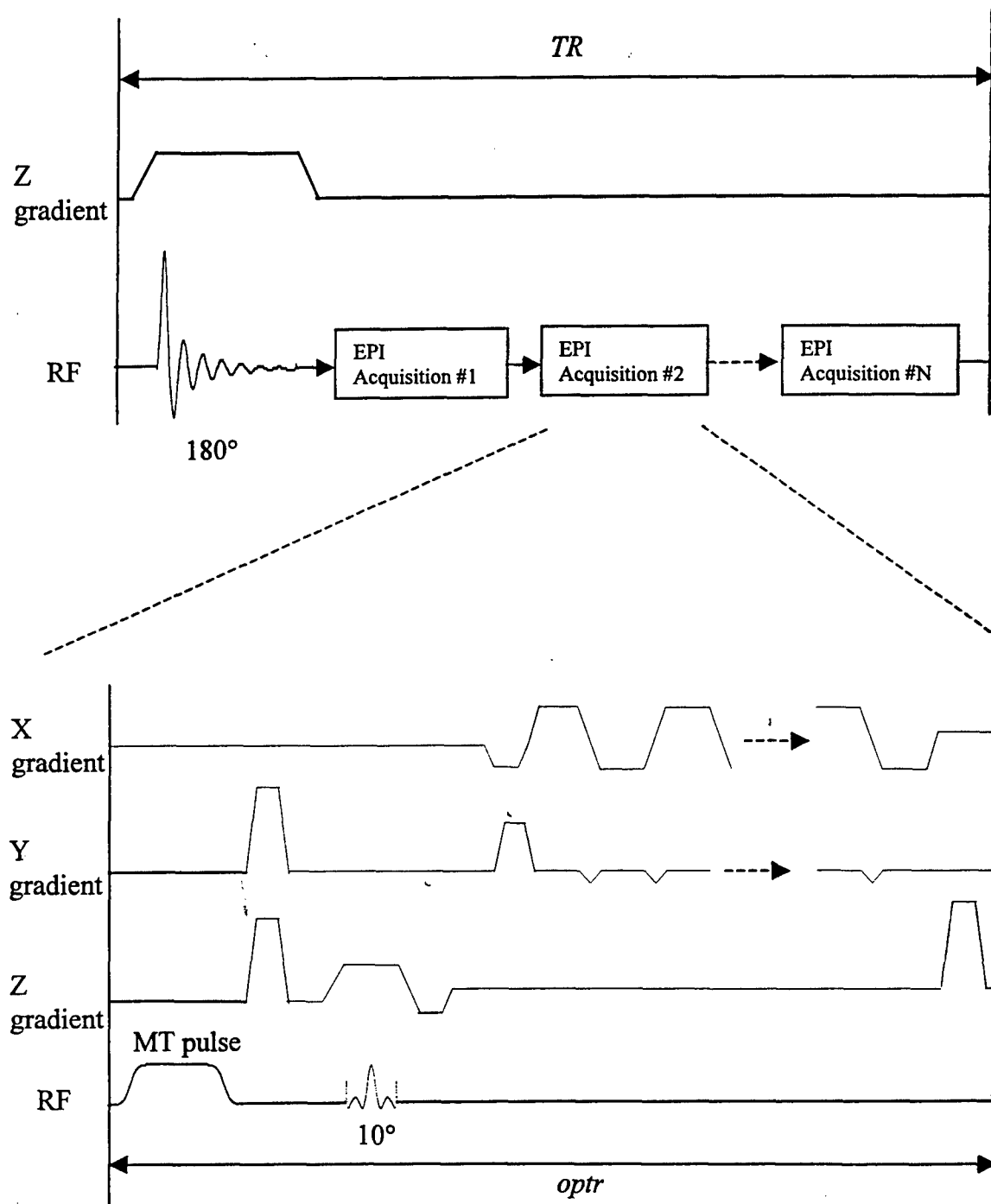
Figure 5.12. The EPI based spin tagging sequence with MT pulses incorporated. The odd-number interleave EPI technique discussed is implemented in data acquisition. The upper figure shows the timing diagram for each interleave at acquisition. A 180° degree RF pulse is followed by N repeated EPI data acquisitions (as shown at the lower figure).

capture the ideal spin recovery after the application of the spin tagging inversion RF

pulse under the Selective or Non-selective tagging condition. The images acquired can

be used to extract the T_1's under the Selective and Non-selective conditions, and then

the perfusion parameter f/λ can be calculated. The techniques of data extraction and

processing will be covered in the next chapter.

Chapter 6

Data Processing Techniques

For each slice location to be analyzed after the necessary images are acquired using the arterial spin tagging sequence, the pixel values across all dynamic images are used to calculate the T_1 value for the corresponding pixel location. This chapter will focus on the discussion of the semi-log linear regression method used to extract the T_1 values from the images. Error-reduction techniques used to support this semi-log linear regression method will also be discussed.

6.1. Semi-log Linear Regression Method for T_1 Calculation

A statistical semi-log linear regression technique has been developed based on the comparison between the signal from undisturbed spins under the Regular condition, and the signal from inverted spins under the Selective or Non-selective condition (Figure 6.1). The b value (the inverse of T_{1s} or T_{1n}) is equal to the negative slope of the regression line. The semi-log linear regression equations, which will be derived, are shown below based on two arbitrary data points (the ith and jth data points) of the T_1 recovery curve:

$$b_s = \frac{1}{T_{1s}} = - \frac{\ln(S_{reg} - S_{sel}(i)) - \ln(S_{reg} - S_{sel}(j))}{TI_{br}(i) - TI_{br}(j)} \qquad (6.1)$$

$$b_n = \frac{1}{T_{1n}} = - \frac{\ln(S_{reg} - S_{non}(i)) - \ln(S_{reg} - S_{non}(j))}{TI_{br}(i) - TI_{br}(j)} \qquad (6.2)$$

The steady-state signal intensity
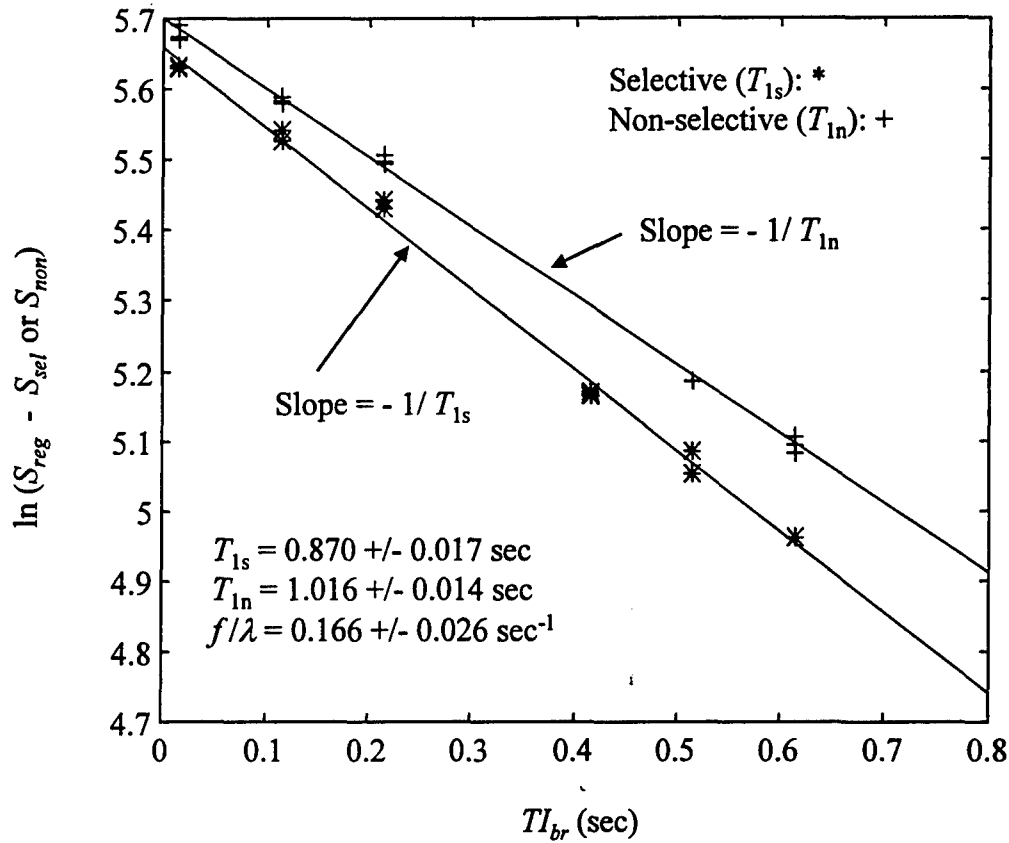difference in log scale at different *TI*

Figure 6.1. An example of semi-log linear regression for T_1 calculation. This figure shows an example of the use of the semi-log linear regression method in calculating T_1 values (T_{1s} at Selective condition, and T_{1n} at Non-selective condition) and the relative perfusion rate f/λ. The calculation results are based on the number of points left after the application of the minimum-mean-square-error technique. TI_{br} is the starting time of image acquisition after the spins are inverted. S_{reg} is the average signal intensity at one pixel from the last three images at the Regular condition. S_{sel} is the signal intensity at one pixel from one of the steady-state images at the Selective condition, S_{non} is the signal intensity at one pixel from one of the steady-state images at the Non-selective condition.

where

S_{reg} = the average signal intensity at a pixel location from the steady-state

images under the Regular condition,

$TI_{br}(i)$ or $TI_{br}(j)$ = the starting time for image data acquisition after spin

inversion at the ith or jth timing condition,

$S_{sel}(i)$ or $S_{sel}(j)$ = the signal intensity at a pixel location for a steady-state image

at the ith or jth timing condition under the Selective condition,

$S_{non}(i)$ or $S_{non}(j)$ = the signal intensity at a pixel location for a steady-state

image at the ith or jth timing condition under the Non-

selective condition.

The value of f/λ is the difference between the inverse of the T_1 values as expressed in

Eq. (4.7), and is restated here:

$$\frac{f}{\lambda} = b_s - b_n \qquad (4.7)$$

The linear regression equations, Eqs. (6.1) and (6.2), are derived below.

In this derivation, the following ideal situation is assumed: The read-out RF

pulse causes such a small flip angle that its continuous application for all the phase-

encoding steps (in either 2D fast SPGR or EPI) does not disturb the natural recovery

of the inverted spins under the tagging conditions and the equilibrium states of the

spins under the non-tagging condition.

Given this assumption, under a spin tagging condition, the steady-state

longitudinal magnetization at the end of each TR period just before the next inversion

pulse can be derived from Eq. (2.34) with flip angle $\alpha = 180°$. The result is:

$$M_{t0ss} = M_0\,(1-e^{-b\,TR}) - M_{t0ss}\,e^{-b\,TR} \qquad (6.3)$$

where,

M_{t0ss} = the steady-state longitudinal magnetization at the end of each TR

period,

M_0 = the longitudinal magnetization under fully relaxed conditions,

$$b = \begin{cases} \dfrac{1}{T_{1s}} & \text{for the Selective condition} \\[2ex] \dfrac{1}{T_{1n}} & \text{for the Non-selective condition} \end{cases} \quad,$$

TR = the repetition time.

Thus,

$$M_{t0ss} = M_0\,\frac{1-e^{-b\,TR}}{1+e^{-b\,TR}} \qquad (6.4)$$

The longitudinal magnetization at time t after the spin inversion at steady-state is

$$\begin{aligned} M_t(t) &= M_0(1-e^{-bt}) - M_{t0ss}e^{-bt} \\ &= M_0(1-e^{-bt}) - M_0\frac{1-e^{-bTR}}{1+e^{-bTR}}e^{-bt} \\ &= M_0(1-e^{-bt} - \frac{1-e^{-bTR}}{1+e^{-bTR}}e^{-bt}) \\ &= M_0(1 - \frac{2e^{-bt}}{1+e^{-bTR}}) \end{aligned}$$

or

$$M_t(t) = M_0(1 - \frac{2e^{-bt}}{1 + e^{-bTR}}) \qquad (6.5)$$

As a result, the signal measured at echo time *TE* is

$$S_t = M_0(1 - \frac{2e^{-bTI}}{1 + e^{-bTR}})\sin(\theta)e^{-\frac{TE}{T2}} \qquad (6.6)$$

where,

  TI = the time between the inversion pulse and the effective center of k space,

  TE = the time of echo at each read-out period,

  θ = the read-out RF flip angle.

  Under the spin non-tagging condition (Regular condition), based on the given assumption, the longitudinal magnetization $M_{reg}(t)$ at any time t stays at equilibrium. Specifically,

$$M_{reg}(t) = M_0 \qquad (6.7)$$

The signal measured at echo time *TE* becomes

$$S_{reg} = M_0 \sin(\theta)e^{-\frac{TE}{T2}} \qquad (6.8)$$

Thus,

$$\frac{S_t}{S_{reg}} = 1 - \frac{2e^{-bTI}}{1 + e^{-bTR}} \qquad (6.9)$$

Then,

$$1 - \frac{S_t}{S_{reg}} = \frac{2e^{-bTI}}{1 + e^{-bTR}}$$

or

$$\frac{S_{reg} - S_t}{S_{reg}} = \frac{2e^{-bTI}}{1 + e^{-bTR}}$$

Thus,

$$\frac{S_{reg} - S_t(i)}{S_{reg} - S_t(j)} = \frac{e^{-bTI(i)}}{e^{-bTI(j)}}$$
$$= e^{-b(TI(i) - TI(j))}$$

(6.10)

where,

$TI(i)$ = the time of inversion at the ith TI cycle,

$S_t(i)$ = the signal at a pixel when $TI(i)$ is used,

$TI(j)$ = the time of inversion at the jth TI cycle,

$S_t(j)$ = the signal at a pixel when $TI(j)$ is used.

Then,

$$\ln(S_{reg} - S_t(i)) - \ln(S_{reg} - S_t(j)) = -b(TI(i) - TI(j))$$

Thus,

$$b = -\frac{\ln(S_{reg} - S_t(i)) - \ln(S_{reg} - S_t(j))}{TI(i) - TI(j)}$$

(6.11)

The above equation shows the semi-log linear regression relationship between (S_{reg} - S_t) and TI. It can be applied to both Selective and Non-selective tagging conditions. The exact locations of the effective TIs are uncertain, but they should contain the same amount of shift from their apparent positions (the times from the spin inversion to the starting point of data acquisition). Because of the subtraction of $TI(i)$ and $TI(j)$, the uncertainty of the effective TI is cancelled out. Therefore, the $TI(i)$ and $TI(j)$ in Eq.

(6.11) can be replaced with $TI_{br}(i)$ and $TI_{br}(j)$, which have been defined in Eqs. (6.1) and (6.2). Then Eq. (6.11) becomes

$$b = -\frac{\ln(S_{reg} - S_t(i)) - \ln(S_{reg} - S_t(j))}{TI_{br}(i) - TI_{br}(j)} \qquad (6.12)$$

Eq. (6.12) can be expanded to a higher level of detail. The result is Eqs. (6.1) and (6.2) that have been stated in the early part of this chapter, and can be restated below:

$$b_s = \frac{1}{T_{1s}} = -\frac{\ln(S_{reg} - S_{sel}(i)) - \ln(S_{reg} - S_{sel}(j))}{TI_{br}(i) - TI_{br}(j)} \qquad (6.1)$$

$$b_n = \frac{1}{T_{1n}} = -\frac{\ln(S_{reg} - S_{non}(i)) - \ln(S_{reg} - S_{non}(j))}{TI_{br}(i) - TI_{br}(j)} \qquad (6.2)$$

Eq. (6.1) also allows for the elimination of the effect of the geometric mismatch between the inversion and data acquisition slice profiles on T_{1s} calculation. The RF excitation pulses used for the spin inversion and the data acquisition are different. Under the Selective condition, geometric mismatch occurs between the inversion and data acquisition slice profiles. (Under the Non-selective condition, this is not a problem because the RF inversion pulse inverts spins everywhere.) Eq. (6.1) can be used to address this problem as discussed below:

The geometric mismatch between the inversion and read-out profiles can lead to signal contamination by signal from non-inverted spins. Thus the apparent signal from the Selective condition can be modeled as

$$S_{sel_{app}} = (1 - err) \cdot S_{sel} + err \cdot S_{reg} \qquad (6.13)$$

where,

$S_{sel_{app}}$ = the signal of the same pixel actually measured,

S_{sel} = the signal of a pixel if there is no slice profile mismatch,

err = the fraction of error due to slice profile mismatch.

Then,

$$\frac{S_{sel_{app}}}{S_{reg}} = (1 - err)\frac{S_{sel}}{S_{reg}} + err$$

And

$$\frac{S_{sel}}{S_{reg}} = \frac{\dfrac{S_{sel_{app}}}{S_{reg}} - err}{1 - err}$$

$$1 - \frac{S_{sel}}{S_{reg}} = 1 - \frac{\dfrac{S_{sel_{app}}}{S_{reg}} - err}{1 - err}$$

$$\frac{S_{reg} - S_{sel}}{S_{reg}} = \frac{1 - err - \dfrac{S_{sel_{app}}}{S_{reg}} + err}{1 - err}$$

$$= \frac{1 - \dfrac{S_{sel_{app}}}{S_{reg}}}{1 - err}$$

Thus,

$$\frac{S_{reg} - S_{sel}(i)}{S_{reg} - S_{sel}(j)} = \frac{1 - \dfrac{S_{sel_{app}}(i)}{S_{reg}}}{1 - \dfrac{S_{sel_{app}}(j)}{S_{reg}}}$$

$$= \frac{S_{reg} - S_{sel_{app}}(i)}{S_{reg} - S_{sel_{app}}(j)} \qquad (6.14)$$

Comparing with Eq. (6.10), we have

$$\frac{S_{reg} - S_{sel_{app}}(i)}{S_{reg} - S_{sel_{app}}(j)} = e^{-b_s \cdot (TI(i) - TI(j))}$$

where,

$$b_s = \frac{1}{T_{1s}} = \frac{1}{T_1} + \frac{f}{\lambda} = \text{the } b \text{ value under the Selective condition}.$$

Thus,

$$b_s = \frac{\ln(S_{reg} - S_{sel_{app}}(i)) - \ln(S_{reg} - S_{sel_{app}}(j))}{TI(i) - TI(j)}$$

$$= \frac{\ln(S_{reg} - S_{sel_{app}}(i)) - \ln(S_{reg} - S_{sel_{app}}(j))}{TI_{br}(i) - TI_{br}(j)} \qquad (6.15)$$

Eq. (6.15) corresponds exactly to Eq. (6.1). In other words, by using the semi-log

linear regression method, the problem due to geometric mismatch between the

inversion and read-out slice profiles is eliminated. For simplicity of the notations, the

subscript "*app*" has not been used in Eqs. (6.1) and (6.2), but the S_{sel} and S_{non} in these

two equations actually represent the apparent signals at a pixel.

6.2. Error-Reduction Techniques for T_1 Calculation

Error-reduction techniques that are based on three different approaches have

been used to support the semi-log linear regression method for T_1 calculation. These

approaches involve the elimination of the uncertain data points, pixel averaging, and minimum mean-square-error optimization.

Elimination of uncertain data points during data processing is considered first. In the fast SPGR based spin tagging pulse sequence, four images are acquired in each of the seven TI cycles. The last three images have achieved steady state and are extracted for the linear regression calculation. This is the case for the Selective and Non-selective conditions, thus, there are a total of 21 points for the calculation of T_{1s} or T_{1n}. Five images are acquired under the Regular condition. Similarly, the last three images have achieved steady state and are extracted for the linear regression calculation. All images acquired are represented as magnitude images, but the actual signal under the zero line of the T_1 recovery curve is negative (Figure 4.3). These image signals must be negated in order to use the above equations. The three points (acquired at a same TI) that are located the closest to the zero value are usually eliminated because it is difficult to decipher whether these points are above or below the zero line. As a result, a total of 18 points contribute to the calculation of T_1.

The T_1 and f/λ calculations based on this pulse sequence are very sensitive to noise, especially displacement artifacts. Thus the second and third error-reduction techniques are the noise-reduction techniques that have been implemented to reduce this problem. For the second technique, the resolution of each image is reduced from 256×256 to a lower resolution, for example, 64×64, by pixel averaging. This helps to reduce white noise as well as the effect of possible small object displacement among the 61 images being analyzed.

For the third error-reduction technique, an approach with minimum-mean-square-error optimization is used for the calculation of T_1 values. A maximum of five noisy data points can be eliminated to maximize T_1 calculation precision, and to avoid inaccuracy caused by over-elimination of data points (Figure 6.2). The algorithm can be outlined as following:

1. Start with all 18 points.
2. Calculate the b value $(1/T_1)$ and its standard deviation, the slope and the Y axis-intercept of the line.
3. If the number of points used for calculation is equal to 13, or the standard deviation of the b value is greater than the previous one calculated, stop and go to Step 7, else continue.
4. Calculate the distance between the line and each of the points.
5. Eliminate the point with the maximum distance.
6. Go to Step 2.
7. Output the b value and its standard deviation.
8. End.

The algorithm presented above is used to ensure that a data point containing excessive noise is not used for T_1 calculation. However, there is a limit to the number of points that can be eliminated, since over elimination can lead to bias calculation. Here, a maximum of five points can be eliminated: three points from an undesirable TI timing condition can be eliminated and two noisy points from other TI timing conditions can also be eliminated.

For the EPI based spin tagging pulse sequence, steady state is not a concern in the T_1 calculation because all dynamic data is acquired after a single RF inversion pulse. All dynamic pixel signals measured after the inversion pulse, except the one or two points closest to the zero line, are used for the T_1 calculation. Therefore, the above approaches can also be used but in this case will include more data points.
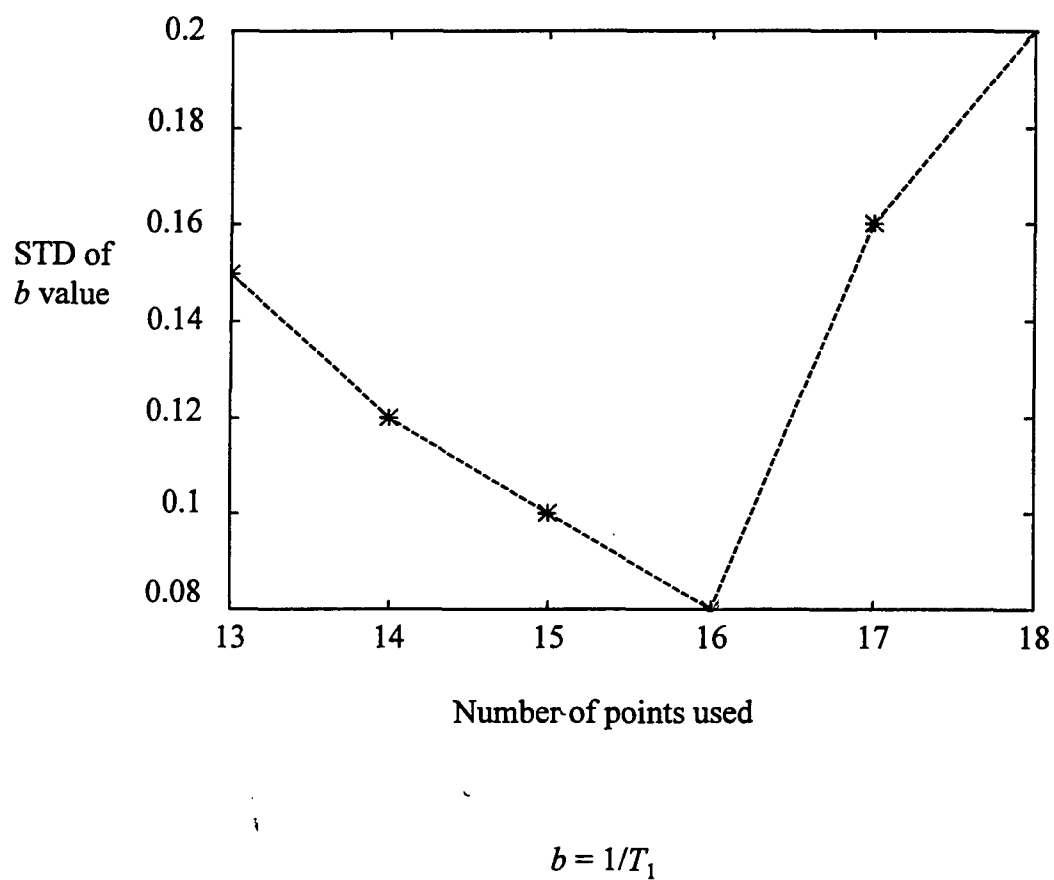
$$b = 1/T_1$$

Figure 6.2. The minimum-mean-square-error approach to find the optimal solution for the T_1 values.

This chapter has focused on the discussion of the semi-log linear regression method used to extract the T_1 values from the images. Error-reduction approaches (the elimination of the uncertain data points, pixel averaging and minimum mean-square-error) have been used to support this semi-log linear regression method. The semi-log linear regression method has been evaluated and compared to the traditional zero-crossing method, which determines the T_1 value based on the zero-crossing point of the T_1 recovery curve, and the curve fitting technique based on the exponential nature of the T_1 recovery. Neither the zero-crossing method nor the curve fitting technique has been able to provide an accurate T_1 calculation due the uncertainty of the effective TI values and the RF slice profiles geometric mismatch that have been discussed earlier in this chapter. The performance of the semi-log linear regression method, along with the three error-reduction approaches, is clearly superior to the zero-crossing and curve fitting techniques. Thus the semi-log linear regression method and the three error-reduction approaches are applied to all the data used in this work.

In the following chapter, an image processing technique that was used to further improve the T_1 calculation accuracy through object displacement artifact reduction will be discussed. Additionally, image visualization and analysis techniques that allow for the application of the calculation results, which obtained from the data processing techniques presented in this chapter, to breast cancer detection will be presented.

Chapter 7

Image Processing Techniques

Motion artifacts are always problematic for dynamic images collected over a period of time. How should they be corrected? After the T_{1s}, T_{1n}, and f/λ values have been calculated for the slices being investigated, how can they be visualized in a clear manner? How can these values be used to aid clinicians in making better decisions in identifying cancerous regions? In this chapter, techniques developed to solve these problems are discussed.

7.1. Binary Segmentation Technique for Displacement Artifact Correction

An important image processing technique that has been developed in this project reduces the displacement artifacts that can cause inaccuracies in T_1 calculations. Both breast objects (referring to the two objects seen on each individual image) are expected to be in the same relative position for all images acquired at one slice location. Unfortunately, the relative position of the breast objects might change during the three-minute scan in the fast SPGR based spin tagging pulse sequence. Researchers would like to know the amount of displacement and correct it when necessary. A typical breast perfusion study generates 61 images at each slice location, and 10 locations are analyzed, giving a total of 610 images. Due to the large number of images, an algorithm requiring intensive computation to estimate and correct object displacement is not appropriate. A fast and effective technique is needed. This goal has been achieved by estimating dislocation based on binary segmentation of the 61

images acquired from a typical breast study using the fast SPGR based spin tagging sequence. When the EPI based spin tagging sequence is used, the images are collected in much less time, and motion artifacts become less problematic. The displacement artifact correction technique presented here can still be applied to these images as well as be generalized to other types of dynamic studies.

Knowledge about a dynamic study usually can help to improve the accuracy and efficiency of image processing, and certainly reduces the complexity of the algorithm design. During scanning, the subject is restricted on the scanner table, and thus rotation of the breasts is virtually impossible. Only lateral displacement in the X and Y directions needs to be considered. Fortunately the displacement is not large, most likely within a range of +/-1 cm. The approximate shapes, sizes and positions of the objects are known. Although signal intensity varies greatly from one image to another, with some images having poor object-background separation, the breast objects are still separable from the background. This knowledge leads to the implementation of a binary segmentation technique discussed below.

The 61st image is obtained at the steady state of the Regular condition, and is proton-density weighted. It has a good object-background separation and thus binary segmentation is clean, so it is used as the reference. A threshold is easily chosen for the reference image to separate the objects from their background. Based on this threshold, almost all the pixels on the breast objects are labeled as ones and almost all the pixels on the background are labeled as zeros. In this way, a good reference

segmentation image is created. For all other 60 images, once a threshold is determined as discussed in the next paragraph, binary segmentation images are created similarly.

Since the reference image has a very clean object-background separation, the total number of pixels in the two breast objects (population of object pixels) is approximately equal to the mass of the binary segmentation image (or the total number of ones). When one of the other 60 images is analyzed, a histogram of pixel values is created first. The pixel value that separates the populations of object and background pixels is the threshold used for binary segmentation [51].

Cross correlation is done between the segmentation image to be realigned and the reference segmentation image. Maximum cross correlation occurs when the two images overlap. Since the range of breast object displacement is short, only a local cross correlation is needed (Figure 7.1). This greatly reduces the computation time. This also takes advantage of the fact that the pixel values at the outer parts of the objects can be separated better from their backgrounds than those at the inner parts of the objects.

To further speed up the computation, two iterations are used to compute the cross correlation:

Range of computation: -10 to 10 pixels in both X and Y directions,
Iteration # 1: -8, -4, 0, 4, 8,
Iteration # 2: -2, -1, 0, 1, 2.

The displacement estimation and correction algorithm was implemented using the C language and was evaluated on an SGI O2 (195 MHz, MIPS, R10000) workstation. For the analysis of the 61 images, the run time was 2.2 minutes.
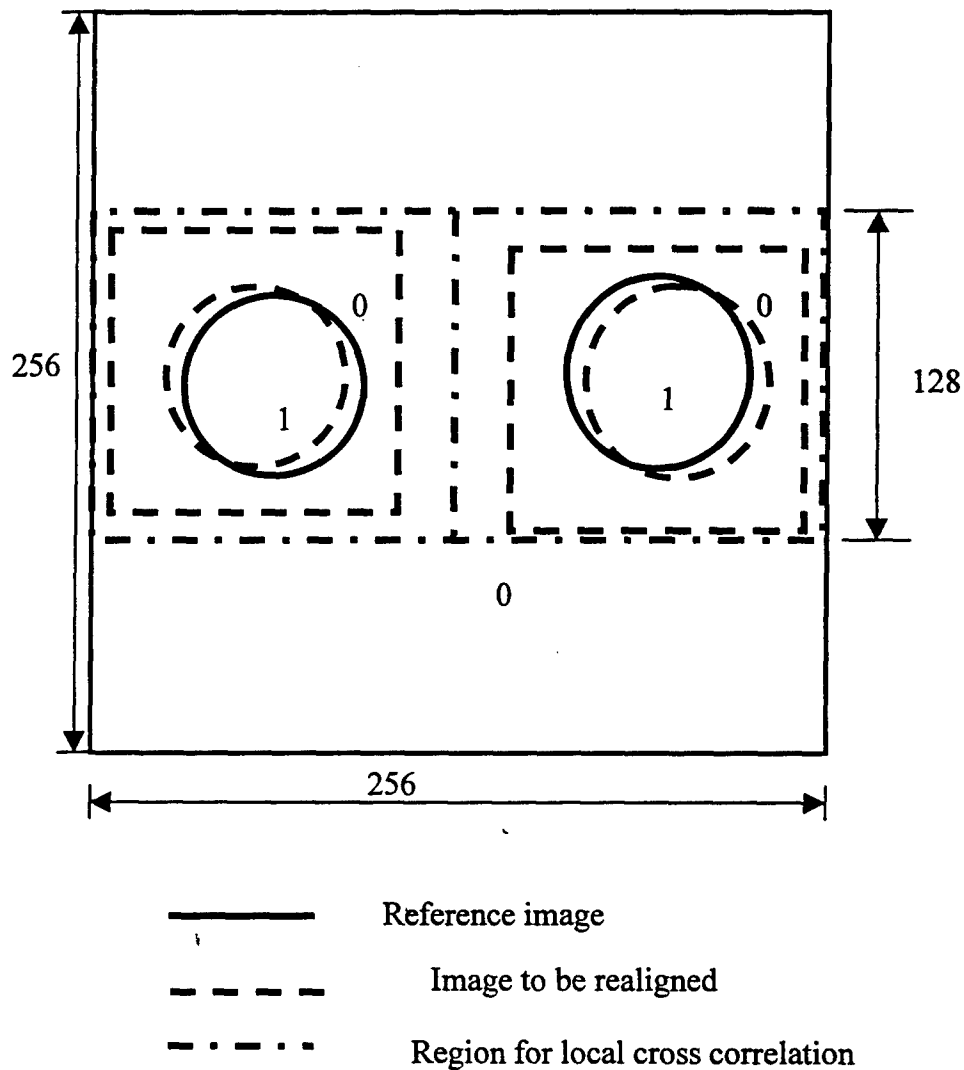
Figure 7.1. Object displacement estimation based on local cross correlation. Local cross correlation is performed between the binary image for realignment against the reference binary image. The maximum correlation occurs when two objects overlap.

Figure 7.2 shows the displacement correction applied to an artificially introduced displacement. The average mis-calculation of object displacement was 0.39 pixel. This result was found to be superior to the edge-detection technique and other binary segmentation techniques that had been attempted by the author. Since the threshold is automatically determined, this technique has high portability.

7.2 Image Visualization and Segmentation

After the necessary displacement correction, the values of T_{1s}, T_{1n} and f/λ at different pixel locations on each slice can be calculated based on the semi-log linear regression technique. Images can be formed based on these values. They are called feature images because they represent the characteristics of breast tissue. The most useful feature images for tissue characterization are the T_1 image based on the T_{1n} values in the units of sec, the perfusion image based on the f/λ values in the units of sec^{-1} and the error perfusion image based on the standard deviations of the f/λ values also in the units of sec^{-1}. These feature images contain pixels with a wide range of values. But the values of T_1, f/λ and the standard deviation of f/λ of breast tissues should be within reasonable ranges. Pixel values below or above certain values are not useful and can be misleading. To display these feature images, an appropriate positive shift, scaling and window size should be applied (Figure 7.3) [52]. Linear scaling is applied to preserve the characteristics of the data. The details of these manipulations are shown in Table 7.1 below:
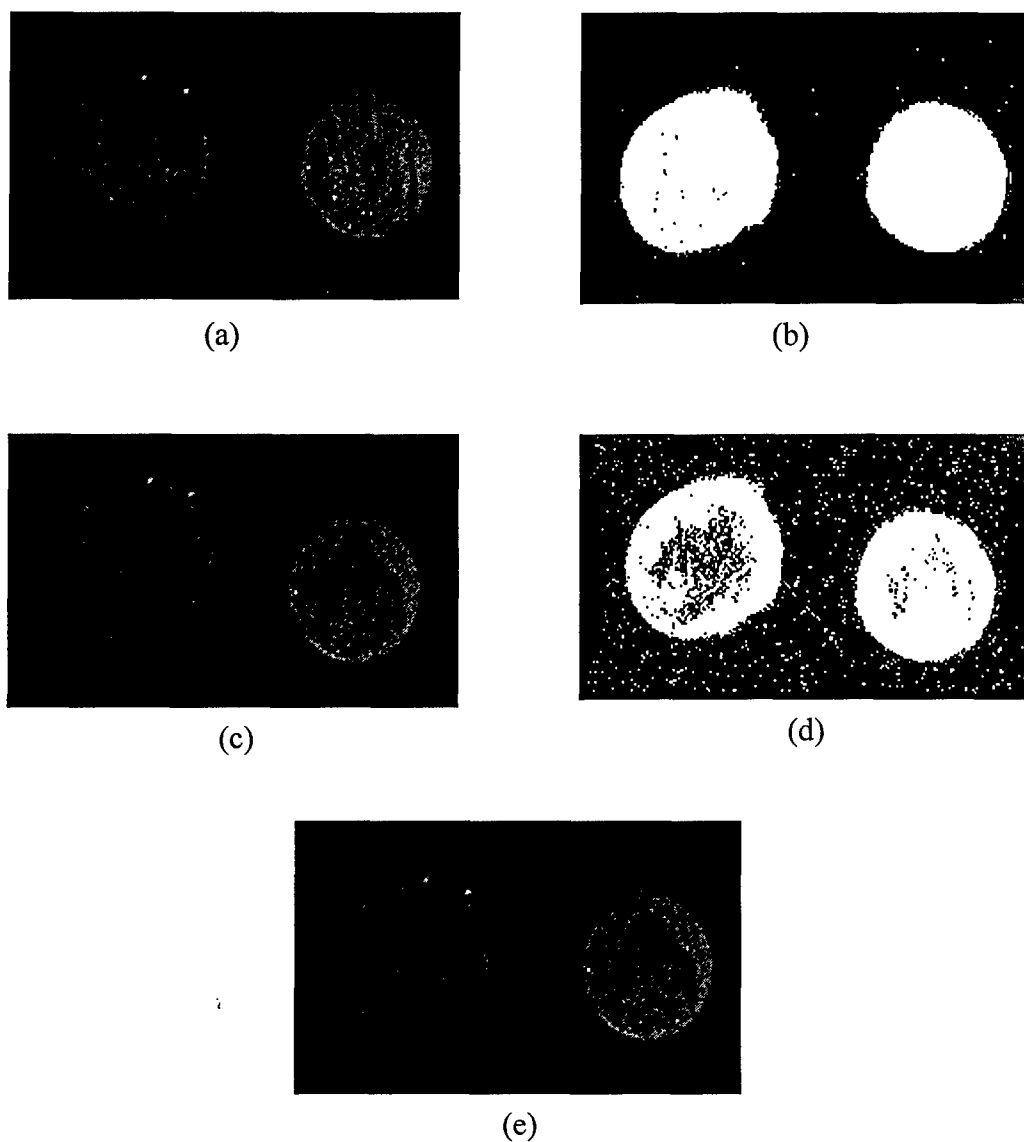
Figure 7.2. Displacement restoration based on binary segmentation. (a) Reference (Image 61). (b) The segmented binary image of Figure (a) with threshold 100. (c) Displacement was artificially introduced to Image 8. The left object was shifted to the right by four pixels and shifted up by five pixels. The right object was shifted to the left by six pixels and shifted down by six pixels. (d) The segmented binary image of Figure (c) with threshold 70. (e) The restored image of Figure (c).
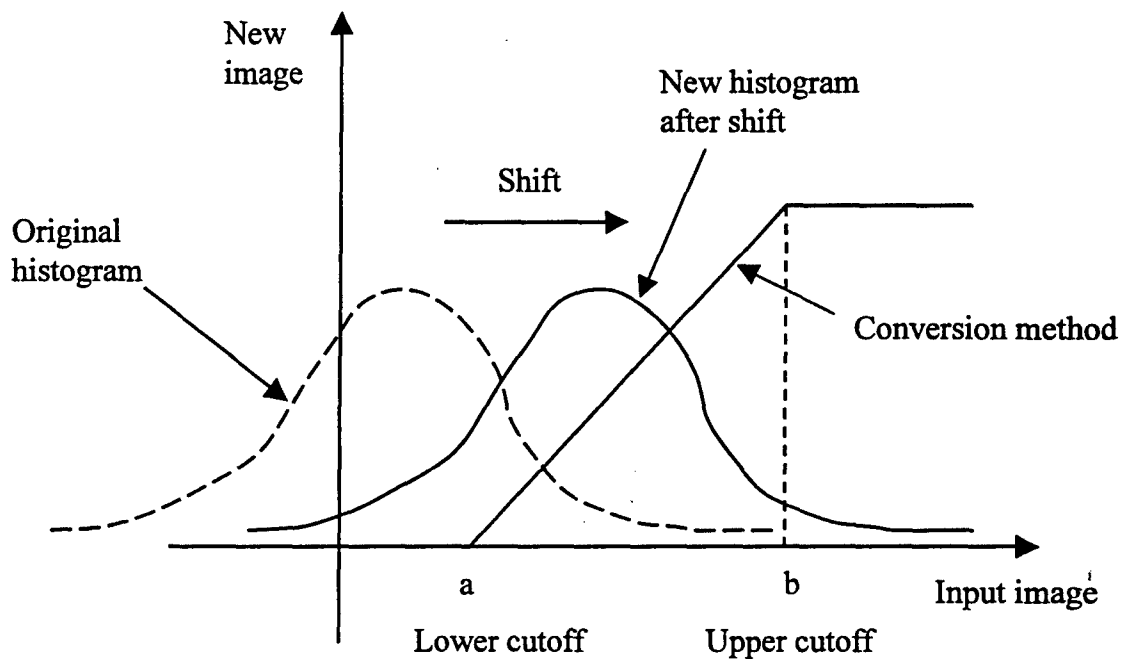
Figure 7.3. Feature image display conversion. Before a feature image is displayed, it needs to be processed to provide a meaningful display range and a reasonable contrast level by contrast stretching with appropriate cutoff, offset shift and scaling.

Table 7.1. The Contrast Stretching Parameters Used for the
Display of the Three Feature Images

Feature images	T_1 image (sec)	f/λ image (sec^{-1})	STD of f/λ image (sec^{-1})
Possible range of values	from 0 to 4	from -4 to 4	from -5 to 5
Range of interest	from 0 to 1.5	from -0.5 to 0.8	from -0.5 to 0.5
Positive shift	0	0.5	0.5
Upper cutoff	1.5	0.8	0.5
Lower cutoff	0	-0.5	-0.5
Scaling factor	1000	1000	1000

A visualization computer program called BreastView has been developed by the author on an SGI workstation based on C language, X Window System and Motif 1.2. This program will be used to interpret these three feature images for the recognition of suspicious cancer regions. Since a sizable tumor extends to several pixels, these pixels should have similar tissue characteristics. Specifically, they should have high T_1 values that are approximately equal to each other, and high perfusion rates. When a pixel is found to have a high T_1 and a high f/λ, and the standard deviation of the f/λ is low, its surrounding pixels within the same slice and across slices would be checked to see if they have similar characteristics. The level of suspicion for this pixel is calculated based on the percentage of its surrounding pixels (including this central pixel) containing the similar suspicious characteristics. For a pixel on an edge slice, there is a total of 18 pixels to check; otherwise, there is a total of 27 pixels to check. By applying this method to all pixels in all slices, maps of suspicion are created. If the pixel has a total level of suspicion exceeding a cutoff

value, such as 20%, this pixel would be identified as a cancer pixel. The goal is to develop an analytical tool for breast cancer detection. The exact cutoff will depend on the judgement of researchers and clinicians. The suspicion level cutoff, as well as the cutoffs for f/λ, T_1 and the standard deviation of f/λ should be obtained based on a large set of studies. Based on the small set of studies that have been done, the approximate cutoffs that can be used to identify cancer pixels are listed:

T_1: > 0.5 sec
f/λ: > 0.1 sec^{-1}
STD of f/λ: < 0.1 sec^{-1}.
Suspicion level threshold: > 20 %.

Researchers will be able to use the BreastView program to manipulate the above cutoffs and to observe the change of the suspicion maps. This visualization program can simultaneously display the feature images and clinical images. Parameters T_1, f/λ, and the standard deviation of f/λ at any pixel location of the breast objects can be found by a simple click of the mouse. If a dynamic contrast enhancement study has been done, a click of the mouse can also activate the program to plot the dynamic change of signal intensity at this location. The suspicious cancer pixels can also be mapped to high-resolution traditional clinical images (256×256), which are always acquired for comparison during each subject study. This mapping provides a radiologist with the traditional view of the breast images with the suspicious cancer regions identified. BreastView is designed to allow easy pixel cross-registration and comparison between results from different MR imaging techniques. This would provide rich information for clinicians in making more accurate decisions.

Appendix B provides more detail information on the installation and operation of this program.

Images from a patient with a suspicious mass found by palpation in her right breast were used to verify the image processing methods presented. Figure 7.4 shows the three feature images created along with an image acquired under the Regular condition of the breast sequence for comparison. All three feature images have the resolution of 64×64. The T_1 image has a good SNR. It clearly defines the distribution of T_1 values on the slice. The brighter areas at the inner regions of the breasts indicate higher T_1 values and thus higher water content. This perfusion image appears to have a good SNR though sometimes the perfusion image is quite noisy. This happens because the intensity of the white noise is within the range of the f/λ values. A pixel would not stand out unless it had a very high f/λ value. For both the T_1 and the perfusion images, some pixels at the edge of the breasts have a high intensity, but they are just edge artifacts due to high calculation error at the edges. Since pixel values at the edges are sensitive to breast object displacement as well as ringing artifacts, high calculation error can happen at these pixels. The error levels of the f/λ calculation can be found on the error perfusion image. Pixels with low T_1 values generally contain more error in the calculation of perfusion because the equations (Eqs. (6.1) and (6.2)) used for the calculation of perfusion are more sensitive to the fluctuation of T_1 at low T_1 values. Fortunately, this does not cause much trouble because cancer tissue should have relatively high T_1 values (> 500 ms).
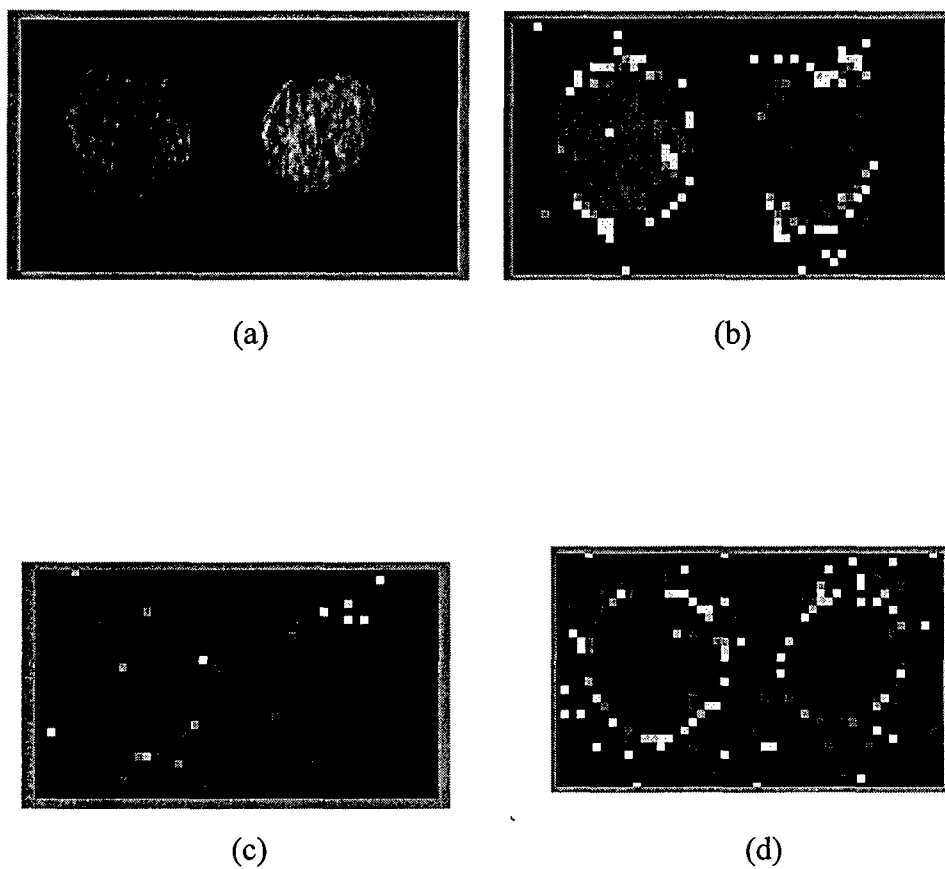
Figure 7.4. Three feature images derived for one slice location in one subject study. (a) The last image under the Regular condition is displayed for comparison. The three feature images are (b) the T_1 image, (c) the perfusion image based on f/λ, and (d) the error perfusion image based on the standard deviation of f/λ.

Figure 7.5 shows the mapping of suspicious cancer pixels onto high-resolution traditional clinical images according to the methods discussed. The suspicious regions identified by the pure white pixels on the right breasts in Slices 6, 7 are considered one connected region. These pure white pixels are actually red in the visualization program BreastView. This suspicious region is at, or right next to, the benign mass that appears bright in both clinical images. The malignancy of this suspicious region was later confirmed by needle biopsy. In general, for positive identification of cancer, these suspicious regions identified in the breast sequence should be compared with traditional clinical MR images, as well as X-ray mammography and ultrasound images. It is often unclear whether abnormal masses found by palpation, traditional MRI and X-ray mammography are malignant or not. Suspicious cancer regions identified by this method provide important information in confirming the malignancy of the abnormal masses.

7.3. Bayesian Technique and ROC

The suspicious cancer pixel identification based on thresholds provides the basic approach for cancer recognition in this work. The number of cases studied here is limited. However, if a large pool of case studies is available, the Bayesian decision technique [53] in cancer identification can be applied. The Bayesian technique to be discussed can be extended to the ROC (receiver operating characteristic) curve that is commonly used for the evaluation of a diagnostic algorithm in radiology.
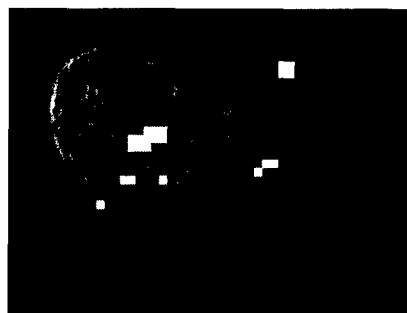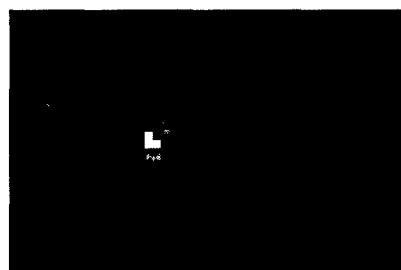
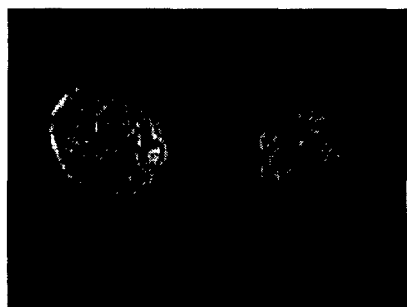Proton Density Weighted, Slice 6 T_2 Weighted, Slice 6
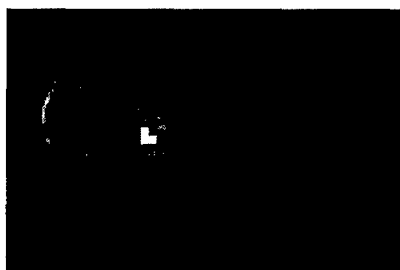
Proton Density Weighted, Slice 7 T_2 Weighted, Slice 7

Proton Density Weighted, Slice 8 T_2 Weighted, Slice 8

Figure 7.5. Suspicious cancer region color mapping. The identified suspicious cancer pixels are mapped onto the high-resolution traditional clinical MR images according to their corresponding slice locations. These images are from three consecutive 3mm slices with inter-slice distance of 10 mm. The pure white mapping pixels are actually red in the visualization program BreastView.

This Bayesian technique can be outlined as follows:

Let vector space $\mathbf{x} = (T_1, f/\lambda, \text{STD of } f/\lambda)$ for a ROI (region of interest) in a

breast. The risks associated with a given vector $\mathbf{x}$ are

$$\text{Risk(Label Benign} \mid \mathbf{x}) = r(\text{Label Benign} \mid \text{Malignant}) P(\text{Malignant} \mid \mathbf{x})$$
$$+ r(\text{Label Benign} \mid \text{Benign}) P(\text{Benign} \mid \mathbf{x}) \qquad (7.1)$$

$$\text{Risk(Label Malignant} \mid \mathbf{x}) = r(\text{Label Malignant} \mid \text{Malignant}) P(\text{Malignant} \mid \mathbf{x})$$
$$+ r(\text{Label Malignant} \mid \text{Benign}) P(\text{Benign} \mid \mathbf{x}) \qquad (7.2)$$

where,

Risk(Label Benign | $\mathbf{x}$) = the risk value to label a ROI "Benign" for a given $\mathbf{x}$,

Risk(Label Malignant | $\mathbf{x}$) = the risk value to label a ROI "Malignant" for a

given $\mathbf{x}$,

r(Label Benign | Malignant) = the risk factor to label a ROI "Benign" but

actually be malignant,

r(Label Benign | Benign) = the risk factor to label a ROI "Benign" and actually

be benign,

r(Label Malignant | Malignant) = the risk factor to label a ROI "Malignant"

and actually be malignant,

r(Label Malignant | Benign) = the risk factor to label a ROI "Malignant" but

actually be benign,

P(Malignant | $\mathbf{x}$) = the probability of being malignant for a given $\mathbf{x}$,

P(Benign | $\mathbf{x}$) = the probability of being benign for a given $\mathbf{x}$.

Generally there is not any risk for correct labeling, and thus

$$r(\text{Label Benign} \mid \text{Benign}) = 0$$

and

$$r(\text{Label Malignant} \mid \text{Malignant}) = 0$$

Then Eq. (7.1) and (7.2) become

$$\text{Risk}(\text{Label Benign} \mid \mathbf{x}) = r(\text{Label Benign} \mid \text{Malignant}) \, P(\text{Malignant} \mid \mathbf{x}) \qquad (7.3)$$

$$\text{Risk}(\text{Label Malignant} \mid \mathbf{x}) = r(\text{Label Malignant} \mid \text{Benign}) \, P(\text{Benign} \mid \mathbf{x}) \qquad (7.4)$$

Since,

$$P(\text{Malignant} \mid \mathbf{x}) = \frac{p(\mathbf{x} \mid \text{Malignant}) P(\text{Malignant})}{p(\mathbf{x})} \qquad (7.5)$$

and

$$P(\text{Benign} \mid \mathbf{x}) = \frac{p(\mathbf{x} \mid \text{Benign}) P(\text{Benign})}{p(\mathbf{x})} \qquad (7.6)$$

where,

$p(\mathbf{x} \mid \text{Malignant})$ = the probability density of vector $\mathbf{x}$ given that the ROI is

malignant,

$P(\text{Malignant})$ = the probability of being malignant for a ROI

$p(\mathbf{x} \mid \text{Benign})$ = the probability density of vector $\mathbf{x}$ given that the ROI is benign,

$P(\text{Benign})$ = the probability of being benign for a ROI,

$p(\mathbf{x})$ = the probability density of vector $\mathbf{x}$.

$$\text{Risk Ratio} = \frac{\text{Risk(Label Benign} \mid \mathbf{x})}{\text{Risk(Label Malignant} \mid \mathbf{x})}$$

$$= \frac{r(\text{Label Benign} \mid \text{Malignant}) \, P(\text{Malignant} \mid \mathbf{x})}{r(\text{Label Malignant} \mid \text{Benign}) \, P(\text{Benign} \mid \mathbf{x})} \qquad (7.7)$$

$$= \frac{r(\text{Label Benign} \mid \text{Malignant})}{r(\text{Label Malignant} \mid \text{Benign})} \, \frac{p(\mathbf{x} \mid \text{Malignant})}{p(\mathbf{x} \mid \text{Benign})} \, \frac{P(\text{Malignant})}{P(\text{Benign})}$$

The ratio $\dfrac{r(\text{Label Benign} \mid \text{Malignant})}{r(\text{Label Malignant} \mid \text{Benign})}$ is chosen by the clinician or researcher.

The ratio $\dfrac{p(\mathbf{x} \mid \text{Malignant})}{p(\mathbf{x} \mid \text{Benign})}$ is composed from a training data set. The ratio

$\dfrac{P(\text{Malignant})}{P(\text{Benign})}$ can be obtained from literature or estimated from the training data set;

but the source of this ratio obtained must correspond with the source of subjects used

in the breast study. Estimation of the two ratios, $\dfrac{p(\mathbf{x} \mid \text{Malignant})}{p(\mathbf{x} \mid \text{Benign})}$ and $\dfrac{P(\text{Malignant})}{P(\text{Benign})}$,

requires a large training data set to be statistically significant.

If the Risk Ratio is greater than 1, the ROI would be labeled "Malignant".

Otherwise, the ROI would be labeled "Benign". Or

Risk Ratio	ROI Label
> 1	Malignant
≤ 1	Benign

The values of risk factors are determined by the clinician or the researcher

based on his/her experience. For example, if the clinician thinks that it is too risky to

label a malignant mass to be "Benign", he/she would give a high value for r(Label

Benign | Malignant), and a relative low value for r(Label Malignant | Benign).

Choosing the different values of the risk factor ratio $\frac{r(\text{Label Benign} \mid \text{Malignant})}{r(\text{Label Malignant} \mid \text{Benign})}$ is

equivalent to choosing different values of the decision threshold. The pairs of false

positive and true positive fractions resulting from the different values of the risk factor

ratio would allow for the creation of an ROC curve, which can be used to evaluate the

performance of the technique presented [1].

This chapter has covered the binary segmentation technique used for

displacement artifact correction, the methods of image visualization and segmentation

used for cancer identification, the Bayesian decision technique used for cancer

recognition, and the ROC curve used for statistical analysis. The binary segmentation

technique has been shown to be effective in estimating and correcting displacement

artifacts. The availability of the user-friendly BreastView program that was written to

implement the image visualization and segmentation methods presented in this chapter

to clinicians and researchers should allow for more confidence in the identification of

cancerous breast tissues. The Bayesian technique can be used for the identification of

cancerous breast tissue if a large pool of case studies is available.

Chapter 8

Results and Discussion

The performance of the methods based on the arterial spin tagging sequences to measure T_1 and perfusion has been verified with a flow phantom, meat phantoms, normal breasts, and breasts with abnormal masses. Most of these studies were performed on a Signa Advantage 1.5T GE MR system and the rest were performed on a Signa Horizon LX 1.5T GE MR system (GE Medical Systems Inc., Milwaukee). A dual phased array breast imaging RF receiving coil (Medical Advance, Inc., Milwaukee) was used for the breast studies. All spin tagging studies were done in coronal view with the subject lying down in a prone position. The coronal view is parallel to the body and is expected to be perpendicular to the direction of maximum net blood flow in the breasts.

8.1. Flow Phantom Study

Perfusion studies using a controllable flow phantom were the first set of and the most important verification studies done. A flow phantom was assembled from a kidney dialysis tube. This dialysis tube is composed of artificial capillaries that allow the exchange of molecules during dialysis for a kidney patient. The kidney dialysis tube is a very good tissue model for perfusion studies. It has a length of about 25 cm, an internal diameter of about 5 cm, about 1000 capillaries and an approximate λ of 0.15 (the fraction of the "blood" volume relative to the total volume including the "blood" and the "interstitial fluid"). This "blood" volume is assumed to be the total

volume flowing out of the dialysis tube after it is filled up. It was measured to be 20 ml. The "interstitial fluid" is assumed to be the total volume that can fill up the space inside the tube but outside of the capillaries. It was measured to be 113 ml. For the convenience of physical measurement, the perfusion of the flow phantom was only verified in one direction, instead of multiple directions that occur in actual tissue. The flow is fed through long rubber tubes, and is driven by an external electrical mechanical pump outside the magnet room to avoid hazards associated with the strong magnetic field (Figure 8.1). The fluid used in the phantom was purified drinking water doped with manganese chloride to have a T_1 value of approximately 895 ms, which is within the range of T_1 value of body fluid. The flow rate was controlled by adjusting the mechanical pump and was physically measured using a stop watch and a graduated cylinder.

The fast SPGR based pulse sequence developed has been optimized for perfusion measurements by compromising between scan time and the precision of f/λ value. All phantom studies showed that there was a linear relationship between f/λ and the actual flow applied within the range of tissue perfusion (Figure 8.2). In these studies, the T_{1n} values during non-selective inversion at four different flow rates were about the same as expected: 1.232 +/- 0.034 sec. To improve measurement sensitivity, the "interstitial fluid" was not filled. So the actual value of the λ in this phantom should be within the range of [0.15, 1]. It can be estimated based on the physically measured flow rate and the f/λ value measured by the spin tagging technique. For example, at a physical average input flow rate of 0.0222 ml/sec/cm^2 through the cross
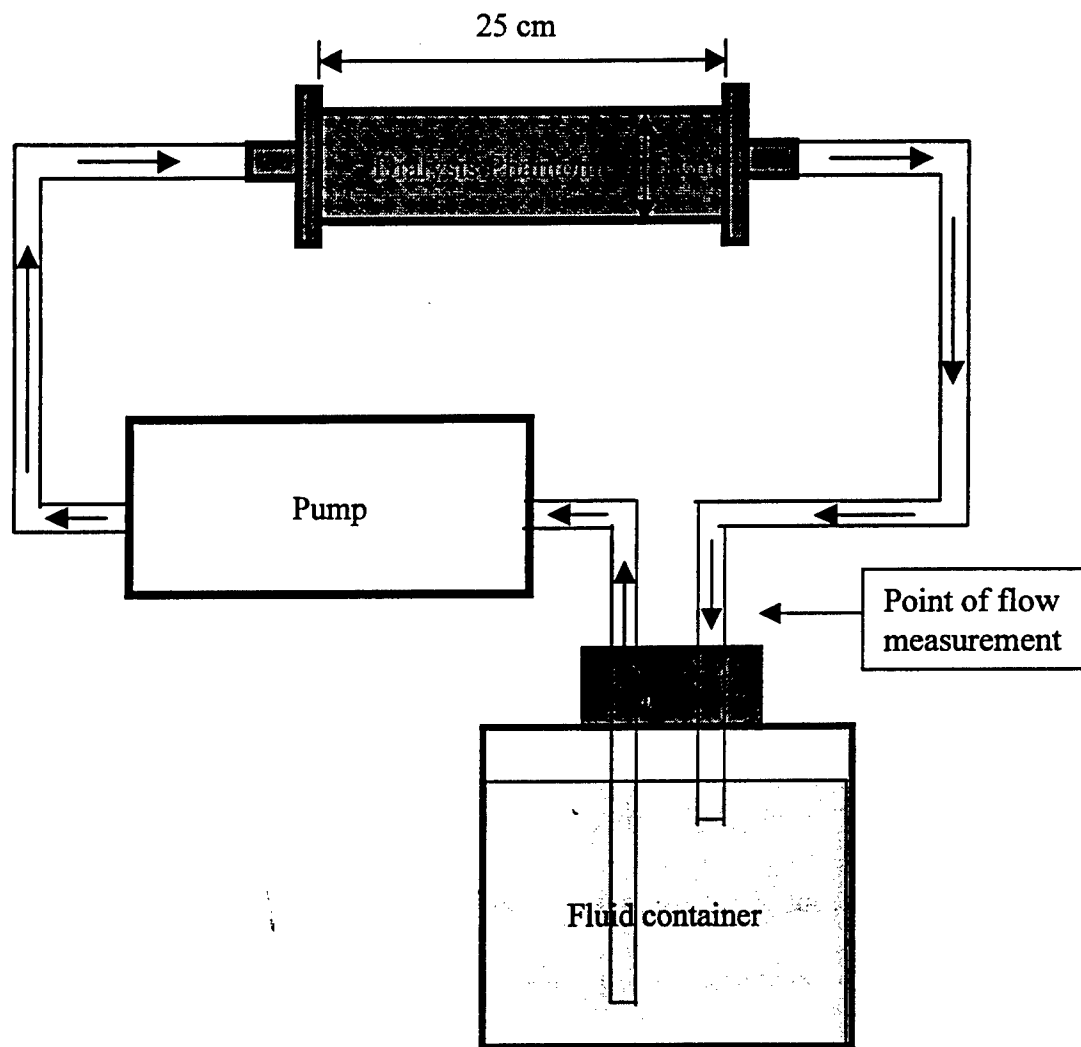
Figure 8.1. The setup of the kidney dialysis phantom. The figure shows
the mechanical setup of the kidney dialysis phantom (1000 capillary
tubes) and accessories. The flow rate can be controlled through the pump.
The flow rate can be measured through the fluid receiving end of the tube
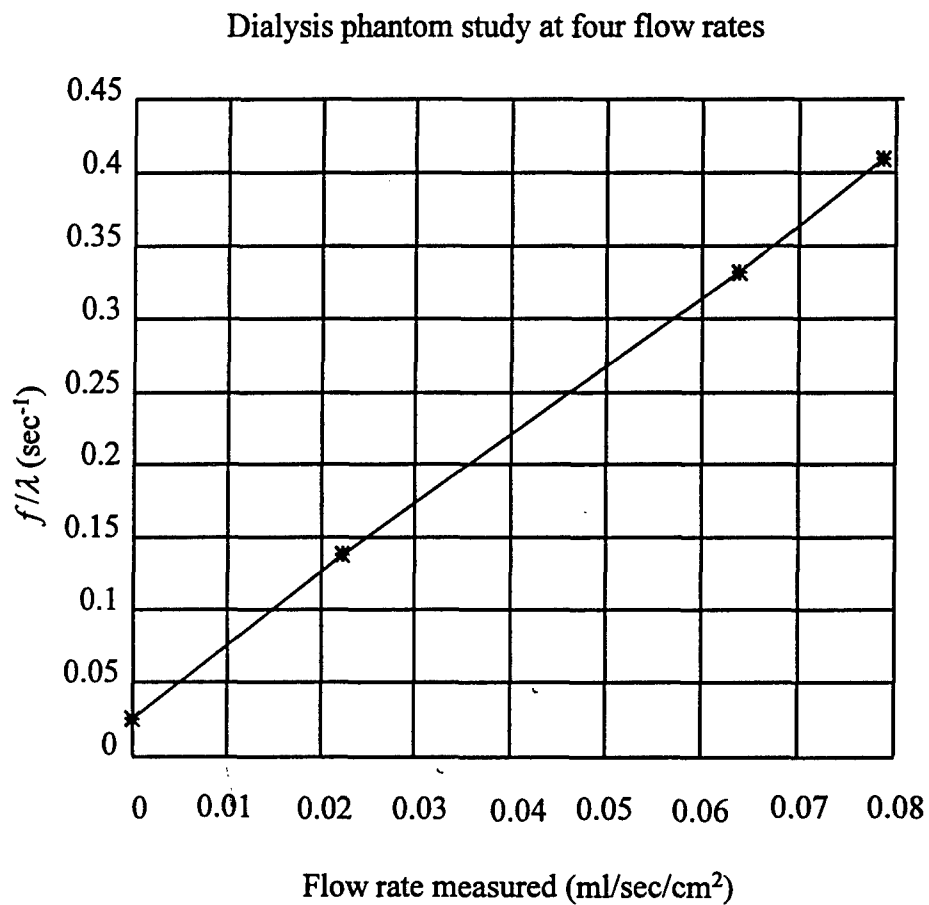after it is pulled out from the fluid container.

Figure 8.2. Results from the kidney dialysis phantom perfusion study. The arterial spin-tagging sequence was applied at four different low flow rates with 0, 0.0222, 0.0640 and 0.0787 ml/sec/cm². The corresponding f/λ values calculated were 0.0251, 0.138, 0.331 and 0.409 sec⁻¹.

section of the phantom, the f/λ value was measured to be 0.138 sec^{-1} through the spin tagging technique. Since a slice thickness of 0.3 cm was used in the scan, the physical input flow rate of 0.0222 ml/sec/cm^2 is equivalent to a perfusion value f of 0.0740 sec^{-1}, which is obtained by the simple relationship below:

$$f = \frac{\text{flow rate (ml / sec / cm}^2)}{\text{slice thickness (cm)}} \qquad (8.1)$$

Then the λ value is calculated to be 0.536 based on these f and f/λ values. It is within the range of [0.15, 1] as expected.

8.2. Meat/Fat Phantom Study

The meat/fat phantom study is used to verify the applicability of the sequence to tissue similar to breast. The two meat/fat phantoms are made of pork meat enclosed with both pork fat and chicken fat in two plastic cups. Each plastic cup has a height of 6 cm, a top diameter of 9 cm and a bottom diameter of 7 cm. Since the tissue in this phantom is not alive, it should have nearly zero perfusion. The perfusion measured should just be caused by the random motion of water molecules within the tissue. Since the water molecules are constrained by the meat and fat tissues, their motion should be very limited. Four slice locations are analyzed. Thirty-eight regions of interest (ROIs) at the meat and 21 ROIs at the fat from these four slice locations are chosen for analysis (Figure 8.3). The size of each ROI was 35 mm^2. Figure 8.4 graphically shows the distribution of T_{1n} and f/λ in meat and fat. The distribution of T_{1n} and f/λ is summarized in Table 8.1 below:
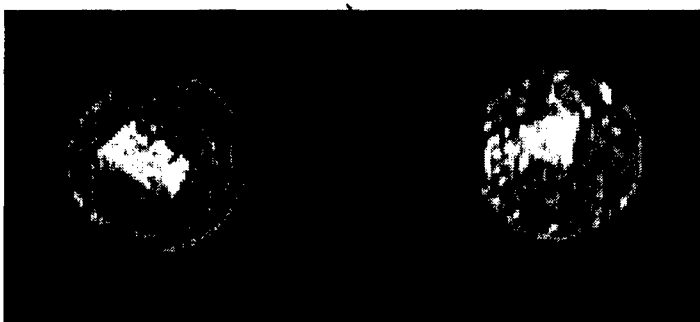
(a)
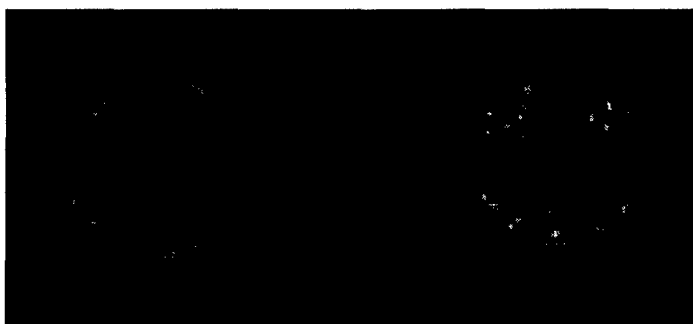
(b)

(c)

Figure 8.3. The meat/fat phantom images obtained with the fast SPGR based spin tagging sequence. The above figures show images obtained at (a) Selective, (b) Non-Selective and (c) Regular conditions at one slice location. All images are displayed using the window level of Min/Max: 0/516. The center darker area in Images (a) and (b) or the equivalent brighter area in Image (c) is meat and the rest of the area in the two objects is fat.
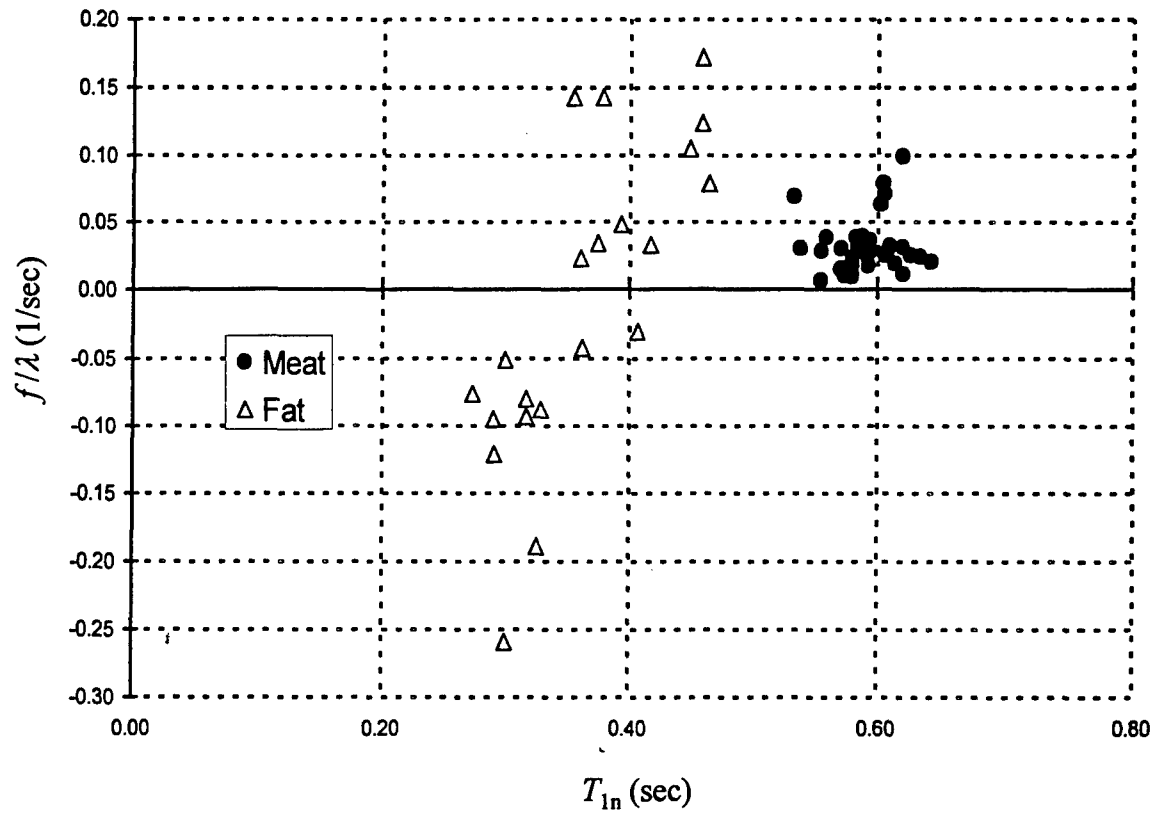
Figure 8.4. The T_{1n} and f/λ distribution comparison between meat and fat in the meat/fat phantom.

Table 8.1. Meat-Fat Characteristic Comparison in
Meat/Fat Phantom

	Mean of T_{1n} (sec)	STD of T_{1n} (sec)	Mean of f/λ (sec^{-1})	STD of f/λ (sec^{-1})
Fat	0.363	0.061	-0.010	0.116
Meat	0.598	0.043	0.022	0.086

The T_{1n} of meat is higher than that of fat. The f/λ value of fat is closer to zero than

that of meat because the water content in fat is lower than that in meat. The higher

standard deviation in the calculation of T_{1n} and f/λ is due to the higher b values (the

inverse of T_1 values).

8.3. Human Subject Studies

Eighteen subjects participated in the breast studies. One subject also

participated in the first-pass contrast enhanced dynamic comparison study. All

volunteers signed the consent form of research agreement that had been approved by

the human subjects research committee at University of California, Davis. At each

study, some simple but effective procedures were used to reduce motion artifacts: (1)

the volunteer would be strapped on the scan table in a prone position (Figure 8.5); (2)

the volunteer was instructed not to move and to breathe smoothly during scanning.

Besides the examination using the arterial spin tagging pulse sequence, other

examinations using traditional clinical techniques were also done. The following
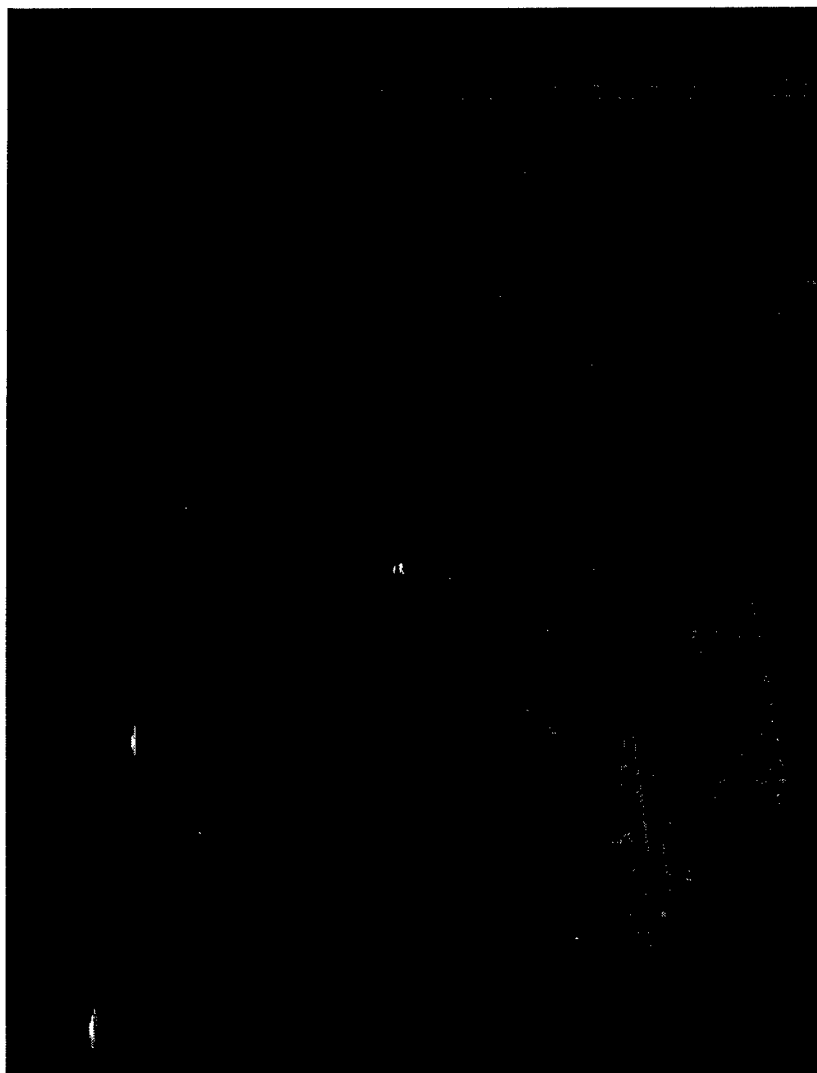
procedure was followed for each study:

Figure 8.5. Subject preparation for breast imaging.

1. 2D spin echo scan at the axial plane: this T_1 weighted multi-slice scan acts as a localizer to provide the overview of the whole breasts and neighboring tissues and helps to detect the existence of any abnormal mass.

2. 2D fast spin echo scan at the coronal plane: this proton density-weighted and T_2-weighted scan provides the traditional clinical breast images. The resulting images are used to compare with the images obtained from the arterial spin tagging sequence.

3. Arterial spin tagging pulse sequence at the coronal plane: about 10 slices centering around the abnormal masses that have been identified by the patient and/or the patient's physician or have been identified in the two previous clinical scans. For normal subjects, about 10 slices locations are chosen at the central regions of the breasts with inter-slice distance of 10 mm. The 10 slices should be at the same locations as the ones obtained in the 2D fast spin echo scan, and should have the same field of view. This would allow for direct comparison between clinical techniques and the arterial spin tagging technique.

If the first-pass contrast enhanced dynamic study is also carried out, three additional scans would be done:

4. Pre-contrast 3D SPGR scan: the proton density-weighted scan is done before the injection of the contrast material. The resulting images would be used to compare with resulting images after contrast material has reached a steady state.

5. 2D fast SPGR multi-slice dynamic contrast study: fourteen identical 25-second scans are performed continuously with an inter-scan time of 5 sec. At each scan, about 11 slice locations are imaged. Three scans are performed before the injection of the contrast material. The contrast-material injection and the fourth scan start at the same time. The total scan time for the whole dynamic contrast study is about 7 minutes.

6. Post-contrast 3D SPGR scan: the same scan as Scan 4 is done after the injection of the contrast material. The effect of the contrast material has reached a steady state. The resulting images would be used to compare with those obtained before the contrast material was administrated.

Examples of the scan procedure and the details of the scan protocols used for the breast studies are shown in Appendix C. In the following section, three case studies with normal breasts, breasts with benign abnormal masses, and breasts with malignant tumors will be discussed.

8.3.1 Normal Breast Study

In this study, no first-pass dynamic contrast enhanced study was performed. Ten slice locations were studied. Figure 8.6 shows images at one slice location at the Selective, Non-selective and Regular conditions in the arterial spin tagging scan. As shown in this figure as well as in clinical images, the fat and non-fat regions are well separated geometrically. The non-fat region is at the inner part of the breasts while the fat region is at the outer part. Based on the nice separation, regions of interest (ROIs) can be easily isolated for the characteristic comparison between fat and non-fat areas

(b)

(a)
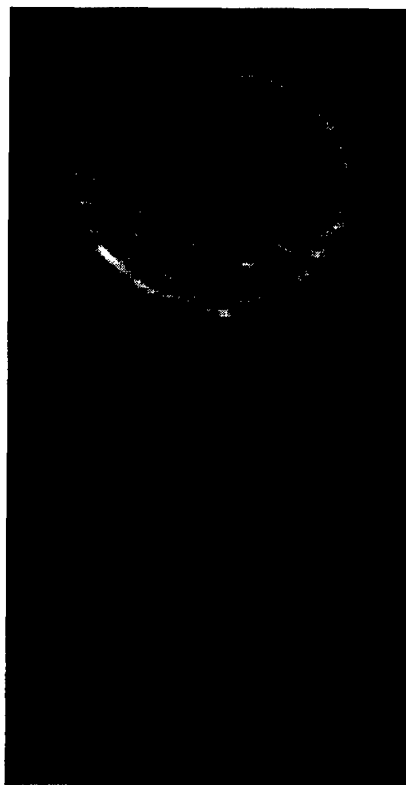
(c)

Figure 8.6. Arterial spin tagging images from normal breasts. The above images are selected from one slice location of the arterial spin tagging resulting images. This is a normal subject study. The images shown are from (a) Selective, (b) Non-selective and (c) Regular conditions. All images are displayed at the same widow level with the maximum at 302 and minimum at 151.

of the breast. The ROIs with the size of 35 mm^2 have been identified from all 10 slices

acquired from the arterial spin tagging sequence. Figure 8.7 shows the f/λ and T_{1n}

distribution for this study, and can be summarized in Table 8.2 below:

Table 8.2. The f/λ and T_{1n} Summary for a Study with Normal Breasts

	Mean of T_{1n} (sec)	STD of T_{1n} (sec)	Mean of f/λ (sec^{-1})	STD of f/λ (sec^{-1})
Fat	0.435	0.207	- 0.005	0.135
Non-fat	1.446	0.403	0.033	0.044

8.3.2 Breast Study with a Benign Abnormal Mass

No first pass contrast enhanced study was performed in this study either. Ten

slice locations were studied. Figure 8.8 shows images at one slice location from

clinical scans as well as from the arterial spin tagging scan. A rod-shape abnormal

mass was easily identified in the clinical scans (Figure 8.8 (d) and (e)). This mass was

considered benign because the volunteer acknowledged that it had been there and had

remained the same size for more than 10 years. ROIs with the size of 35 mm^2 have

been isolated from the edge and the center of the abnormal mass as well as non-fat

area outside of the abnormal mass for the MR tissue characteristic comparison. Figure

8.9 shows the f/λ and T_{1n} distribution for these different tissues, and can be

summarized in the table following (Table 8.3):

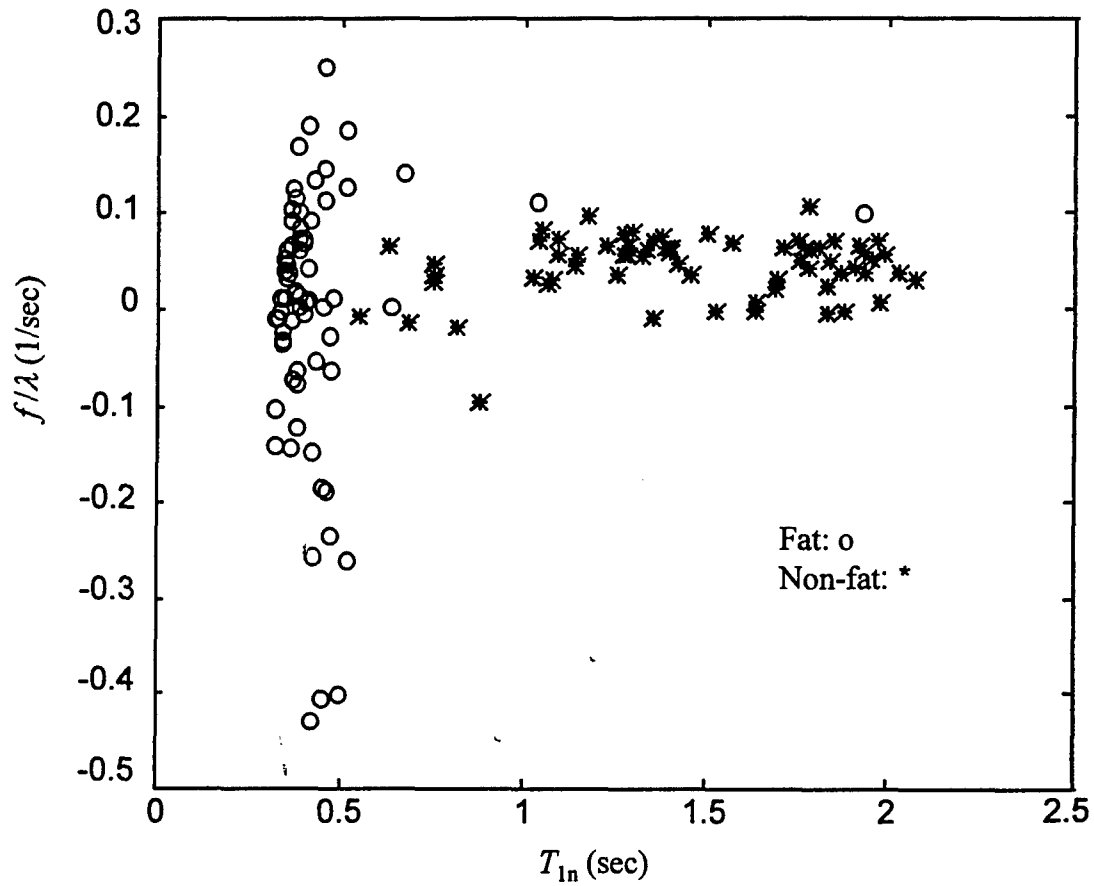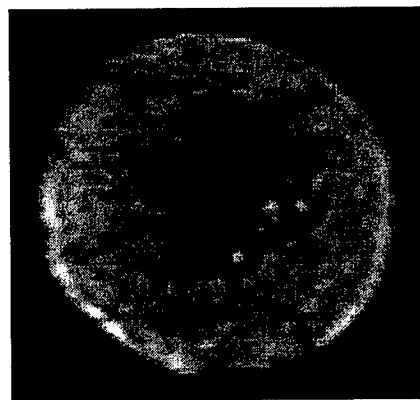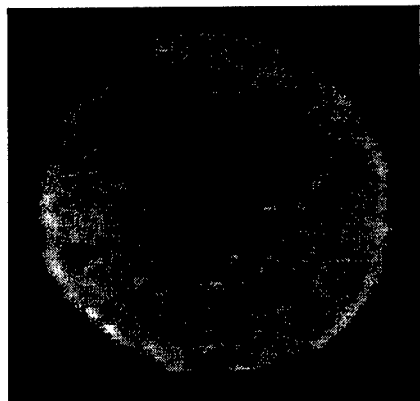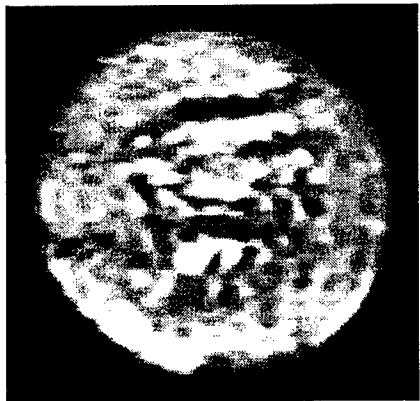f/λ and T_{1n} Distribution for Normal Breast Tissue

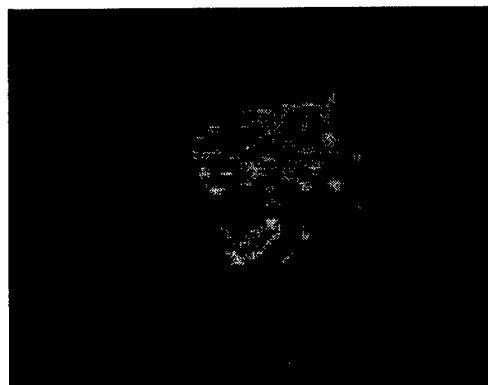Figure 8.7. The f/λ and T_{1n} distribution for one of the studies with normal breasts.

Figure 8.8. Images of a breast with a benign lesion. These images are all obtained from the same slice location. The first three images are from the arterial spin tagging scan at (a) Selective, (b) Non-selective and (c) Regular conditions. The other two images are from clinical scans: (d) T_2 FSE fat-suppressed, and (e) T_1 SPGR with fat suppressed. All images are displayed at the same widow level with the maximum at 390 and the minimum at 195.

f/λ and T_{1n} Distribution for Benign Breast Lesion
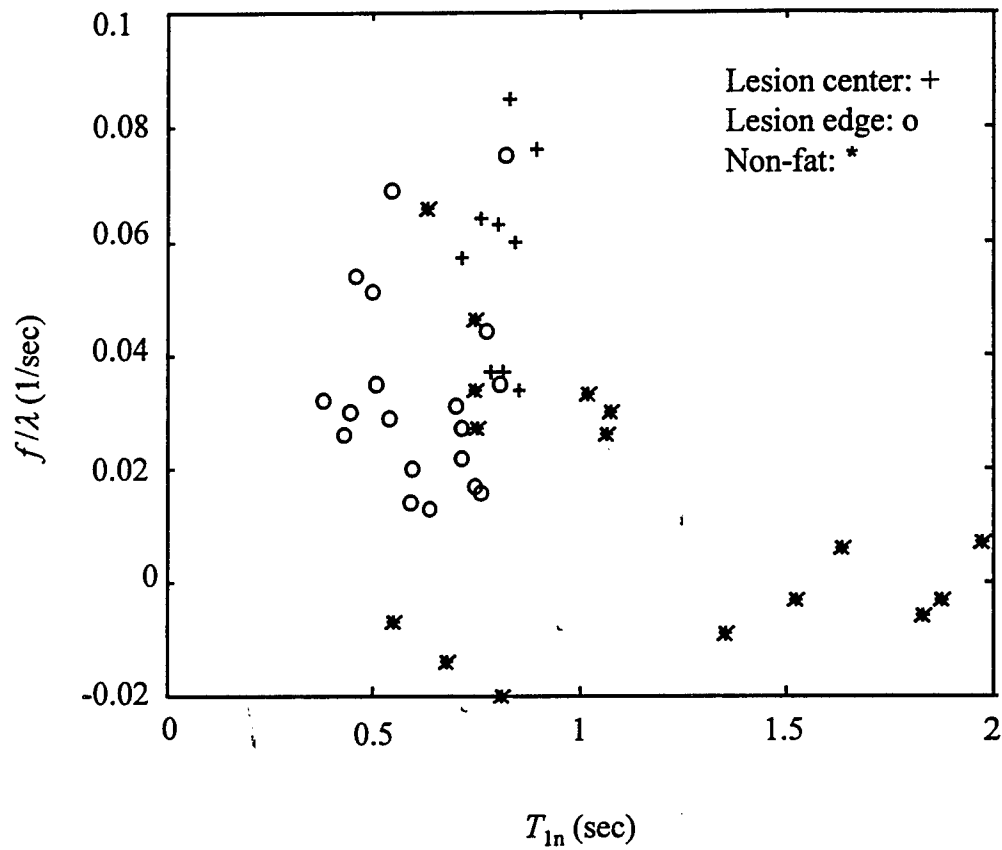

Figure 8.9. The f/λ and T_{1n} distribution for one breast study with a benign lesion.

Table 8.3. The f/λ and T_{1n} Summary for a Breast Study
with a Benign Abnormal Mass

|	Mean of T_{1n} (sec)	STD of T_{1n} (sec)	Mean of f/λ (sec^{-1})	STD of f/λ (sec^{-1})
Lesion Center	0.813	0.053	0.057	0.018
Lesion Edge	0.615	0.140	0.034	0.018
Non-fat Tissue	1.142	0.487	0.013	0.025

8.3.3 Breast Study with a Malignant Tumor

No first pass contrast enhanced study was performed in this study either. Three

slice locations centering around the abnormal mass were studied. The malignant

regions were identified based on the image processing and visualization techniques

discussed in Chapter 7 and were labeled by color mapping onto the clinical images

(Figure 8.10). These regions were close to the abnormal mass that could be palpated,

and its malignancy was later confirmed by needle biopsy. ROIs with the size of 35

mm^2 has been isolated at the tumor, non-fat regions outside the tumor as well as fat

tissue for MR tissue characteristic comparison. Figure 8.11 shows the f/λ and T_{1n}

distribution for these different areas, and can be summarized in the table below (Table

8.4):

Table 8.4. The f/λ and T_{1n} Summary for a Breast Study
with a Malignant Tumor

	Mean of T_{1n} (sec)	STD of T_{1n} (sec)	Mean of f/λ (sec^{-1})	STD of f/λ (sec^{-1})
Fat	0.385	0.085	-0.177	0.592
Non-fat	0.842	0.392	0.035	0.266
Tumor	1.145	0.372	0.111	0.142

As shown in Figure 8.11, because fat has T_{1n}'s much lower than those of the other two

groups of tissue, it can be separated out easily based on T_{1n} value alone. The mean
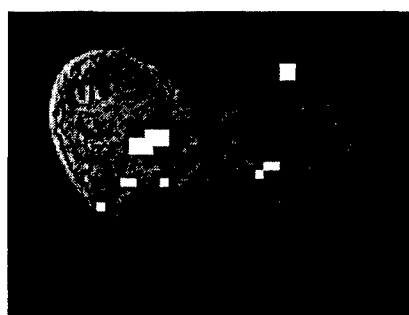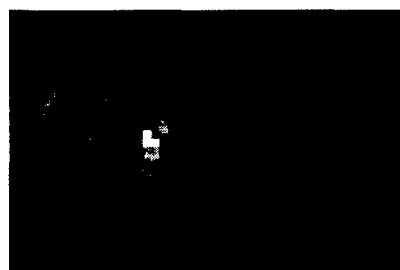
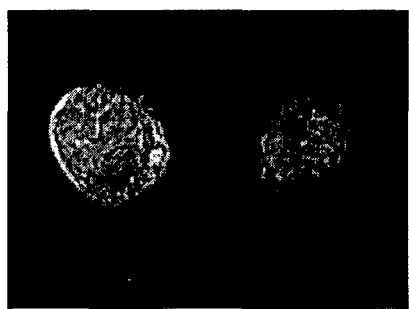Proton Density Weighted, Slice 6 T_2 Weighted, Slice 6

Proton Density Weighted, Slice 7 T_2 Weighted, Slice 7

Proton Density Weighted, Slice 8 T_2 Weighted, Slice 8

Figure 8.10. Suspicious cancer region color mapping. The identified suspicious cancer pixels are mapped onto the high-resolution traditional clinical MR images according to their corresponding slice locations. These images are from three consecutive 3mm slices with inter-slice distance of 10 mm. The white mapping pixels are actually red in the visualization program BreastView.

f/λ and T_{1n} Distribution for Breast Tissue with a Malignant Tumor

Δ: Fat   +: Non-fat   o: Tumor

(a)
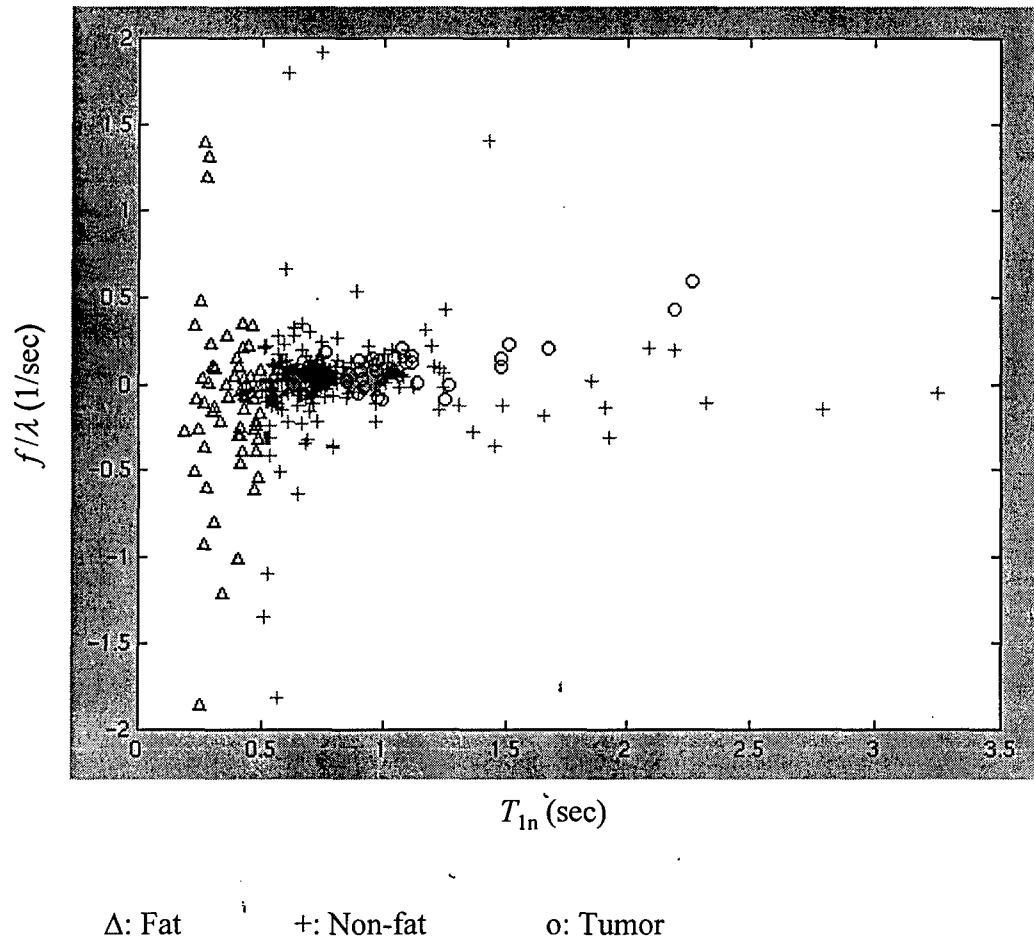
Figure 8.11. The f/λ and T_{1n} distribution for breast tissue with a malignant tumor. Figure (b) is a magnification of Figure (a).

f/λ and T_{1n} Distribution for Breast Tissue with a Malignant Tumor

Δ: Fat   +: Non-fat   o: Tumor
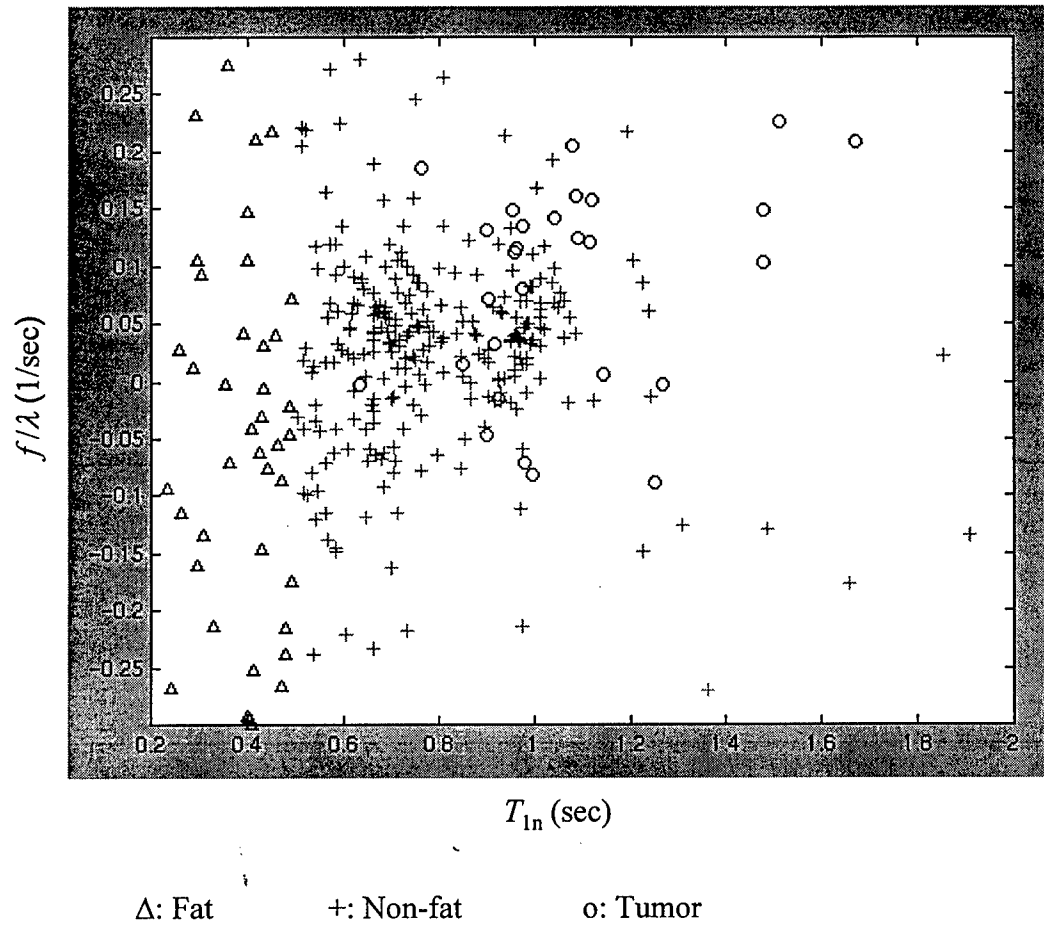
(b)

Figure 8.11. (continued)

and standard deviation of the f/λ for fat have a wide range, and thus f/λ does not provide any value for fat tissue recognition. Since tumor tissue is non-fat tissue and should have T_{1n} value at the range of healthy non-fat tissue, the overlap between fat and tumor is minimal. However, to separate tumor tissue from non-fat tissue, both the T_{1n} and f/λ values should be used. For example, as shown in Table 8.4 and Figure 8.11, both the T_{1n} and f/λ values at tumor tissue are relatively higher than those at non-fat tissue, but with some overlap.

8.3.4. Patient Study Summary

Eighteen subjects, including 11 patients referred by their physicians and seven volunteers referred by themselves, participated in the breast studies. Three patients and two volunteers were eliminated from the analysis because either the studies were not done according to protocol, there was excessive motion during scanning, the abnormal mass was too close to the chest wall to be measured reliably, or no patient biopsy was performed to confirm the results of the MR study. There were a total of 13 useful cases left for analysis. For all these cases, the suspicious pixels were identified based on the following criteria as was suggested in Chapter 7:

T_{1n}: > 0.5 sec
f/λ: > 0.1 sec^{-1}
STD of f/λ: < 0.1 sec^{-1}

and the suspicion level threshold was set at 20.2%. Analysis has been done using the program BreastView. Appendix D shows three case studies using this program. For information on how to use this program, refer to Appendixes B and G. Table 8.5 shows the result of these 13 cases.

Table 8.5. Summary of Breast Case Studies

Date of Study	Subject Referred by	Palpable (Yes or No) ?	Seen on Clinical MRI ?	Level of Suspicion Based on T_{1n} and f/λ	Assessment Based on Suspicion Level	Abnormal Mass Type
05/03/97	Physician	No	Yes	Low	Negative	Benign (Fibroadenoma)
05/23/97	Physician	Yes	Indeter-minable	Moderate High	Positive	Malignant (Ductal Carcinoma)
08/01/97	Physician	Yes	No	High	Positive	Malignant (Ductal Carcinoma)
11/15/97	Physician	Yes	No	Low	Negative	Benign
12/10/97	Physician	Yes	No	High	Positive	Benign
04/13/98	Physician	Yes	Indeter-minable	Moderate High	Positive	Benign
07/27/98	Physician	Yes	No	Low	Negative	Benign
08/07/98	Physician	Yes	No	High	Positive	Benign
02/07/97	Herself	No	No	Low	Negative	Normal
03/05/97	Herself	Yes	Yes	Low	Negative	Benign (Fibroadenoma)
07/26/97	Herself	No	No	Low	Negative	Normal
11/16/97	Herself	Yes	Yes	Low	Negative	Benign (Fibroadenoma)
12/14/97	Herself	No	No	Low	Negative	Normal

Normal = normal subject who does not have any tumor based on reliable health
  history,
Abnormal Mass Type = determined based on biopsy or reliable health history.

Based on the summary shown in Table 8.5, the number of true positive (TP) is

2; the number of false negative (FN) is 0; the number of false positive (FP) is 3 and

the number of true negative (TN) is 8. Therefore, the true-positive fraction or

sensitivity is 100%, calculated by TP/(TP+FN). The false-positive fraction is 27.3%,

calculated as FP/(FP+TN). The specificity is 72.7%, which is equal to one minus the

false-positive fraction. Because the number of cases investigated was limited, these statistical figures cannot provide enough confidence in evaluating the technique. If more breast cases have been studied, a ROC curve, commonly used to evaluate the performance of a technique in radiology, can be built by using different suspicion level thresholds or different thresholds of $T_{1n}, f/\lambda$ and STD of f/λ. If a large pool of case studies is available, a more sophisticated Bayesian statistical model discussed in Chapter 7 can also be built. This model can be used to evaluate the imaging technique, and more importantly, it can be used to evaluate new case studies.

Chapter 9

Summary, Conclusions and Recommendations

The arterial spin tagging technique based on 2D fast SPGR has been developed and implemented in both EPIC 5.4 for the Signa Advantage MR system and EPIC LX 8.2.5 for the Signa Horizon LX MR system. Its accuracy in perfusion measurement has been proven through phantom experiments. It has also been successfully applied to tissue classification and tumor identification. Its applicability is enhanced through the graphical-user-interface analysis software, BreastView, which has been developed by the author for the necessary image visualization, threshold analysis, and cross-registration between different MR breast imaging techniques. Based on the 13 case studies analyzed, a sensitivity of 100% and a specificity of 72.7% have been achieved using the fast SPGR based arterial spin tagging sequence and the associated analytical techniques.

However, the fast SPGR based spin tagging technique as well as the data analysis technique used has limited the accuracy of the T_1 and f/λ estimation due to two ideal assumptions. First, it has been assumed that data acquisition would not disturb the recovery curves of the inverted spins or the equilibrium states of the non-inverted spins. This assumption indeed never holds. Simulation showed that the T_1 calculated based on the techniques presented was slightly lower than the true T_1. The better approach is to replace the 2D fast SPGR data acquisition scheme with an echo planar data acquisition scheme. In echo planar imaging (EPI), only one read-out RF

pulse is used for the complete data acquisition of a whole image. The disturbance due to the read-out RF pulses to the recovery curves of the inverted spins or the equilibrium states of the non-inverted spins would be small. Since EPI is faster than 2D fast SPGR, the total scan time would be shortened also. This would enhance its value as a breast-screening tool. However, EPI places high demands on gradient amplitudes and slew rates, and introduces hard-to-remove N/2 ghost artifacts. Thus the 2D fast SPGR based spin tagging sequence can still play a useful role in research sites without sufficient hardware capability. This EPI based spin tagging sequence has been implemented successfully in the simulation level in EPIC LX 8.2.5 for the Signal Horizon LX MR systems. It has not been able to run successfully on the LX system yet due to hardware problems that GE Medical System Inc. is still attempting to resolve.

The other assumption for the 2D fast SPGR based spin tagging sequence is that the contribution of magnetization transfer in Eq. (4.1) is negligible. RF and gradient pulses dedicated to magnetization transfer have been implemented in the EPI based arterial spin tagging pulse sequence. This would potentially improve the calculation of the T_1 values. Relatively higher magnetization transfers have also been detected in malignant tumor [36]. Thus, the magnetization transfer parameters detected might add another feature in determining lesion malignancy. Analysis of the magnetization parameters has not been done in this dissertation, but remains as a recommendation for the further development of this project.

The pulse sequence and post-processing techniques presented may be suitable for all specific clinical indications that have been reported for first-pass contrast enhanced imaging. They may in fact be more convenient and equally reliable for identifying the regions of tissue changes that give rise to contrast enhancement. However, contrast enhancement is regarded as essential in MRI breast evaluation, and is unlikely to be supplanted. The recommendation is to perform the first-pass contrast enhancement comparison study along with all the arterial spin tagging studies. This would allow the direct comparison in accuracy, precision as well as ease of application.

For the further development of this project, more case studies using all the sequences developed should be conducted to develop a meaningful statistical model appropriate for Bayesian analysis as discussed in Chapter 7. To make it successful, strong collaboration with referring physicians and surgeons is recommended. This would allow sufficient numbers of patient volunteers. Needle biopsies should be performed on all volunteers with palpable masses or suspicious masses identified in any imaging modality, so that results from arterial spin tagging studies as well as first-pass contrast enhanced studies can be confirmed.

Appendix A

Computer Simulation and Scanner Operation for the Fast SPGR Based

Arterial Spin Tagging Pulse Sequence

The fast SPGR based arterial spin tagging pulse sequence (BreFgre) has been

developed in the EPIC LX 8.2.5 environment on an SGI workstation with an operation

system of IRIX 6.3 or higher. It can be simulated on an SGI workstation or run on a

Signa Horizon LX system.

A.1. Simulation

At the directory containing the BreFgre pulse sequence source code, run the

EPIC tool by typing:

WTools.x &

Build the PSD first if it has not been done yet. To see the simulation, click the "Load

cv" button at the Evaltool page, and then load the file, "GoodSimCVs1.txt" or

"GoodSimCVs2.txt". The file "GoodSimCVs1.txt" is for a full simulation. The file

"GoodSimCVs2.txt" is for a fast simulation without going through all the repetition

steps. Be sure to press the return key after each entry to ensure that the value is

accepted. Follow the steps for simulation at the IPGSim page to view the waveform.

The CVs from these two files only serve as example CVs; they can be changed as

desired. The CVs used in the two simulation files are defined as following:

```
opfast = the fast scan flag with 1 = on,
BreScan = the breast scan flag with 1 = on,
opacqo = the acquisition mode with 0 = interleaved and 1 = sequential,
opmph = the flag for multi-phase data acquisition with 1 = on,
```

opfphases = the total images acquired at each slice location in the multi-phase
case,

opdeprep = the flag for DE prep pulse with 0 = off and 1 = on,

opirprep = the flag for IR prep pulse with 0 = off and 1 = on,

opirmode = the type of IR or GRASS/MPGR used,

slquant1 = the total number of images acquired,

phorder = the phase/view ordering with 0 = normal, 1 = centric and 2 =
interleaved,

br_norm = the number of images acquired at the regular condition,

br_tino = the number of TI choices used,

ti_inc = the step size of TI increment (ms),

br_acqs = the number of images repeatedly acquired at each TI value at the
spin tagging condition.

A.2. Scanner Operation

The breast sequence scans only at one slice location at a time. After the scan is finished at each location, the series should be copied, and the slice location should be updated. After this, click through the sequence of "Save Series", "Prepare to Scan" and "Scan". It is not necessary to do the full prescan at every slice location; every other slice location is sufficient. This reduces the overall scan time. To skip the prescan, run "manual prescan", but abort it prematurely, so that the old prescan values will be kept.

The following is a complete example prescription for a breast study using the BreFgre sequence:

Patient ID: 0000027
Patient Name: amy doe
Landmark: Xyphoid
Patient position: Prone
Patient Entry: Head First
Coil: BREASTPA
Series Description: david's breast seq
Plan: coronal
Mode: 2D

Pulse Seq: SPGR
Imaging Options: Seq, Fast, Mph
Psd Name: /psd/dzhu/BreFgre
TE: Minimum
Flip Angle: 10°
Bandwidth: 31 kHz
FOV: 34 cm
Slice Thickness: 3.0 mm
Spacing: 1.0 mm
Freq: 256
Phase: 256
NEX: 1
Phase FOV: 0.5
Freq Dir: R/L
Auto Center Freq: Water
Start: A44
End: A44
Slices: 1
At Multi Phase Screen:
      Phase Per Location: 61
      Phase Acq. Order: Sequential
      Delay After Acq.: Minimum

After all the necessary CVs have been entered, click through the sequence of "Save Series", "Prepare to Scan" and "Scan". After the scan is finished, the images would be reconstructed and displayed on the console.

Appendix B

Instructions for the BreastView Program

The BreastView program has been designed to be user-friendly. The graphical-user-interface guides the user through the entire visualization and analysis process for a breast study. The assumption is that the necessary analysis has been done correctly beforehand. After executing the BreastView program on the command line by typing "BreastView", there is a "Help" button on the first page of the interface. Clicking the "Help" button allows the user to view the full html file with the following instructions:

Installation

At the program directory of BreastView, create the following symbolic linkage:

    ln -s /CDROM DataInCD

    ln -s /data2/zhudata/BreastData DataInOther

    ln -s /data2/zhudata/BreastAnaly AnalyDir

To run BreastView, type

BreastView &

Data Loading

Click the "Load Data Directory" button to open the directory where data is stored. The data is in

    DataInCD

    or

    DataInOther

After the data directory is loaded, the "Show Study Info" and "Load Analysis Directory" buttons will come up. Clicking the "Show Study Info" button will show the information of the breast study that has been done.

Click the "Load Analysis Directory" button to open the directory where analytical results are stored. The analysis directory should be in

AnalyDir

If this directory has been loaded correctly, all the action buttons will come up. Otherwise the program will ask you to reload the analysis or data directory.

Data Preview

Clicking the "Display Histogram for All" button displays the histogram of T_1 and f/λ for all the slices investigated.

Create Suspicious Cancer Regions

The detection images have normally been created according to the default threshold settings. They can be recreated based on the researcher's choice of thresholds. After the detection thresholds have been specified, simply click the "Create Detection Image" button to create a new set of detection images.

View All Images

Clicking the "Display All Images" button should lead to the display of the eight types of images that are most useful for making decisions.

This button offers two choices:

1) Contrast enhancement dynamic study images will be shown.

2) No contrast enhancement dynamic study images will be shown. All feature

images will be displayed instead.

Tips in Viewing Images

After all eight types of images are displayed, the user can do the following:

1) The Maximum and Minimum values of each image are displayed automatically.

The image contrast can be changed by moving the "Max" and "Min" bars.

2) Slices of investigation can be displayed by moving the sliding bars. By moving

the sliding bars, the slice locations of different types of study can be approximately

matched.

3Dslice#: Select the slice of the 3D images.

DySlice#: Select the slice for the dynamic study, and the corresponding

slices of the 3D studies.

BrSlice#: Select the slice for all the feature images resulted from the spin

tagging sequence and the slices of the corresponding dynamic studies.

HiSlice#: Select the slice of the high-resolution clinical images (Proton-

weighted and T_2-weighted).

AxSlice#: Select the slice of the axial view images.

3) To determine an individual pixel value, simply click the left mouse button on

the pixel of interest on any image except the axial image. Other images should

display the pixel values at the corresponding pixel location also. The units of the pixel values are indicated if known.

4) Click the "Suspicion mapping" button to show the color mapping in clinical and dynamic rise images. The color mapping corresponds with the range setting for the Suspicion map. Changing the range setting of the Suspicion map through the "Max" and "Min" sliding bars should automatically display the new color mappings.

5) Click the "Plot" button to open a window for plotting the dynamic study. Select "Point" for pixel by pixel display. Clicking the left mouse button on a pixel in any image except the axial image will show the dynamic plot.

Select "Roi" to show the dynamic plot of the ROI (region of interest) specified earlier.

6) After activating "Draw ROI ...", the ROI can be specified by the user: left mouse button to specify the starting point of the ROI, right mouse button to create the ROI, and middle button to finish the task.

7) If the dynamic study images are displayed, you have a choice of choosing the "Axial Cut" or the "Dynamic Rise" images.

8) Click the "Histogram" button to display the total histogram including all the slices investigated.

Click the "Pixel" button: the T_1 and f/λ values will be mapped onto the total histogram while clicking the left mouse button on the images displayed.

Click the "Roi" button to map the distribution of T_1 and f/λ of the ROI specified on the total histogram.

Click the "No Mapping" button to stop the above mapping.

9) The slice selection bars have been designed to view the appropriate images. By dragging them, the user can see how they work.

10) Click the "Redraw All Images" button to redraw all the images.

11) An active window can be closed by selecting "Close" from the pull-down manual at the upper-left corner.

Close Current Study and Open Another One

To close the current study, just click the "Close Study" button, then you are ready to analyze another study.

Appendix C

Breast Study Procedures and Protocols

Two example procedures with and without a first-pass contrast enhanced dynamic study are shown in Sections C.1 and C.2. The investigator must write down the relevant information during the study. If there is an abnormal mass for the subject, the subject or her physician should be asked to localize the masses on the figure provided (as shown in Section C.3). The other protocols are shown in Sections C.4 to C.8.

C.1. Example Procedure without a First-Pass Contrast Study

Date of study: 11/16/97

Breast Sequence Study

by Michael Buonocore and David Zhu

Type of study: phantom( ), subject (x), Patient ( )

Name: Age: 38

Preparation:

Ask subject to have a good fit of the foam pads and a good strap, not to move, and breath smoothly during scanning.

Procedures:

    1. 2D Spin Echo axial cut (Series 1) FOV = 40 cm

      I 84 to s 84 , loc: 29 . Scan thick = 5 mm, Inter = 1 mm.

2. 2D Fast Spin Echo (Series 2)   FOV = 34 cm

P 7 to A 55 , loc: 12 , scan thick = 5 mm, inter = 1 mm.

3. David's breast sequence coronal cut: fgt1_new3d, FOV = 34 cm

Seven TI cycles: br_TR = 2.7 s, br_TI = 15 ms, ti_inc = 100 ms.

TI decreases from 615 ms to 15 ms.

Acquisition slice thickness: 3 mm, Selective slice thickness: 3mm

Frequency direction: R/L for all locations

series 3:   location:P7   R1 = 6 , R2 = 15 , TG = 153

series 4:   location:P1   R1 = 6 , R2 = 15 , TG = 154

series 5:   location:A5   R1 = 6 , R2 = 15 , TG = 153

series 6:   location:A11   R1 = 6 , R2 = 15 , TG = 154

series 7:   location:A17   R1 = 6 , R2 = 15 , TG = 160

series 8:   location:A23   R1 = 6 , R2 = 15 , TG = 160

series 9:   location:A29   R1 = 6 , R2 = 15 , TG = 160

series 10:   location:A35   R1 = 6 , R2 = 15 , TG = 167

Comments:

Fibroadenoma in the left breast, about 1/3 in from nipple, and about 3 o'clock

position.

C.2. Example Procedure with a First-Pass Contrast Study

Date of study: 8/7/98

Breast Study with Contrast

by Michael Buonocore and David Zhu

Type of study: phantom( ), normal subject ( ), subject w/ suspicious lesion (x)

Name: Age: 37   Weight: 135

Preparation:

Ask subject to have a good fit of the foam pads and a good strap, not to move, and

breath smoothly during scanning.

Procedures: (Protocol: # 64)   (Study # 04817)

      1. 2D Spin Echo axial cut (Series 1 -> axial) FOV = 40 cm

        I 84 to s 84 , loc: 29   . Scan thick = 5 mm, Inter = 1 mm.

      2. 2D Fast Spin Echo (Series 2 -> highres)   FOV = 34 cm

        P 10 to A 50 , loc:11 , scan thick = 5 mm, inter = 1 mm.

      3. David's breast sequence coronal cut: fgt1_new3d, FOV = 34 cm

        Seven TI cycles: br_TR = 2.7 s, br_TI = 15 ms, ti_inc = 100 ms.

        TI decreases from 615 ms to 15 ms.

        Acquisition slice thickness: 3 mm, Selective slice thickness: 3 mm

        Frequency direction: R/L for all locations

        series 3:   location: P10 R1 = 6 , R2 = 15 , TG = 146

        series 4:   location: P4   R1 = , R2 =   , TG =

series 5:　·　location: A2　R1 = 6 , R2 = 15　, TG = 150

series 6:　　location: A8　R1 = 6 , R2 = 15　, TG = 149

series 7:　　location: A14　R1 =　, R2 =　, TG =

series 8:　　location: A20　R1 = 6 , R2 = 15　, TG = 146

series 9:　　location: A26　R1 =　, R2 =　, TG =

series 10:　　location: A32　R1 = 6 , R2 = 15 , TG = 149

series 11:　　location: A38　R1 =　, R2 = , TG =

series 12:　　location: A44　R1 = 6　, R2 = 15　, TG = 158

series 13:　　location: A50　R1 = 6 , R2 = 15　, TG = 151

4. Pre-contrast 3D scan (scan #2 in protocol, 2'37") (flip angle = 65)

(series 14　-> pre_3d_a)

(Center at A22.7 with 28 locs, 3 mm slice thickness)

5. More David's breast sequence coronal cut: fgt1_new3d, FOV = 34 cm

series 15:　　location: A23　R1 = 6 , R2 = 15　, TG = 145

series 16:　　location: A17　R1 =　, R2 =　, TG =

series 17:　　location: A29　R1 = 6 , R2 = 15　, TG = 148

The patient is pulled out to set up contrast injection in the following scans:

6. Pre-contrast 3D scan (scan #2 in protocol, 2'37") (flip angle = 65)

(series 18 -> pre_3d)

(Repeat the pre_contrast) (Center at A22.7 with 28 locs, 3 mm slice thickness)

7. Fast SPGR contrast dynamic study (total 7 minutes) (scan #1 in protocol):

(Series 19 -> dynamic)

Each scan has a scan time of 25 sec, with an approximate inter-scan time of 5 sec, for a total of 30 sec.

(1) 3 scans are done before injection.

(2) Begin injection and press SCAN to begin the 4th scan.

(3) Continue on the same fashion until the 14th scan.

8. Post-contrast 3D scan (scan #2 in protocol, 2'37"), same as #6 above.

(Series 20 -> post_3d)

(Center at A22.7 with 28 locs, 3 mm slice thickness)

Comments:

Patient claims that the tumor is located at 10 o'clock in the right breast.

The patient has small breasts. Foam packs have been adjusted to avoid motion artifacts. Might need to consider image displacement correction.

Based on the analysis of the perfusion study, this patient appears to have a malignant tumor in the right breast.

Biopsy later indicated that the lesion(s) was benign.

C.3. A Simple Questionnaire for the Localization of the Abnormal Masses

Volunteer name: Date of study:

View from side

Right   Left

View from top

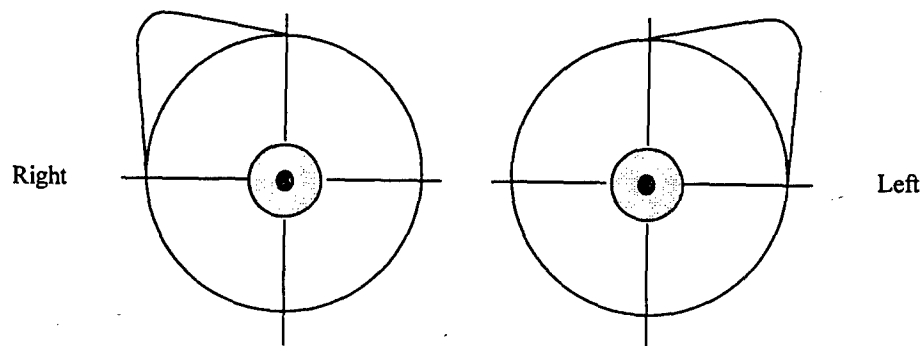Right   Left

View from front

Right   Left

C.4. 2D Spin Echo Scan in the Axial Plane

Patient Entry: head first
Patient Position: prone
Landmark: sternal notch
Coil: other: LS45
Plane: axial
Mode: 2D   Monitor SAR
Pulse Sequence: spin echo
        Resp   Flow
        comp   comp
Number of Echo = 1
TE = Minimum Full (20 ms)
TR = 600 msec
Autoshim
Auto Center Freq: Water
FOV = 40 cm
Slice Thickness = 5.0 mm
Inter-slice Gap = 1 mm
Start: I84, End: S84   => Number of Locations: 29
Acq Time:
        Freq: 256
        Phase: 128
        Freq Dir: R/L
        Phase FOV: 40 cm
        1 NEX: 3 min 38 sec

C.5. 2D Fast Spin Echo in the Coronal Plane

Patient Entry: head first
Patient Position: prone
Landmark: sternal notch
Coil: other: LS45
Plane: Coronal
Mode: 2D   Monitor SAR
Pulse Sequence: Spin Echo
                Fast
FSE Optimization: 1
Echo Train: 8
Number of Echo: 2
Eff TE: 17 ms
Eff TE2: 128 ms
Rep Time: 3600 ms

Autoshim Off (only need to do once for the whole study)
Auto Center Freq: Water
FAT SAT
FOV = 34 cm
Slice Thickness = 6 mm
Inter-slice Gap = 1 mm
Suggest Range:
      Start: P10, End: A62 => Number of Locations: 13
Acq Time:
      Freq: 256
      Phase: 192
      Freq Dir: R/L
      1 NEX: 3 min 12 sec
Reps before pause: None

C.6. Fast SPGR Based Arterial Spin Tagging Pulse Sequence in the Coronal

Plane in Signa Advantage System

Patient Entry: head first
Patient Position: prone
Landmark: sternal notch
Coil: other: LS45
Plane: Coronal
Mode: 2D   Turn off monitor SAR
Pulse Sequence: SPGR
      sequential
      fast
      multiphase
Psd Name: zhud/fgt1_new3d
Phase Per Location: 61
Phase Acq. Order: sequential
Delay After Acq.: minimum
Flip Angle: 10 degree
Minimum TE
Autoshim Off
Auto Center Freq: Water
Bandwidth: 32 kHZ
FOV = 34 cm
Slice Thickness: 3.0 mm
Inter-slice Gap: 2.5 mm
Start: A30, End: A30 (or other locations) => Number of Locations: 1
Acq Time:

Freq: 256
Phase: 256
Freq Dir: R/L
Phase FOV: 34 cm
1 NEX

Use the following default parameters :

br_tino = 7, br_TI = 15ms, br_TR = 2.7 s, br_opyres = 120, br_opyresh = 120,
yhybrid = 1, opfphases = 61, br_tino = 7, br_reps = 1, br_norm = 5, br_acqs = 5,
br_TI = 15 ms, ti_inc = 100 ms.

The protocol for the fast SPGR based arterial spin tagging sequence in Signa

Horizon LX can be referred to Appendix A.

C.7. 3D SPGR Scan

Patient Entry: head first
Patient Position: prone
Landmark: sternal notch
Coil: other: LS45
Plane: Coronal
Mode: 3D   Monitor SAR
Pulse Seq: SPGR
        Flow Comp
        Graphic RX
Flip Angle: 20 degree
TE = Minimum
TR = 50 msec
Autoshim Off
Auto Center Freq: Water
FAT SAT
FOV = 34 cm
Slice Thickness: 3.0 mm
Number of Locations: 28
Acq Time:
        Freq: 256
        Phase: 128
        Freq Dir: R/L
        Phase FOV: 3/4 => 25.5 cm
        1 NEX: 2 min 37 sec

C.8. First-Pass Contrast Enhanced Dynamic Study using Multi-slice Fast SPGR

Patient Entry: head first
Patient Position: prone
Landmark: sternal notch
Coil: other: LS45
Plane: Coronal
Mode: 2D   Monitor SAR
Pulse Seq: SPGR
          Fast
Flip Angle: 30 degree
TE = 4.2 msec
TR = 11.7 msec
Autoshim Off
Auto Center Freq: Water
FOV = 34 cm
Slice Thickness: 5 mm
Inter-slice Gap: 2 mm
Start: , End: => Number of Locations: 11

Acq Time:
        Freq: 256
        Phase: 128
        Freq Dir: R/L
        Phase FOV: 3/4 => 25.5 cm
        2 NEX: 25 sec

Appendix D

Example Breast Case Studies

For all these cases, the suspicious pixels were identified based on the following criteria as was suggested in Chapter 7:

T_{1n}: > 0.5 sec
f/λ: > 0.1 sec^{-1}
STD of f/λ: < 0.1 sec^{-1}

and the suspicion level threshold was set at 20.2%. Analysis has been done using the program BreastView.

Case Study #1: Palpable mass

Date of study: Nov 16, 1997

Level of suspicion based on T_{1n} and perfusion: Low

Clinical MR images: Positive (lesion visualized, consistent with palpation)

Assessment based on spin tagging: Negative for malignancy

Abnormal mass type: Benign based on reliable health history (CONSISTENT with spin tagging result)

Discussion: The low level of suspicion, based on T_{1n} relaxation time and perfusion, at and around the palpated lesion location was a strong indication that the lesion was benign. Only one suspicious pixel was found at that location at the 20.2% threshold. It was judged that the breasts did not contain malignant tissue. This case is shown in Figures A.1(a)-(d).

Case Study #2: Palpable mass

Date of study: Aug 6, 1997

Level of suspicion based on T_{1n} and perfusion: High

Clinical MR images: Negative (mass not clearly visualized, prior cyst visualized)

Assessment based on spin tagging: Positive for malignancy

Biopsy result: Positive (spin tagging CONSISTENT with biopsy)

Discussion: The high level of suspicion, based on T_{1n} relaxation time and perfusion, at and around the lesion detected by palpation, was a strong indication that the lesion was malignant. This case is shown in Figure A.2(a)-(d).

Case Study #3: Palpable mass

Date of study: Aug7, 1998

Level of suspicion based on T_{1n} and perfusion: High

Clinical MR images: Positive (lesion visualized)

Assessment based on spin tagging: Positive for malignancy

Assessment based on first-pass contrast enhancement study: Positive for malignancy

Biopsy result: Negative (spin tagging NOT CONSISTENT with biopsy)

Discussion: High levels of suspicion, based on T_{1n} relaxation time and perfusion, were found in several breast regions. The visible lesion location on clinical MRI was consistent with that of the palpable mass. It overlapped but was considerably smaller than that found by the levels of suspicion. First-pass contrast enhancement study results correlated strongly with the high perfusion regions detected by spin tagging.

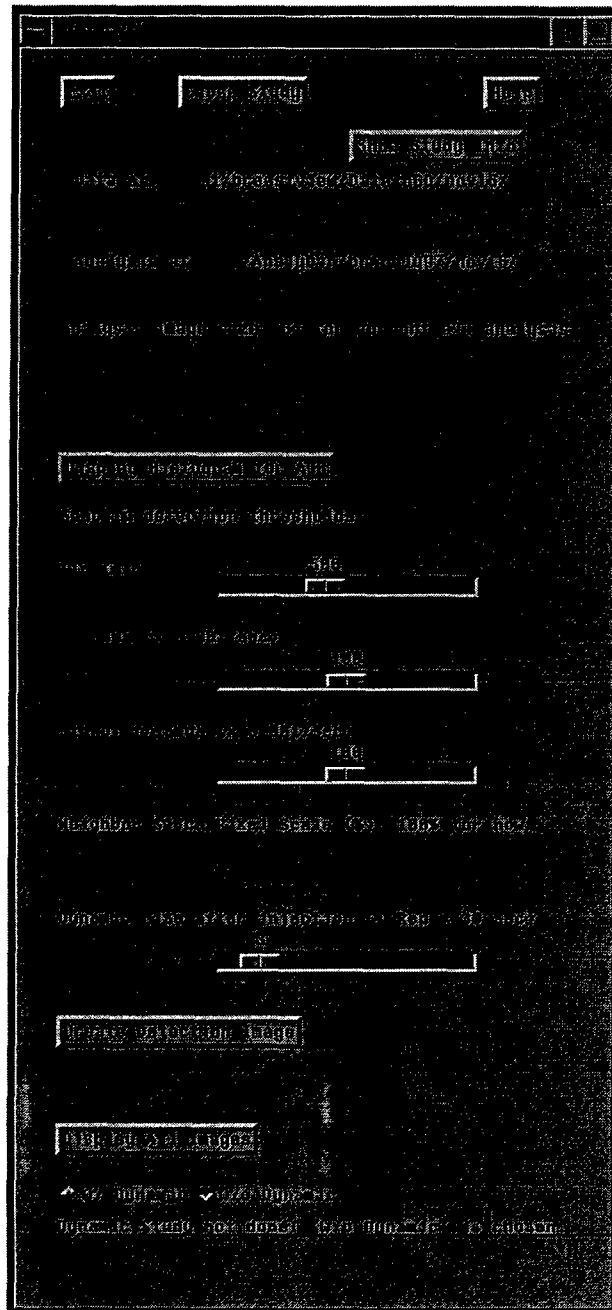Nevertheless, biopsy showed the mass to be benign. This case is shown in Figure

A.3(a)-(d).

Figure A.1(a). Nov 16, 1997 breast study. Suspicion level map
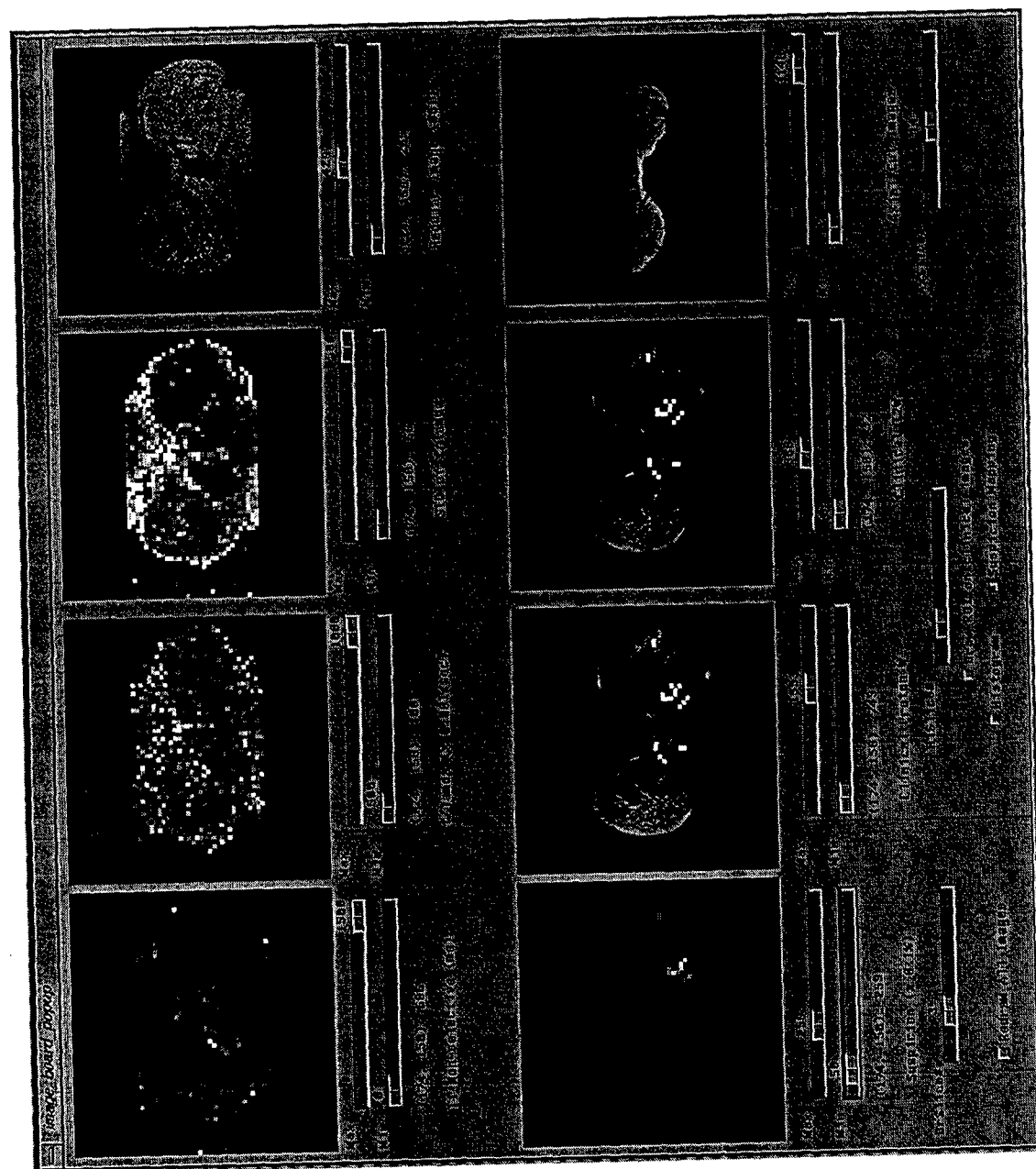is created using the "Create Detection Image" button after
setting the thresholds.

Figure A.1(b). Nov 16, 1997 breast study. Feature images (top row), suspicion level map (bottom left, threshold 0.5%) and mapping (pure white pixels) of the map on proton density and T_2 images (bottom row). Also shown: Axial T_1.
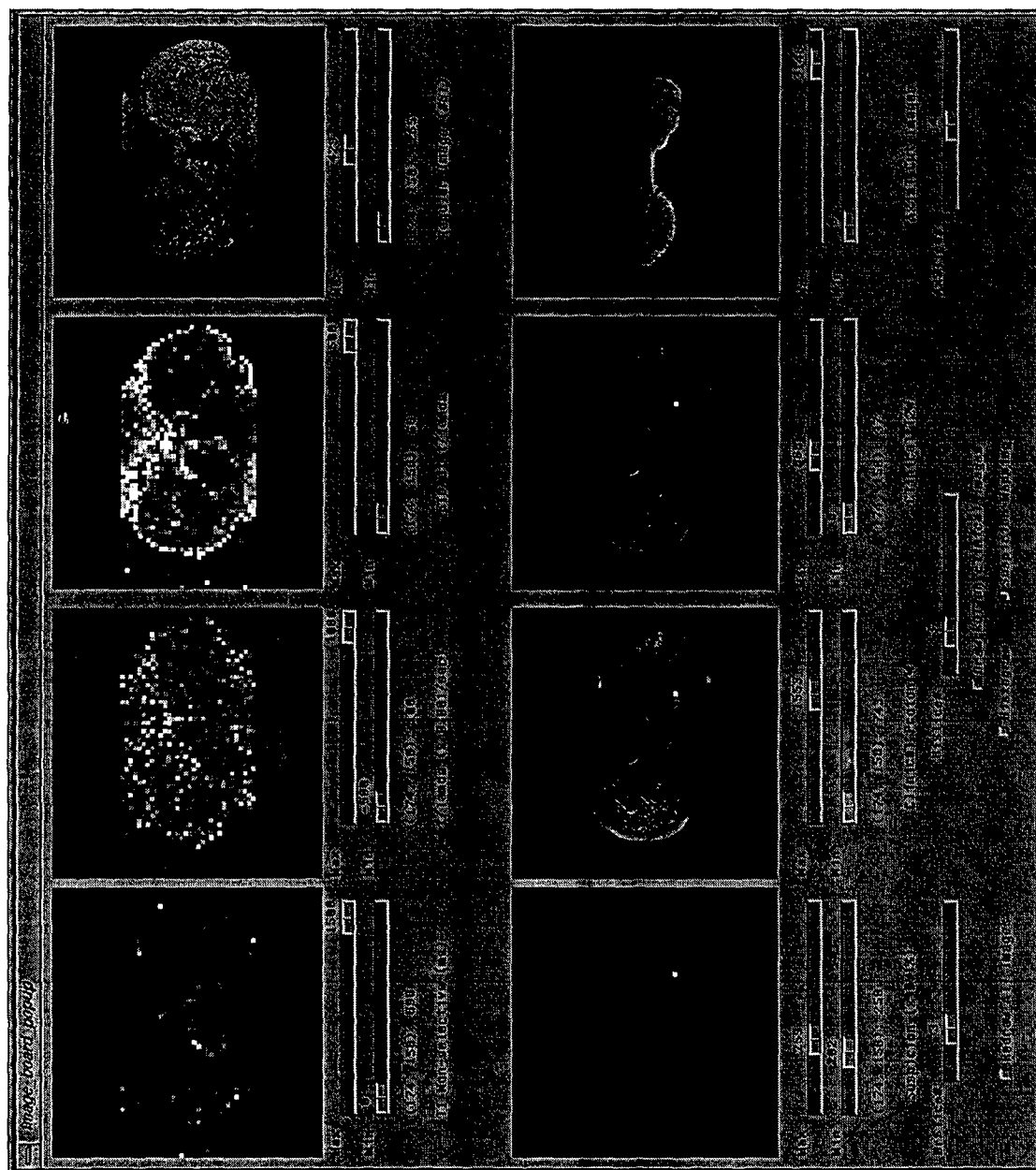
Figure A.1(c). Nov 16, 1997 breast study. Feature images (top row), suspicion map with the suspicion level threshold 20.2% (revealing single pixel) and mapping (pure white pixels) onto proton density and T_2 images. Clicking on pixels display numerical $T_1, f/\lambda$, standard error of f/λ, and suspicion level. Also shown: Axial T_1.

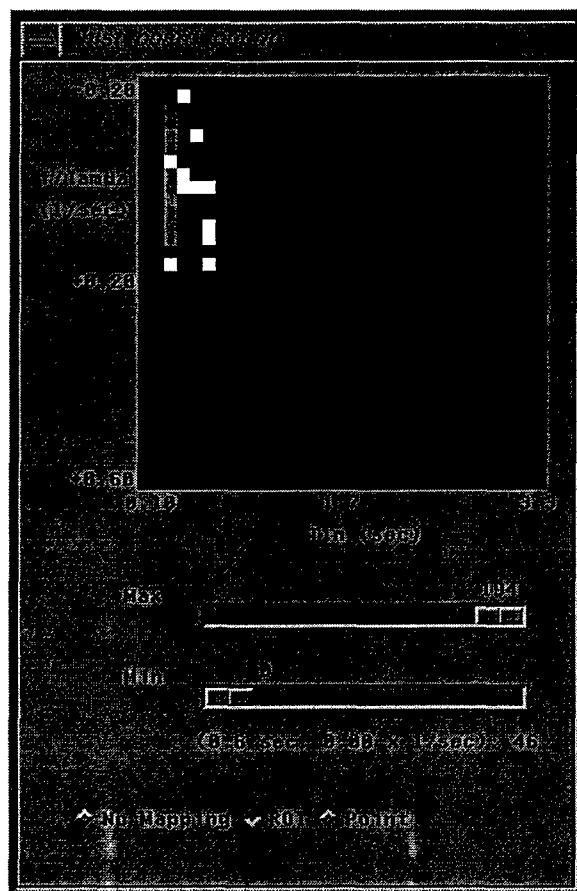Figure A.1(d). Nov 16, 1997 breast study. The T_1 and f/λ values of pixels representing the lesion identified by proton density and T_2 images, are superimposed (by pure white pixels) on the histogram of the T_1 and f/λ values from the entire breast. This figure shows that the criteria for suspicious pixels is based on moderate T_1 and high f/λ. See text for complete criteria.
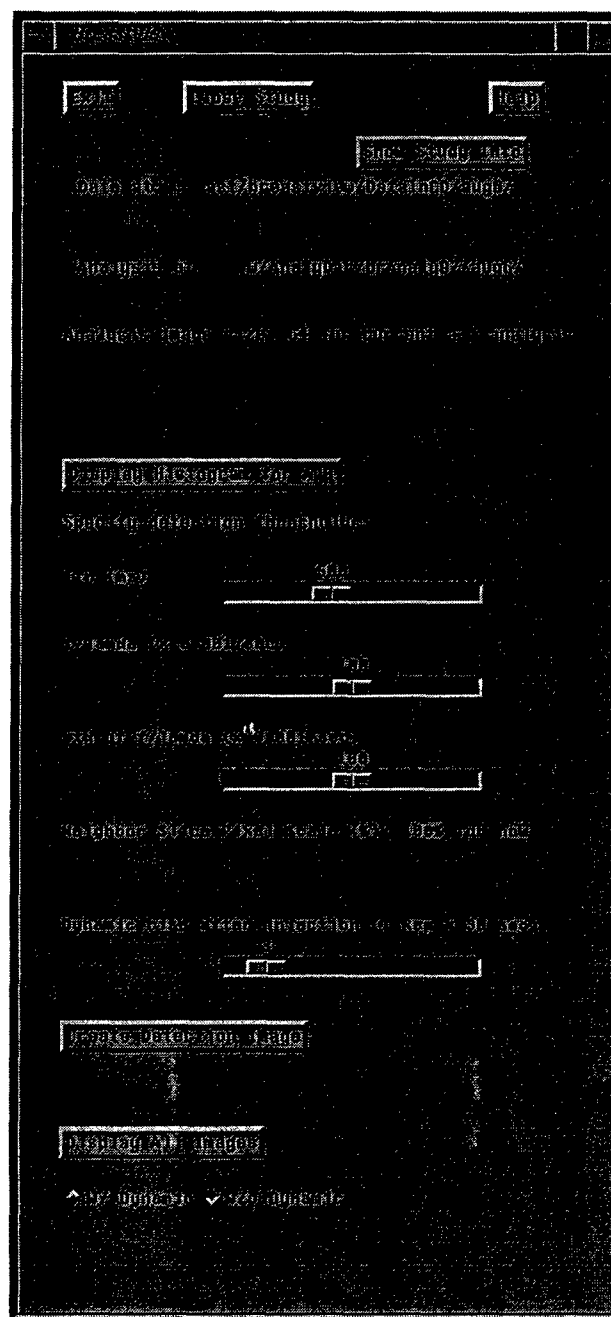
Figure A.2(a). Aug 6, 1997 breast study. Suspicion level map
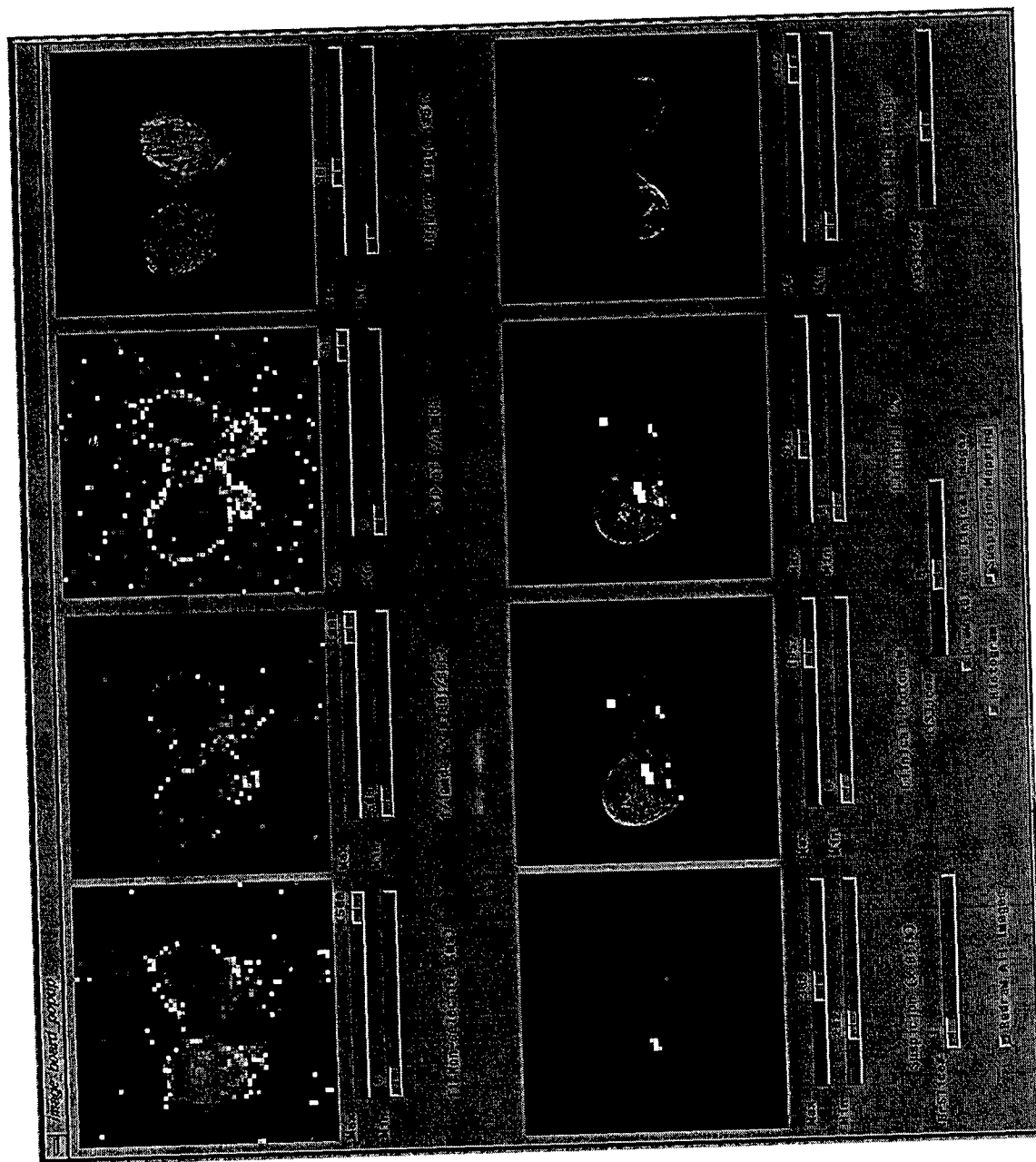is created using the "Create Detection Image" button after
setting the thresholds.

Figure A.2(b). Aug 6, 1997 breast study. Feature images (top row), suspicion level map (bottom left, threshold 20.2%) and mapping (pure white pixels) onto proton density and T_2 images. Also shown: Axial T_1.
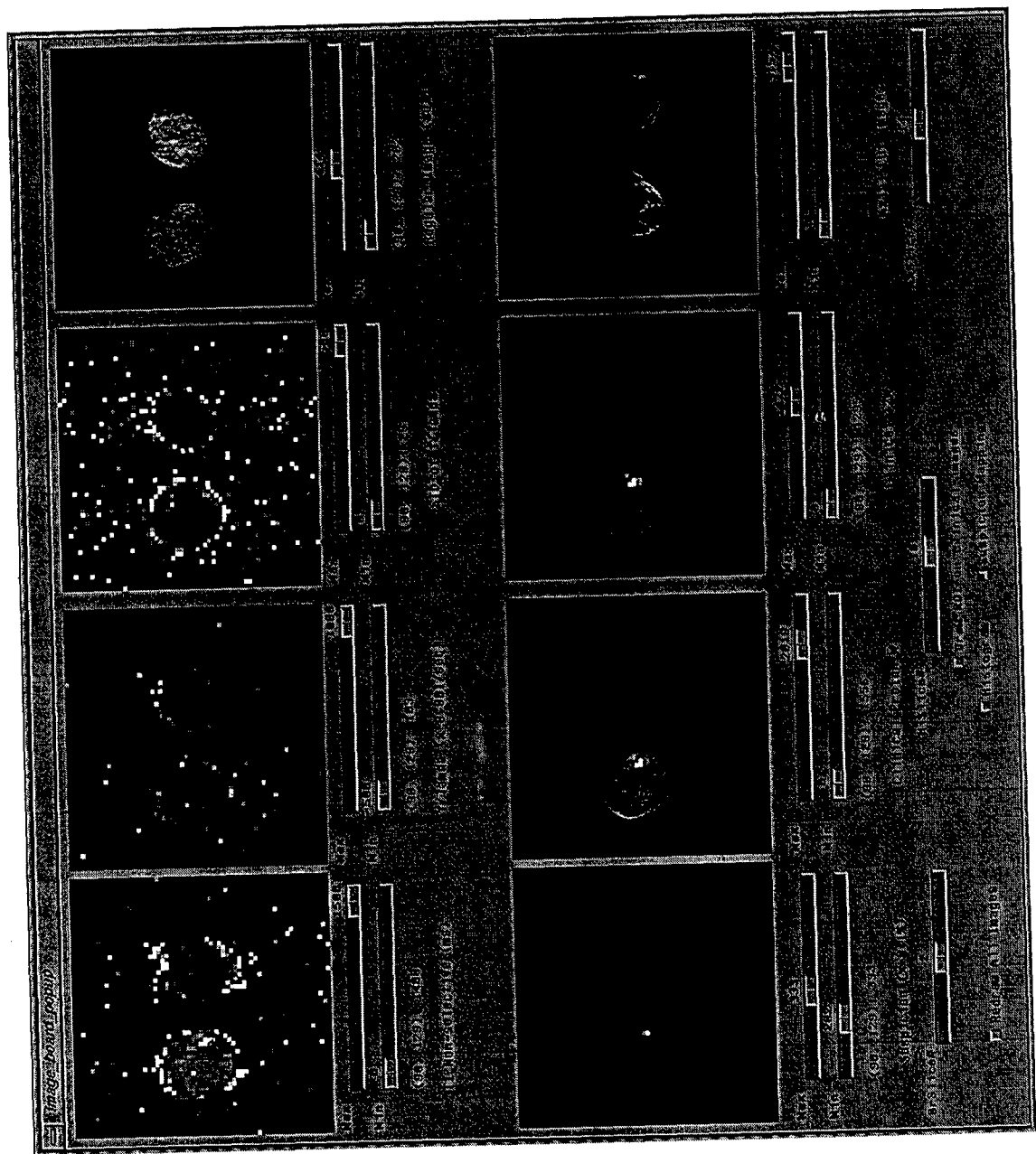
Figure A.2(c). Aug 6, 1997 breast study, slice adjacent to that shown in Figure A.2(b). Feature images (top row), suspicion level map (bottom left, threshold 20.2%) and mapping (pure white pixels) onto proton density and T_2 images. Also shown: Axial T_1.
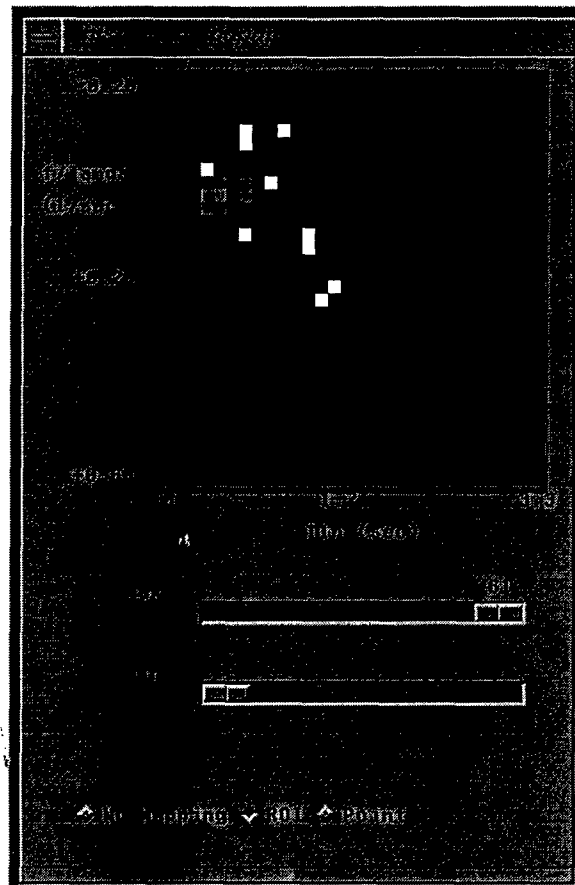
Figure A.2(d). Aug 6, 1997 breast study. The T_1 and f/λ values of pixels representing the lesion identified by proton density and T_2 images in Figure A.2(c), are superimposed (by pure white pixels) on the histogram of the T_1 and f/λ values from the entire breast. This figure shows that the criteria for suspicious pixels is based on moderate T_1 and high f/λ. See text for complete criteria.
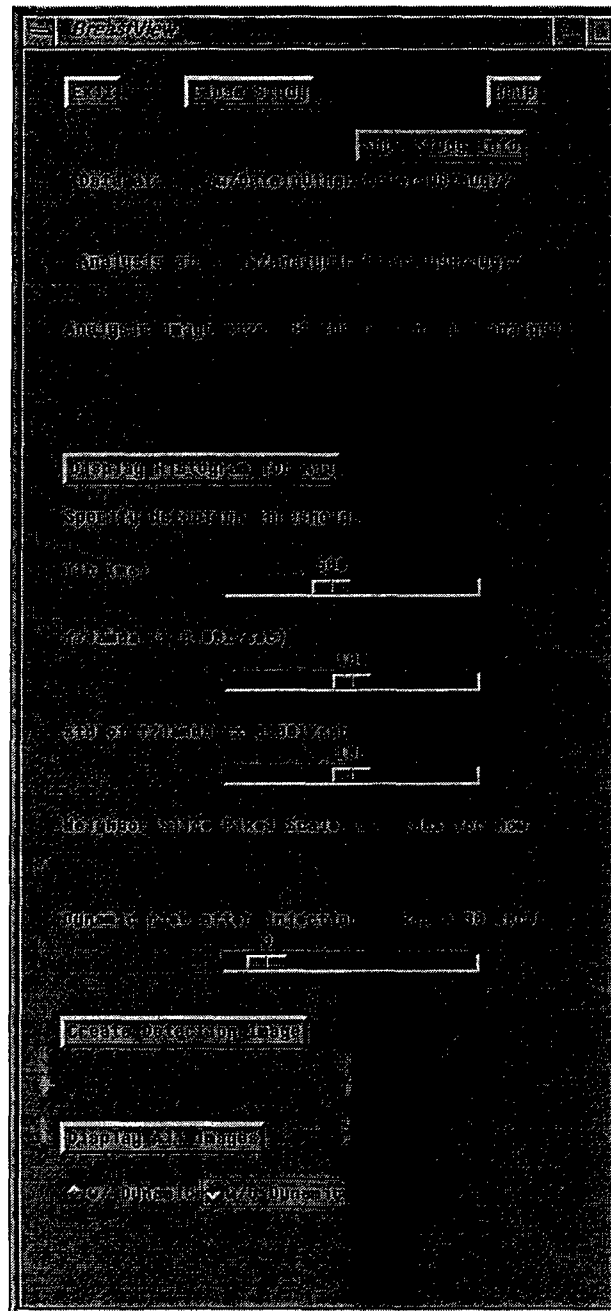
Figure A.3(a). Aug 7, 1998 breast study. Suspicion level map
is created using the "Create Detection Image" button after
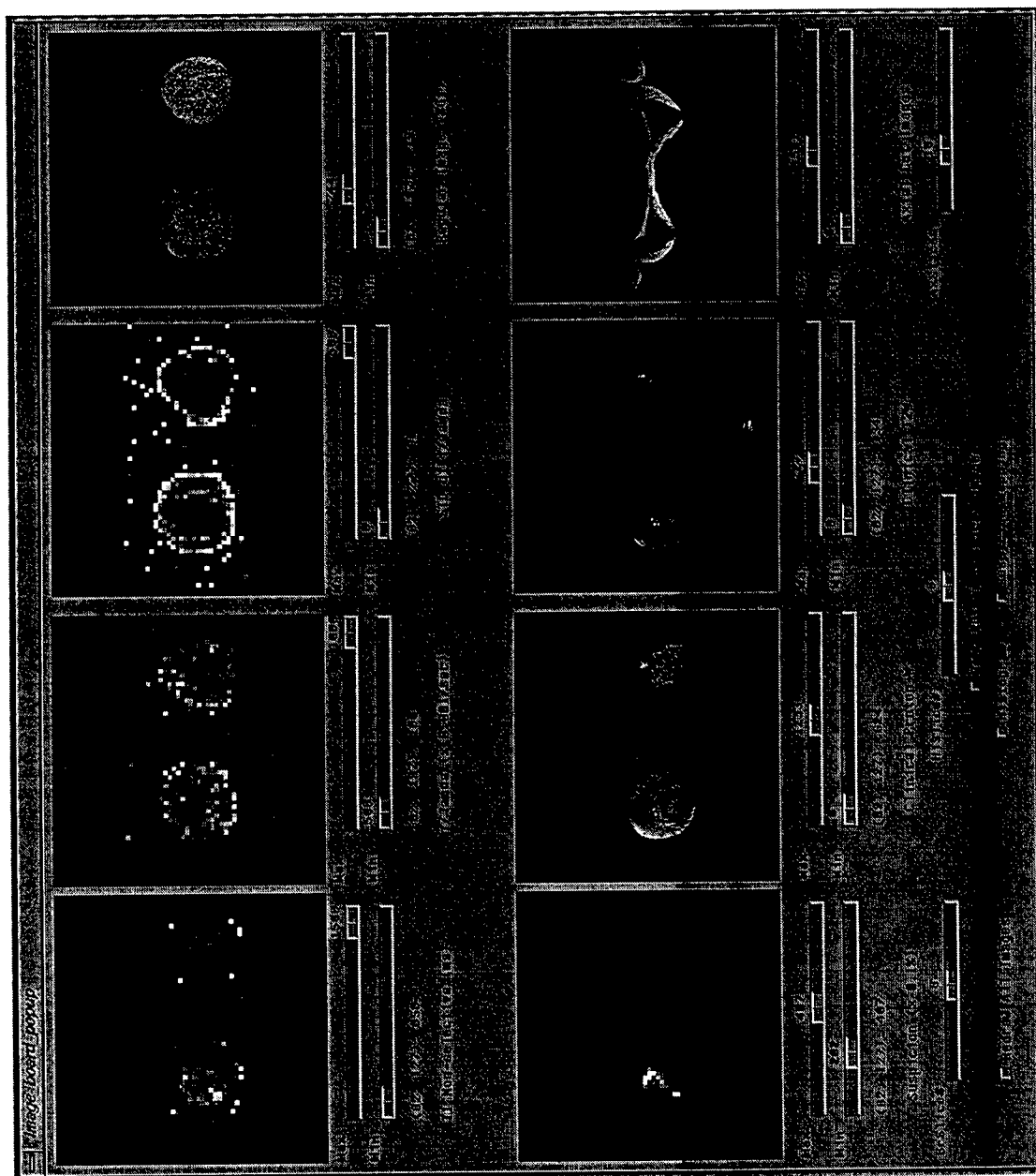setting the thresholds.

Figure A.3(b). Aug 7, 1998 breast study. Feature images (top row), suspicion level map (bottom left, threshold 20.2%). Proton density and T_2 images are shown without suspicion color mapping (bottom row). Also shown: Axial T_1.
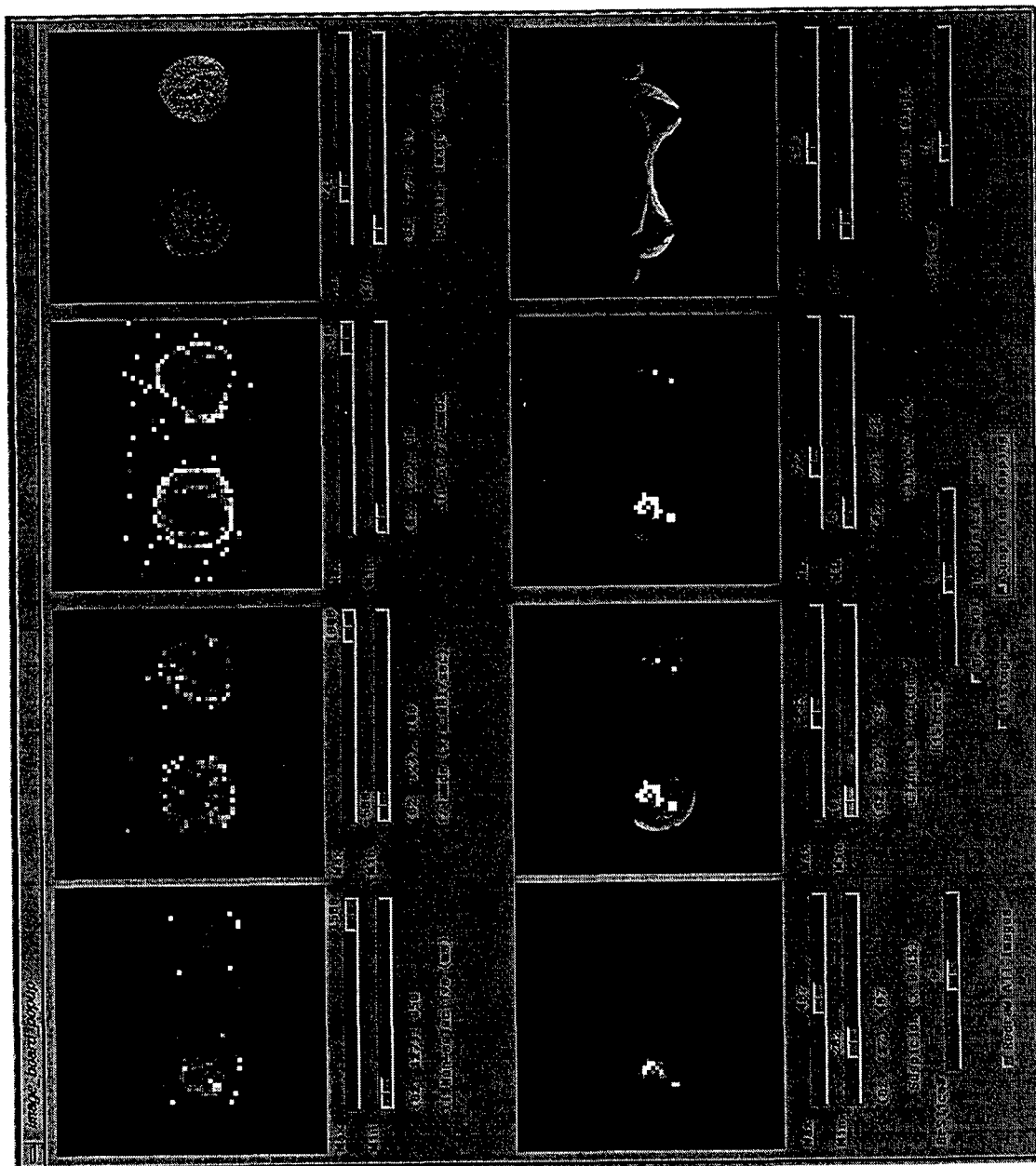
Figure A.3(c). Aug 7, 1998 breast study. Feature images (top row), suspicion level map with threshold at 20.2% (revealing one cluster of pixels) and mapping (pure white pixels) onto proton density and T_2 images. Also shown: Axial T_1.
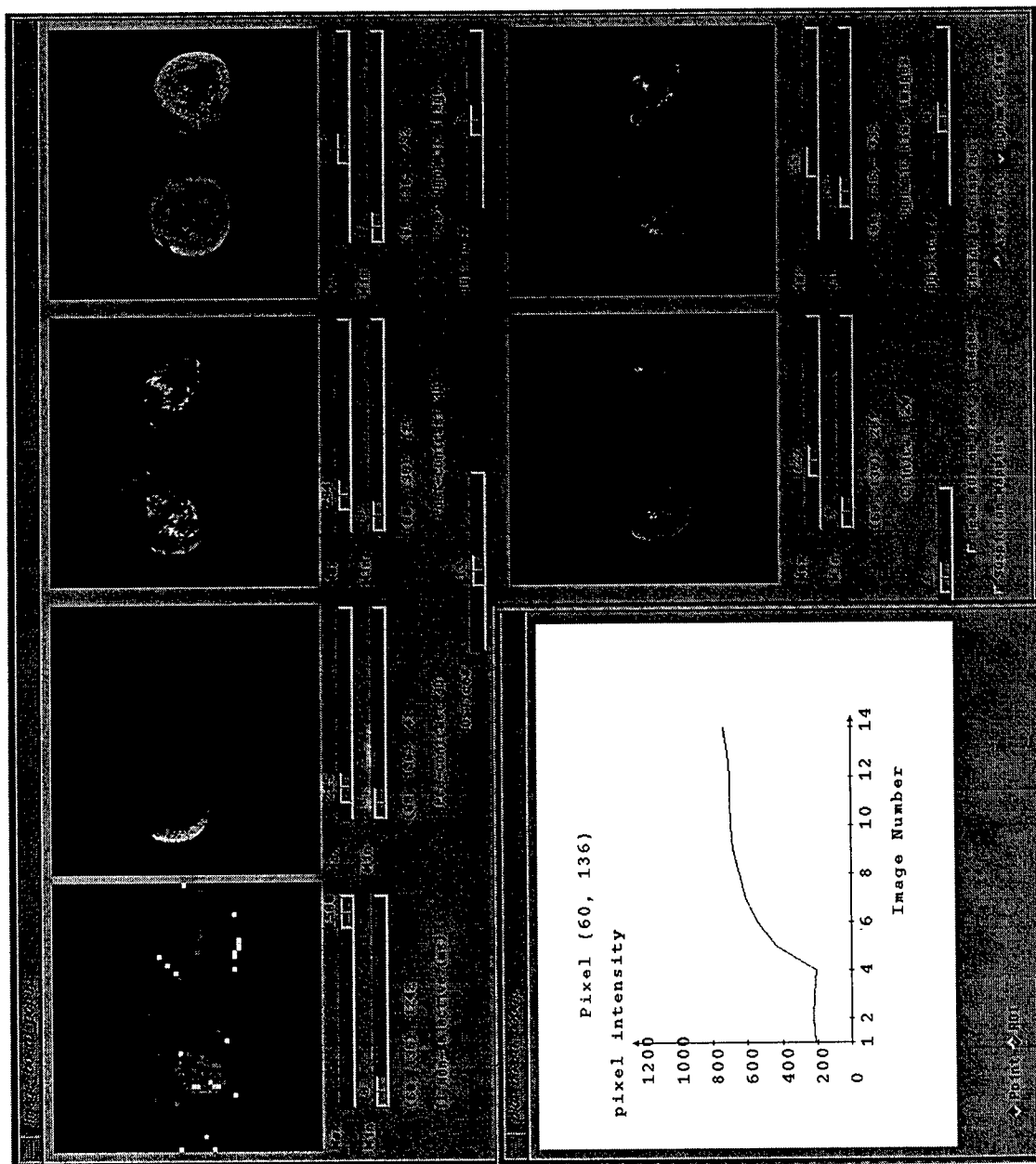
Figure A.3(d). Aug 7, 1998 breast study. Time series of signal changes at a rapidly enhancing pixel during dynamic contrast enhancement. Also shown: T_1 "feature" image (1st from left), pre_contrast 3D image (2nd from left), post-contrast 3D image, last image of dynamic study, T_2 image, and dynamic rise image.

Appendix F

Some Simple and Useful Display and Analysis Programs

This appendix introduces some simple but useful generic image display and analysis programs that have been written by the author or adopted from other sources. They should be beneficial for any research work in MRI. These executable files and source codes are available in the CDROM (zhusoft) if more details are needed. All these programs should run successfully on an SGI workstation with an operating system of IRIX 6.3 or higher.

F.1. dispAlls

This program has been written by the author for the observation and ROI analysis of one image or a series of images without a header or with a header but in GE's I.### format. To see how to use this program, simply type it at the command line without an argument:

> dispAlls

Functions: (1) Display one or a sequence of images with or without a header,

(2) ROI analysis and (3) series plot.

Usage: dispAlls xres yres display_dim image_name headerStatus MaxImagNum

image_name = full name for only 1 image or partial name for a sequence

headerStatus = 1: with header, or 0: without header

MaxImagNum default to 1 when omitted

Example: dispAlls 256 256 256 i 1 29

Example: dispAlls 256 256 256 is 0 80

Example: dispAlls 256 256 256 i.003 1 1

Example: dispAlls 256 256 256 is.003 0 1

Example: dispAlls 256 256 256 i.003 1

F.2. mydisplay and dispGE:

These two programs have been modified from Gao's display_new program

[63]. They are simple display programs for one image with or without a header file. To

see how to use them, type the command without an argument as following:

> mydisplay

Display a no-header image

Usage: mydisplay xres yres display_dim imagefile

> mydispGE

Display a GE I.### image

Usage: mydispGE xres yres display_dim imagefile

F.3. Raw Data Inspection

In pulse sequence development, raw data is often obtained from MR scanning.

The raw data might need to be inspected for the header size, the center of k space, and

whether data is collected correctly in the frequency domain. This purpose can be

achieved through two approaches. The first approach is to use the "od" command in a

UNIX workstation:

To view a P file on an SGI:

od -s Pfile + size_in_bytes_from_beginning_of_file. |more

For example,

    od -s Pfile +39936. |more

To view a P file on a SUN:

    od -s Pfile + size_in_bytes_from_beginning_of_file. |more

For example,

    od -s Pfile +39936. |more

or

    od -iv size_in_bytes_from_beginning_of_file. |more

For example,

    od -iv Pfile +39936. |more

The second approach is to use some simple Matlab routines. This approach

allows the graphical view of the raw data and should provide an easier understanding

of the raw data. A routine written by the author is shown below to serve as an

example:

```
% This routine is to view the P file contents

clear;

pfile = input('The P file  to check is: ', 's');

rawSize = input('The size of the P files (in Bytes) is: ');

fid = fopen(pfile,'r');

[B, count] = fread(fid,(rawSize/2), 'short'); %

fclose(fid);

count
```

```
beginP= input('Set the beginning point for the P file viewing (in short): ');

view_size = input('The view size of data points at a time: ');

for k = 1:1000        % give a large number 1000 to loop forever

  start = input('The chunck number with the view size just set or zero to stop: ');

  start_in_short_at = (start-1)*view_size*2 + beginP

  if start == 0

      break;

  else

      for m = 1:view_size

          realB(m) = B(start_in_short_at + 2*m -1);

          imagB(m) = B(start_in_short_at + 2*m);

      end

      subplot(2,1,1);

      plot(realB);

      title('Real Data Points');

      subplot(2,1,2);

      plot(imagB);

      title('Imaginary Data Points');

  end

end
```

Appendix G

The Companion CDROM Zhusoft

The companion CDROM Zhusoft or its contents can be obtained from the author, David Zhu, or his major professor, Dr. Michael Buonocore in the Department of Radiology at University of California Davis, through necessary research agreements. This CDROM contains the source code developed for this dissertation. It also contains some executable programs that can be run directly from the CDROM on an SGI workstation running IRIX version 6.3 or higher. A full breast study and images from a 4D human cardiac study have also been included so that analysis can be demonstrated for the BreastView program and the dispAlls program respectively. The source code contained in this CDROM can serve as examples and/or building blocks for the further development of the breast and 4D imaging projects as well as the development of MR pulse sequences and graphical-user-interface analysis applications in general. Figure A.4 shows the structure of software and data contained in the CDROM. Each directory contains a "readmefirst.txt" text file that explains the contents of the directory and gives necessary instructions.

Under the directory "4DpcExample", the subdirectory "jul29" contains resulting images from a 4D study. They can be viewed and analyzed using the dispAlls program.

The directory "/Breast/breastview/" contains the breast image analysis program, BreastView, and its source code. Study aug7 serves as an example for the

analysis. The directory "/Breast/Im_process/" contains the entire image processing
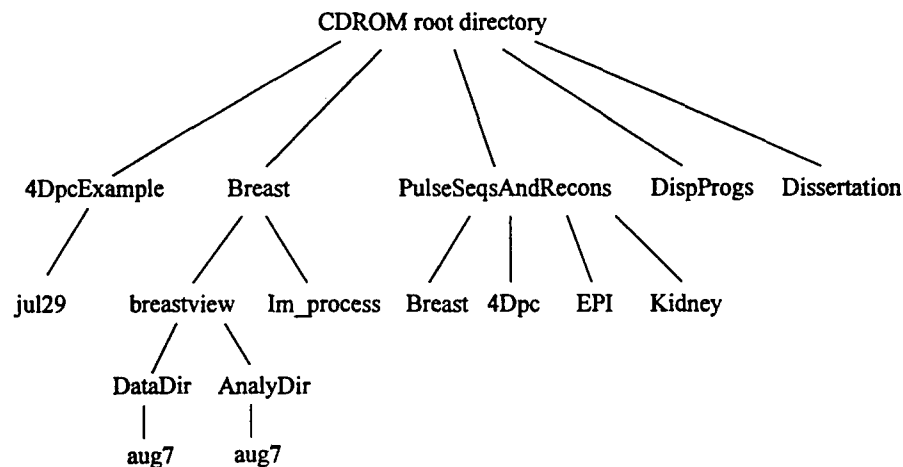
source code for the arterial spin tagging imaging.

Figure A.4. The data and software structure of the companion
CDROM Zhusoft.

The directory "PulseSeqsAndRecons" contains all of the MR pulse sequences

and the necessary image reconstruction programs developed for this dissertation. The

subdirectory "Breast" contains the pulse sequences for the breast project. The

subdirectory "4Dpc" contains the pulse sequences for the 4D project. This

subdirectory also contains the two 4D image reconstruction programs, 4dReconFrLx

and 4dReconFr2AcqLX, and their C code. Although EPI itself and the study of kidney

are not parts of this dissertation, the author has been involved in research in these

areas. Pulse sequences and the necessary image reconstruction programs developed by

the author for the odd-number hybrid EPI technique and for the study of kidney are also included in the CDROM as an extra resource under the subdirectories "EPI" and "Kidney" respectively.

The directory "DispProgs" contains all the generic display programs that have been discussed in Appendix F, including dispAlls, mydisplay, mydispGE, and some Matlab source code for raw data inspection.

The directory "Dissertation" contains the entire dissertation, which can be viewed with Microsoft Word 97 and Microsoft PowerPoint 97 or higher versions.

References

1. Bushberg JT, Seibert JA, Leidholdt EM Jr., Boone JM. *The Essential Physics of Medical Imaging*. Williams & Wilkins, Baltimore, 1994.

2. Berne RM, Levy MN. *Principles of Physiology*. The C. V. Mosby Company, St. Louis, 1990.

3. Carrington A, McLachlan AD. *Introduction to Magnetic Resonance with Applications to Chemistry and Chemical Physics*. Harper & Row, New York, 1967.

4. Fukushima E, Roeder SB. *Experimental Pulse NMR: a Nuts and Bolts Approach*. Addison-Wesley, Reading, 1998.

5. Wehrli FW, Shaw D, Kneeland JB. *Biomedical Magnetic Resonance Imaging: Principles, Methodology, and Applications*. VCH, New York, 1988.

6. Bloembergen N. *Nuclear Magnetic Relaxation*. Schotanus & Jens, Utrecht, 1948.

7. Abragam A. *Principles of Nuclear Magnetism*. Oxford University Press Inc., New York, 1996.

8. Slichter CP. *Principles of Magnetic Resonance*, 3rd edition. Springer-Verlag, New York, 1996.

9. Zur Y, Wood ML, Neuringer LJ. "Spoiling of transverse magnetization in steady-state sequences." *Magn. Reson. Med.*, 1991, 21: 251-263.

10. Callaghan PT. *Principles of Nuclear Magnetic Resonance Microscopy*. Clarendon Press, Oxford, 1991.

11. Meyer CH, Hu BS, Nishimura DG, Macovski A. "Fast spiral coronary artery imaging." *Magn. Reson. Med.*, 1992, 28:202-213.

12. The General Electric Company, *Signa Advantage^{TM} Customer 5.4 EPIC Software Reference Manual*, 1994.

13. The General Electric Company, *Signa Advantage^{TM} Customer 5.4 EPIC ESE User's Manual*, 1994.

14. The General Electric Company, *Signa Advantage^{TM} Customer 5.4 EPIC Tools User's Manual*, 1994.

15. The General Electric Company, *Signa Horizon LX^{TM} Customer LX EPIC Software Reference Manual*, 1998.

16. The General Electric Company, *Signa Horizon LX^{TM} Customer LX EPIC ESE User's Manual*, 1998.

17. The General Electric Company, *Signa Horizon LX^{TM} Customer LX EPIC Tools User's Manual*, 1998.

18. Kaiser WA. *MR mammography*. Springer-Verlag, Berlin, 1993.

19. Rosen PP, *Rosen's Breast Pathology*. Lippincott-Raven, Philadelphia, 1997.

20. Donegan WL, Spratt JS. *Cancer of the Breast*. W.B. Saunders Company, Philadelphia, 1995.

21. Rosenquist CJ, Lindfors KK. "Screening mammography beginning at age 40 years." *Cancer*, 1998, 82(11): 2235-2240.

22. Hoffmann, U, Brix G, Knopp MV, Heβ T, Lorenz WJ. "Pharmacokinetic mapping of the breast: a new method for dynamic MR mammography." *Magn. Reson. Med.*, 1995, 33:506-514.

23. Hickman PF, Moore NR, Shepstone BJ. "The indeterminate breast mass: assessment using contrast enhanced magnetic resonance imaging." *Br. J. Radiol.*, 1994, 67: 14-20.

24. Detre JA, Leigh LS, Williams DS, and Koretsky AP. "Perfusion imaging." *Magn. Reson. Med.*, 1992, 23(1): 37-45.

25. Folkman J, Merler E, Abernathy C, and Williams G. "Isolation of a tumor factor responsible for angiogensis." *J. Exp. Med.* 1971, 133(2): 275-288.

26. Kallinowski F, Schlenger KH, Runkel S, Kloes M, Stohrer M, Okunieff P and Vaupel P. "Blood flow, metabolism, cellular microenvironment and growth rate of human tumor xenografts." *Cancer Res.,* 1989, 49: 3759 - 3764.

27. Gimbrone MA Jr, Leapman SB, Cotran RS, Folkman J. "Tumor dormancy *in vivo* by prevention of neovascularization." *J. Exp. Med.*, 1972, 136:261-276.

28. Jain RK. "Determinants of tumor blood flow: a review." *Cancer Res.*, 1988, 48:2641-2658.

29. Zhu DC, Buonocore MH, Barakat-Pellot C. "Breast tissue differentiation using arterial spin tagging." *Proceedings of the UC Davis Biomedical Engineering Symposium*, Page 35-36, April 25, 1997, Davis CA.

30. Buonocore MH, Zhu DC, Barakat-Pellot C. "Measurement of breast tissue perfusion using arterial spin tagging." *Proceedings of the International Society for*

Magnetic Resonance in Medicine 5th Annual Meeting and Exhibition, 1: 311 (1997).

31. Buonocore MH, Zhu DC, Barakat-Pellot C, Zulim RA. "Noninvasive measurement of blood flow through breast tumors." Poster presentation, *1997 Breast Cancer Research Symposium*, September 16, 1997, Sacramento CA.

32. Buonocore MH, Zhu DC, Pellot-Barakat C, Zulim RA. "Non-invasive measurement of breast tissue perfusion using arterial spin tagging." *Radiology*, November 1997, 205 (P): 162.

33. Buonocore MH, Zhu DC, Zulim RA. "Analysis software for breast imaging studies." *Proceedings of the International Society for Magnetic Resonance in Medicine*, 7th Scientific Meeting and Exhibition 1999;3:2172.

34. Shimada M, Senoo A, Hayashi S, et al. "Assessment of breast cancer with dynamic gadolinium-enhanced MR imaging combined with magnetization transfer contrast using a newly developed breast surface coil for the supine position." *Radiation Medicine*, 1997, 15(2): 85-90.

35. Schreiber WG, Brix G, Knopp MV, Heβ T, Lorenz WJ. "Improved visualization of breast lesions with gadolinium-enhanced magnetization transfer MR imaging." *Magn. Reson. Med.*, 1996, 35:861-869.

36. Yousem DM, Montone KT, Sheppard LM, Rao VM, Weinstein GS, Hayden RE. "Head and neck neoplasms: magnetization transfer analysis." *Radiology*, 1994, 192: 703-707.

37. Edelman RR, Zlatkin MB, Hesselink JR. *Clinical Magnetic Resonance Imaging*. 2nd edition. W. B. Saunders Company, Philadelphia, 1996.

38. Pachot-Clouard M, Darrasse L. "Optimization of T2-selective binomial pulses for magnetization transfer." *Magn. Reson. Med.*, 1995, 34: 462-469.

39. Eng J, Ceckler TL, Balaban RS. "Quantitative ^{1}H magnetization transfer imaging in vivo." *Magn. Reson. Med.*, 1991, 17:304-314.

40. Kwong KK, Chesler DA, Weisskoff RM, Donahue KM, Davis TL, Ostergaard L, Campbell TA, Rosen BR. "MR perfusion studies with T_1-weighted echo planar imaging." *Magn. Reson. Med.*, 1995, 34: 878-887.

41. Wong EC, Buxton RB, Frank LR. "Quantitative imaging of perfusion using a single subtraction (QUIPSS and QUIPSS II)." *Magn. Reson. Med.*, 1998, 39: 702-708.

42. Barbier EL, Silva AC, Kim HJ, Williams DS, Koretsky AP. "Perfusion analysis using dynamic arterial spin labeling." *Magn. Reson. Med.*, 1999, 41: 299-308.

43. Pauly J, Le Roux P, Nishimura D, Macovski A. "Parameter relations for the Shinnar-Le Roux selective excitation pulse design algorithm." *IEEE Trans. Med. Imaging*, 1991, 10(1): 53-65.

44. The General Electric Company, *The original EPIC source code for the 2D SPGR pulse sequence*, 1994.

45. Zhu DC. *Odd-number Hybrid Echo Planar Magnetic Resonance Imaging*. Master's thesis. California State University, Sacramento, 1996.

46. Buonocore MH, Zhu DC. "Odd-number hybrid EPI." *Proceeding of the International Society for Magnetic Resonance in Medicine*, 6th Scientific Meeting and Exhibition 1998, on CD-ROM, Page 1967.

47. Buonocore MH, Zhu DC. "High spatial resolution EPI using an odd-number of interleaves." *Magn. Reson. Med.*, 1999, 41:1199-1205.

48. Buonocore MH, Zhu DC, Bronstein JA. "Ghost artifact suppression for interleaved echo-planar imaging." Scientific paper Abstract. *Radiological Society of North America*, Nov 29 - Dec 5, 1998, Chicago Ill.

49. Buonocore MH, Zhu DC, Bronstein JM. "Ghost artifact suppression for interleaved echo planar imaging using image-based phase correction." *Proceedings of the International Society for Magnetic Resonance in Medicine*, 7th Scientific Meeting and Exhibition 1999;3:1998.

50. Buonocore MH, Gao L. "Ghost artifact reduction for echo planar imaging using image phase correction." *Magn. Reson. Med.*, 1997, 38(1):89-100.

51. Jain R, Kasturi R, Schunck BG. *Machine Vision*. McGraw-Hill, Inc., New York, 1995.

52. Jain AK. *Fundamentals of Digital Image Processing*. Prentice-Hall, Inc., Englewood Cliffs, 1989.

53. Duda RO, Hart PE, Stork DG. *Pattern Classification and Scene Analysis*, 2nd edition. Department of Electrical and Computer Engineering, University of California, Davis, 1997.

54. Nishimura DG, Macovski A, Pauly JM, Conolly SM. "MR angiography by selective inversion recovery." *Magn. Reson. Med.*, 1987, 4: 193-202.

55. Ruggieri PM, Laub GA, Masaryk TJ, Modic MT. "Intracranial circulation: pulse-sequence considerations in three-dimensional (volume) MR angiography." *Radiology*, 1989, 171: 785-791.

56. Dumoulin CL, Souza SP, Walker MF, Wagle W. "Three-dimensional phase contrast angiography." *Magn. Reson. Med.*, 1989, 9: 139-149.

57. Buonocore MH. "Estimation of total coronary artery flow using measurements of flow in the ascending aorta." *Magn. Reson. Med.*, 1994, 32(5): 602-11.

58. Bogren HG, Buonocore MH. "Blood flow measurements in the aorta and major arteries with MR velocity mapping." *J. Magn. Reson. Imaging.*, 1994, 4(2):119-130.

59. Buonocore MH. "Visualizing blood flow patterns using streamlines, arrows, and particle paths." *Magn. Reson. Med.*, 1998, 40(2): 210-226.

60. Pelc N, Bernstein MA, Shimakawa A, Glover GH. "Encoding strategies for three-direction phase-contrast MR imaging of flow." *J. Magn. Reson. Imaging*, 1991, 1:405-413.

61. Gao L. *Magnetic Resonance Blood Flow Measurement through VINNIE*. Ph.D. dissertation, University of California, Davis, 1993.

62. Fredrickson J. *Notes on 4DPC* and *the 4DPC source code based on EPIC 5.6*, Richard M. Lucas Center for Magnetic Resonance Spectroscopy and Imaging, Sanford University, Stanford, 1997.

63. Gao L. *The source code for the display_new program,* University of California,

Davis, 1994.

REPLY TO
ATTENTION OF

MCMR-RMI-S   (70-1y)   1 July 03

MEMORANDUM FOR Administrator, Defense Technical Information
Center (DTIC-OCA), 8725 John J. Kingman Road, Fort Belvoir,
VA 22060-6218

SUBJECT: Request Change in Distribution Statement

1. The U.S. Army Medical Research and Materiel Command has
reexamined the need for the limitation assigned to technical
reports written for this Command. Request the limited
distribution statement for the enclosed accession numbers be
changed to "Approved for public release; distribution
unlimited." These reports should be released to the National
Technical Information Service.

2. Point of contact for this request is Ms. Kristin Morrow at
DSN 343-7327 or by e-mail at Kristin.Morrow@det.amedd.army.mil.

FOR THE COMMANDER:

Encl   PHYLIS M. RINEHART
                                     Deputy Chief of Staff for
                                     Information Management

ADB274518
ADB287328
ADB277943
ADB288221
ADB248332
ADB265760
ADB287619
ADB281577
ADB287600
ADB288422
ADB288375
ADB268297